Studies on Engineering Properties Improvement of Geopolymer and Alkali-Activated Slag

（ジオポリマー，アルカリ活性スラグの工学的特性改善に関する研究）

March 2022

Saludung Apriany

SUMMARY

Alkali-activated materials (AAMs), including those classified as geopolymer, have been studied in the past year. These materials have demonstrated desirable mechanical strengths and high fire resistance properties, making them an ideal substitute for Portland cement in a wide range of applications. However, the extensive application of AAMs in construction fields is limited by several factors. This thesis reports the characterizations of geopolymers and alkali-activated slag and their durability, including fire resistance, alkali leaching, and efflorescence formation.

Five series of geopolymer were prepared with various dosages (0%, 15%, 30%, 45%, and 60%) of ground granulated blast-furnace slag (GGBS) used to replace fly ash. The incorporation of GGBS was found to significantly increase the compressive strength due to the formation of a denser microstructure compared to the matrix containing no GGBS. However, after exposure to elevated temperature, the geopolymer containing a high amount of Ca from GGBS behaved differently from that of low-Ca geopolymer. Low-Ca geopolymer exhibited microstructure densification, while high-Ca geopolymer presents a highly porous microstructure caused by the C-S-H gel decomposition after exposure to a temperature above 500 ℃. Despite exhibiting a highly porous microstructure, the specimens could maintain enough strength when using GGBS up to 45%. When replacing fly ash with 60% GGBS, the specimen suffers from spalling and significant strength loss. Using KOH solution could improve the strength of fly ash/geopolymer by sintering that occurs at a temperature lower than the sintering temperature of geopolymer produced using NaOH solution.

Efflorescence, the white deposits on the surface of the material, is one of the major issues limiting the application of alkali-activated materials. Efflorescence in AAMs is strongly related to the alkali particles that remain unreacted in the matrix. Despite a very compact structure, a rapid efflorescence formation was observed in alkali-activated slag. This finding proves that low-porosity material does not necessarily mean a low tendency to efflorescence. Incorporating a small amount of silica fume up to 15% was found to reduce the efflorescence formation. This indicates that modifying the chemical composition can help control the efflorescence formation in alkali-activated slag.

The extensive application of AAMs is also limited by their brittle behavior. To overcome this issue, epoxy resin was added into a geopolymer mixture. The binder consists of 55% fly ash and 45% slag, while small amounts of epoxy resin (1% and 2.5% of the binder mass) were incorporated to produce geopolymer composite. The results show that the inclusion of epoxy resin significantly enhances the mechanical properties and reduces the total alkali leaching of ambient-cured geopolymer, thus promising the application in construction industry. Interestingly, despite significant loss of alkali, specimens immersed in water present a higher compressive strength than that of cured at ambient temperature.

ACKNOWLEDGEMENTS

A great thanks to my Merciful Lord, Jesus Christ for His grace and all the countless gifts He offered me. His true love always strengthens me throughout my life.

And with boundless love and appreciation, I would like to extend my heartfelt gratitude and appreciation to the people who helped me during my life and my study:

To my supervisor, Prof. Kenji Kawai whose guidance, time spent, encouragement, and advice that helped bring this study into success. It was a privilege to be a student of him;

To Assistant Prof. Yuko Ogawa and Assistant Prof. Riya Chaterine George for their supports, guidance, and time spent during this study;

To Prof. Kenichiro Nakarai and Prof. Takaaki Ohkubo for their advice and constructive comments for the completion of this study;

To all teachers and office staffs of department of civil and environmental engineering, for their invaluable helps;

To all members of Zaiken laboratory, for their unending supports and efforts to make this study possible;

To Yahata Memorial Scholarship Foundation, for providing a financial support during my study for the period of six months;

To Mitsubishi Corporation, for providing a financial support during my study for the period of one year.

A special thanks to Dr. Takeo Miyashita, for his support and encouragement during my study and life in Japan.

And finally, my very deep gratitude to my father, Saludung, my mother, Meti, and to my sisters and brothers, and all of my family for their love, prayers, and supports that brings me to be able to go this far.

Apriany Saludung

Contents

LIST OF FIGURES

LIST OF TABLES

CHAPTER 1. INTRODUCTION

1.1 Background of Study

Nowadays, the demand for construction has increased significantly. Concrete, the most widely used material in construction, has been considered one of the main contributors to global warming and climate change. In particular, the production of cement, the main material for concrete, contributes about 7-8% of global CO_2 emissions (Andrew, 2019; Worrell et al., 2001). Cement manufacture is also a highly energy-intensive manufacturing process. The high CO_2 emission from cement is resulted from the calcination of limestone and the use of fossil fuels (Ebrahimi et al., 2017). Due to the environmental impacts of concrete, cement industry deserves attention in the assessment of global warming potential.

On the other hand, due to the faster growth of industries worldwide, various materials are dumped into the land. One of the most important fossil fuels, coal, supplies over one-third of global electricity generation (Ul Haq et al., 2014). It also plays a crucial role as a key energy source in many industries such as metal production, cement production, and chemical production. However, the use of coal generates a significant amount of byproducts such as fly ash and bottom ash (Hower, 2012; Wilczyńska-Michalik et al., 2014). The composition of fly ash is mainly oxidized compounds of Si, Al, Fe, and Ca, which are similar to natural earthly materials (Tiwari et al., 2014). The concentration of these elements depends on the type of coal (Manz, 1999), combustion process (Wilczyńska-Michalik et al., 2014), and efficiency of emission control devices (Ju and Lee, 2017). Bottom ash is composed mostly of Si, Al, and Fe, but the appearance is comparable to that of river sand (Singh and Siddique, 2014). The disposal of these byproducts generates some problems, including land usage and heavy metal contamination of groundwater. Therefore, reusing these byproducts can reduce the environmental impact. Fly ash is commonly used as a partial

replacement of ordinary Portland cement (OPC) due to its pozzolanic activity. The use of fly ash together with OPC reduces the heat of hydration and improves the durability of concrete (Ebrahimi et al., 2017; Manz, 1999; Poon et al., 2000). Bottom ash, in contrast, has lower pozzolanic activity. However, it can be used as a replacement of fine aggregate in concrete production because of the coarser particles (Rafieizonooz et al., 2016; Singh and Siddique, 2014). Fly ash is suitable for use in concrete; however, the slow rate of hydration of fly ash limits the wide use of high-volume fly ash concrete.

Another important byproduct commonly used in concrete is ground granulated blast-furnace slag (GGBS) (Li and Zhao, 2003; Najimi et al., 2011; Özbay et al., 2016). Ground granulated blast-furnace slag is a byproduct from the blast-furnace of iron manufacture, which is composed of significant oxidized amount of Si, Al, Ca, and Mg. Unlike fly ash, GGBS has latent hydraulic properties, due to which it exhibits excellent cementitious properties when used with Portland cement. The potential use of fly ash and GGBS to replace cement in concrete production can reduce the CO_2 emission associated with OPC manufacture. However, the amount of these byproducts allowed to replace OPC is typically less than 50% (Kurad et al., 2017; Poon et al., 2000).

Alkali-activated materials (AAMs) and geopolymers, the materials hardened by the reaction of aluminosilicate sources and alkali solutions, have been studied in the past years as they appear to be alternative materials that can fully replace the OPC in concrete production. Alkali-activated materials and geopolymers are sometimes mixed up, even though they acquire their strength by chemical reaction between an alkaline soluble sources and aluminosilicate sources. In fact, they are distinct by their reaction pathways and chemical structures of the final products. Although the CO_2 emission from AAMs and geopolymers materials is associated with the manufacture of alkali solutions, Carreño-Gallardo et al. reported that producing AAMs and geopolymers without cement generates 54% less CO_2

than the OPC clinker (Carreño-Gallardo et al., 2018). Thus, the use of AAMs and geopolymers is more sustainable than OPC, not only because of the high CO_2 emission from OPC but also because the use of byproducts such as fly ash and GGBS in AAMs can reduce the environmental impacts raised from their disposal into the landfill. In addition, AAMs and geopolymers can be produced from various range of aluminosilicate sources such as metakaolin, silica fume, rice husk ash, and natural pozzolans such as volcanic ashes and pumices (Liang et al., 2021; Mohseni et al., 2019; Najafi Kani et al., 2012; Nana et al., 2021; H. Y. Zhang et al., 2014b). Moreover, many researchers reported that these materials exhibit comparable or even better mechanical properties and resistance against high temperatures compared to OPC.

Nowadays, the study on the high-temperature resistance of building materials is critical due to the experiences of catastrophic fires. The fire resistance comes under the durability of concrete. OPC concretes generally provide adequate fire resistance for most normal applications. However, when exposed to high temperatures, concretes experience severe microstructural and mechanical changes. Geopolymer has attracted significant attention in recent years due to its excellent fire resistance. Zhang et al. reported that geopolymer specimens produced from metakaolin and fly ash exhibit comparable mechanical strength and higher residual compressive strength than OPC specimens after exposure to elevated temperatures up to 800 ℃ (H. Y. Zhang et al., 2014b). The ceramic-like characteristics of geopolymers make them suitable as fire-resistant materials (Alehyen et al., 2017; Davidovits, 2017). The ability of geopolymer to resist high temperature is believed due to the recrystallization of this material at high temperature. Geopolymers are typically semi-amorphous in structures. Exposure to high temperatures promotes the recrystallization of geopolymer into secondary mineral phases which are dominant minerals of the earth's crust (Alehyen et al., 2017; Kuenzel et al., 2013). Kuenzel et al. investigated

the properties of metakaolin-derived geopolymer after exposure to high temperatures and found the formation of nepheline ($NaAlSiO_4$) at 900 ℃ (Kuenzel et al., 2013). Alehyen et al. also observed the formation of nepheline and other crystalline phases such as albite ($NaAlSiO_8$) and faujasite in fly ash-based geopolymer after exposure to 1000 ℃ (Alehyen et al., 2017). Unlike geopolymer, OPC specimen presents the increase in the amount of alite (C_3S) and belite (C_2S) and the formation of CaO as the result of the thermal decomposition of calcium silicate hydrate after exposure to high temperature (Tantawy, 2017).

Even though geopolymer possesses better heat resistance than Portland cement, some issues limit the extensive application of geopolymer and AAMs in the construction industry, including a high tendency to leach alkali and efflorescence formation. In general, efflorescence refers to the white carbonate deposits on the surface of materials due to the chemical reaction between the water-soluble salts and CO_2 from the atmosphere. In geopolymer and AAMs, the efflorescence is caused by the excess alkali brought to the surface by moisture and reacts with CO_2 in the air. Efflorescence is mainly affected by temperature and humidity. In AAMs and geopolymer, the alkali mobility is the primary cause of efflorescence formation. Ambient-cured geopolymer contains a high amount of unreacted alkali particles, which makes it undergo severe efflorescence compared to heat-cured geopolymer (Najafi Kani et al., 2012; Škvára et al., 2009). Moreover, the efflorescence can occur faster when the geopolymer was subjected to a humid environment. High-temperature curing is an effective way to reduce the efflorescence formation, but this can limit the broad application of geopolymer and AAMs in construction.

The extensive application of AAMs and geopolymers is also limited by their brittle properties and low flexural strength. AAMs and geopolymers exhibit poor cracking resistance due to their brittle, ceramic-like nature (Bernal et al., 2010; Thomas and Peethamparan, 2015). Recently, many studies have been focusing on the development of

geopolymer composites, owing to the enhancement of the mechanical strength, including flexural and compressive strengths, and the improvement of the brittleness. In this framework, several fillers such as steel fibers (Bernal et al., 2010; Carabba et al., 2017; Khan et al., 2018), carbon fibers (Yan et al., 2016; H. Y. Zhang et al., 2014a), cotton fibers (Alomayri et al., 2013; Alomayri and Low, 2013), and organic resins (Chen et al., 2018b; Ferone et al., 2013; Roviello et al., 2015, 2013) are used to modify the toughness and enhance the mechanical properties of AAMs.

1.2 Objectives

As mentioned earlier, the use of AAMs and geopolymers is more sustainable than OPC. Some studies have also proved that geopolymer performed better heat resistance than OPC due to the recrystallization into secondary mineral phases. However, since the chemical composition of starting materials used to produce geopolymer varies depending on the type and origin of materials, more research is required to study the effect of other materials on the fire resistance of geopolymer. Moreover, the preliminary study on the effect of slag addition on the strength of fly ash geopolymer resulted in a significant improvement of compressive strength up to 100 MPa when fly ash was replaced by 60% of slag. However, high strength does not always guarantee high soundness and durability. Therefore, in this study, the fire resistance of geopolymer produced from fly ash and GGBS was further investigated. In addition, some drawbacks limit the use of these materials in construction industry, including low flexural strength and high tendency to efflorescence when cured at ambient temperature. Therefore, main objectives of this research are to:

1) to understand the heat resistance of fly ash/slag-based geopolymer through investigating the effect of slag content and alkali metal type of solution on compressive strength, phase composition, and microstructure after exposure to elevated temperature;

2) to investigate the efflorescence formation in alkali-activated slag incorporating silica fume;
3) to potentially widen the application of geopolymer by introducing an epoxy resin-reinforced geopolymer and investigating their alkali leaching and mechanical performance after curing at different conditions.

In relation to the first objective, few publications have focused on the effect slag addition and different alkali solutions on heat resistance of fly ash/slag-based geopolymer. A previous study has been conducted using potassium hydroxide solution in geopolymer made from fly ash only and found that using potassium-containing solution could improve the compressive strength at high temperature (higher than the initial strength). However, fly ash geopolymer and fly ash/slag geopolymer have different reaction products and properties; thus, it is expected that geopolymer containing slag will behave differently from those made from fly ash only in the response to high temperature attack, and the use of potassium-containing solution may also show different effect on the heat resistance of geopolymer containing both fly ash and GGBS. The compressive strength, phase stability, and microstructure of the unexposed and exposed geopolymer specimens to high temperature were characterized and evaluated.

A study on efflorescence in AAMs is not widely available. The second study aims to investigate the efflorescence formation in alkali-activated slag incorporating silica fume. Although, the previous studies have claimed that geopolymer with low porosity showed less efflorescence formation, this may not be the case for alkali-activated slag, which has different structure and properties from fly ash/slag geopolymer. Since this study employed high concentration of alkali solution and the specimens were cured only at ambient temperature, the efflorescence was expected to excessively form on the surface of specimen. Therefore, to achieve this first objective, different amount of silica fume was incorporated

and its effect on specimens' microstructure, pore size distribution, phase composition, alkali leaching, and efflorescence formation was investigated. Moreover, the efflorescence deposit formed on the surface of specimen was scraped and its elemental and phase compositions were characterized by energy dispersive X-ray spectroscopy (EDS) and X-ray diffraction (XRD), respectively.

The geopolymer composite reinforced by organic polymer has been widely studied. However, the majority of the literature has neither investigated the alkali leaching on the geopolymer composite and the effect of curing conditions, including ambient curing, heat curing, and water curing on the mechanical performance of epoxy resin-reinforced geopolymer composite. The mechanical strength of geopolymer cured in water is crucial to be understood, since geopolymer will leach significant amount of alkali in water. Therefore, to gain further insight, the compressive strength, flexural strength, microstructure, pore size distribution, and phase composition of geopolymer reinforced with different amount of epoxy resin and cured at different condition were characterized.

1.3 Scope of Work

The research utilized low calcium fly ash and GGBS as the base materials for producing geopolymer. The alkali-activated slag (AAS) was also produced under various dosage of silica fume to assess the efflorescence potential. Moreover, fly ash/GGBS-based geopolymer composites reinforced by Bisphenol F epoxy resin were also produced.

The basic properties studied included compressive strength, flexural strength, phase composition, microstructure, porosity, and thermal stability. In addition, the durability including fire resistance and efflorescence formation were also investigated.

1.4 Thesis Outline

The outline of this thesis is shown in Fig. 1.1. Chapter 1 states some backgrounds, including the importance of the research, evaluation of the current situation (advantages/disadvantages) related to the scope of alkali-activated materials and geopolymers, and the research scopes and objectives. Chapter 2 provides a general overview of some topics related to the study, including a brief theory and the development of traditional cement, alkali-activated materials, and geopolymer. This chapter also provides a summary of previous studies by reviewing some literature. Chapter 3 describes the methodology of the research, including the materials used, synthesis, testing procedures, and characterization of the final products. Chapters 4, 5, and 6 present the study results, some of which have been published in the proceeding and international journals. Chapter 7 states the conclusions and some recommendations for the future work related to the study.

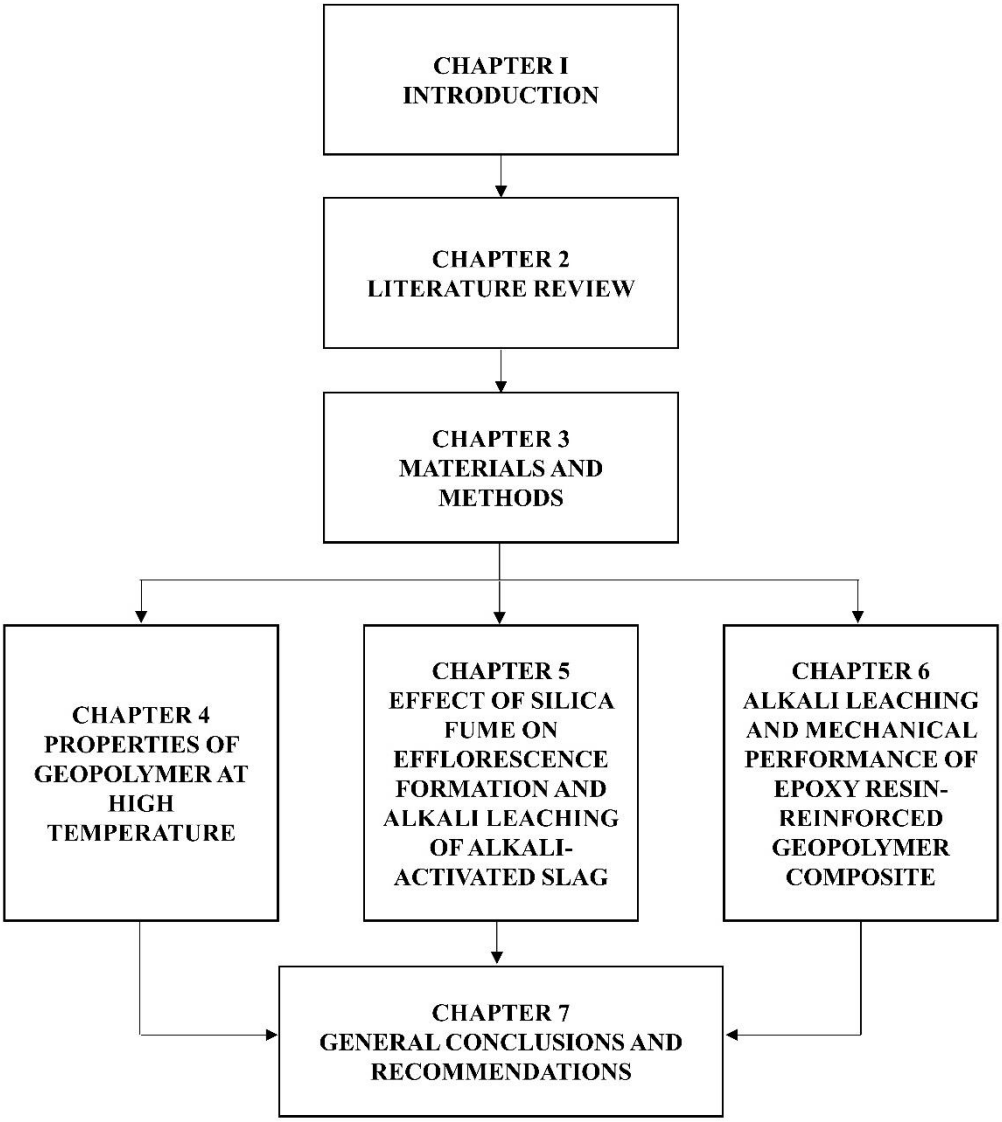

Figure 1.1 Thesis outline

CHAPTER 2. LITERATURE REVIEW

This chapter provides a brief overview of some crucial aspects of traditional cement industries, alkali-activated materials and geopolymers technology by reviewing published literature. A brief historical development, basic theory, characteristics, durability, and the importance of alkali-activated materials and geopolymers are discussed.

2.1 Portland Cement Manufacture

In recent years, the global production of cement has grown rapidly due to the increasing demand for construction worldwide. Ordinary Portland cement (OPC) is an excellent building material widely used as a binder in concrete productions. The main compounds of Portland cement include tricalcium silicate ($3CaO.SiO_2$), dicalcium silicate ($2CaO.SiO_2$), tricalcium aluminate ($3CaO.Al_2O_3$), and a tetra-calcium aluminoferrite ($4CaO.Al_2O_3Fe_2O_3$). These compounds are abbreviated based on the typical atomic symbols as C_3S, C_2S, C_3A, and C_4AF. When mixing with water, C_2S and C_3S react with water molecules to form calcium silicate hydrate (CSH) and calcium hydroxide ($Ca[OH]_2$).

Calcium silicates are the most important hydraulic constituents; therefore, the raw materials used to produce OPC must provide suitable forms and proportions of calcium and silica. Limestone is the common source of calcium, while clays and shales are used as the sources of additional silica.

The raw materials are pulverized and heated in the huge rotary kiln at about 1400-1650 ℃ to form a solid substance called clinker (Gagg, 2014). The fuels commonly used for firing are pulverized coal, oil, or natural gas. After the clinker is cooled, it is pulverized and mixed with small amounts of gypsum and some additives to regulate the initial chemical reaction of the cement (Gagg, 2014). During the calcination of raw materials in the kiln, the following chemical reactions take place:

$$CaCO_3\ (Limestone) \xrightarrow{heat} CaO\ (s)\ +\ CO_2\ (g)$$

$$MgCO_3\ (s) \xrightarrow{heat} MgO\ (s) + CO_2\ (g)$$

$$Clay \xrightarrow{heat} SiO_2 + Al_2O_3 + Fe_2O_3$$

$$Clay\ + Limestone \xrightarrow{Heat} \begin{cases} 3CaO \cdot SiO_2 \\ 2CaO \cdot SiO_2 \\ 3CaO \cdot Al_2O_3 \\ 4CaO \cdot Al_2O_3 \cdot Fe_2O_3 \end{cases}$$

It is estimated that cement manufacture contributes around 7% of global CO_2 emission, making it a major contributor to global warming and climate change (Fry, 2013). Cement production is also a highly energy-intensive process. The emission includes the CO_2 from the calcination of raw materials and the combustion of fossil fuels during the burning process. The specific process of CO_2 emission per ton of cement depends on the ratio of clinker to cement. Some countries have developed technologies that enable the utilization of wastes as alternative raw materials or additives and as alternative fuels. Industrial wastes such as coal ash and blast-furnace slag are blended with clinker to produce blended cement. Reusing industrial waste helps extend the life of existing landfills for waste disposal, and at the same time, reduces the CO_2 emission due to the reduction of clinker amount.

Finally, the environmental impacts arising from Portland cement manufacture have led to the search for alternative binders. Several alternatives, such as alkali-activated cement, calcium sulphoaluminate cement (SAC), magnesium phosphate cement, etc., are being made with some advantages over Portland cement. SAC is typically used in the field of solidification of heavy metals. Among these alternatives, alkali-activated cement produced from industrial wastes has attracted many researchers because this kind of material has shown comparable or even better mechanical strength and durability compared to OPC. Moreover, the use of alkali-activated cement from industrial wastes can solve two major

environmental issues: the CO_2 emission from cement manufacture and the disposal of huge amounts of wastes.

2.2 Alkali-Activated Materials and Geopolymers

In general, 'geopolymers' refer to the low-calcium or calcium-free binders. The reaction products are characterized by zeolite-like phases and a polymeric model resulting in 3D structures, whereas alkali-activated materials are produced using calcium-rich precursors, resulting in the formation of C-S-H gels (Bhardwaj and Kumar, 2019). The variation of the chemical composition of the industrial wastes is one factor that limits the broad application of AAMs and geopolymers in the construction industry.

2.2.1 The chemistry of alkali-activated materials and geopolymers

As mentioned earlier in chapter 1, geopolymer is sometimes mixed up with alkali-activated cement because either of these materials uses alkali solution in their manufactures. Glukhovsky and Krivenko proposed a model for alkaline activation of Si- and Ca-rich materials which were summarized as follows:

$$\equiv Si\text{-}O^- + R^+ = \equiv Si\text{-}O\text{-}R$$
$$\equiv Si\text{-}O\text{-}R + OH^- = \equiv Si\text{-}O\text{-}R\text{-}OH^-$$
$$\equiv Si\text{-}O\text{-}R\text{-}OH^- + Ca^{2+} = \equiv Si\text{-}O\text{-}Ca\text{-}OH + R^+$$

The reaction mechanism of alkaline cement is similar to Portland cement hydration. The alkali solution plays a crucial role in the initial phases of reaction, both in AAMs and geopolymers, because a strong alkali medium is required to dissolve the aluminosilicate precursor. The main hydration product of alkali-activated slag is a calcium silicate hydrate with aluminium in its composition (C-A-S-H), having a lower C/S ratio than Portland cement, while alkali activation of fly ash resulting in the sodium and/or potassium aluminate silicate hydrate (N,K-A-S-H) gel.

Prof. J. Davidovits first coined the term ‘geopolymer’ in 1978, which refers to a class of inorganic polymer, having a chemical composition similar to zeolites but an amorphous structure (Davidovits, 1991). The hardening mechanism involves the chemical reaction of the precursors such as alumino-silicate oxides with alkali polysilicates yielding polymeric Si-O-Al bonds (Davidovits, 1991). The reaction results in the chemical groups are described as following (Davidovits, 2002):

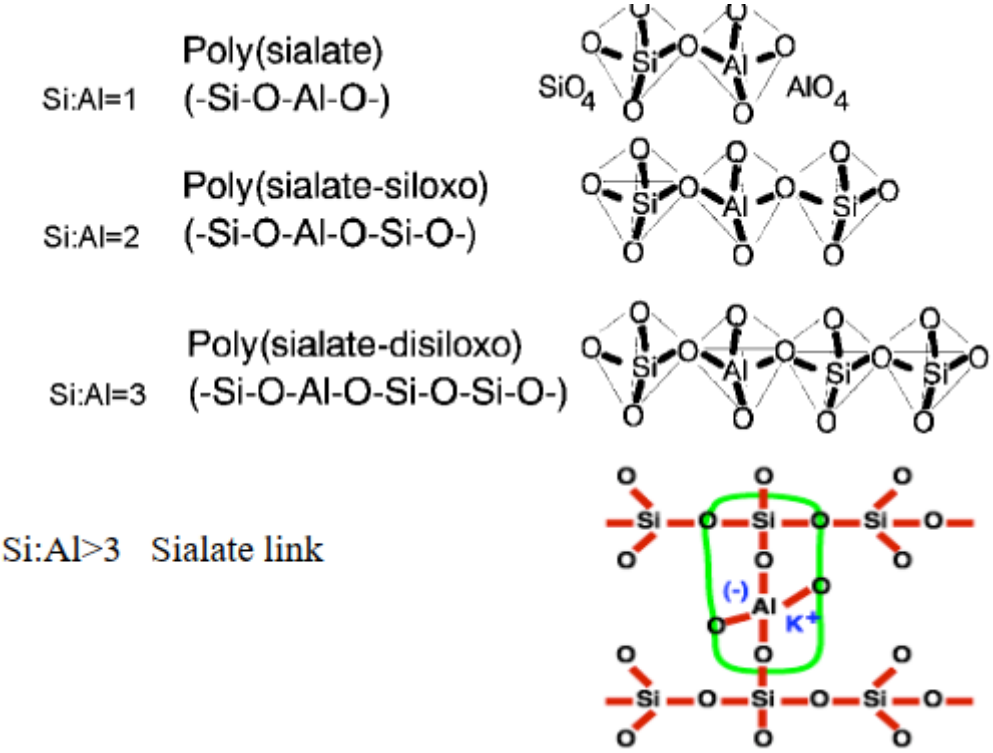

Sialate is an abbreviation for silicon-oxo-aluminate. Hardening of geopolymer occurs at a temperature below 100 °C or room temperature. The nature of geopolymer is amorphous under Bragg diffraction at ambient and medium temperature or crystalline at temperatures above 500 °C.

The mechanism of geopolymerization has been explained by some researchers. The geopolymerization process started with the dissolution of the solid aluminosilicate precursors by alkaline hydrolysis and produced the small reactive [SiO4]- and [AlO4]- tetrahedral units. These units are linked with each other by sharing oxygen atoms to form

polymeric bonds. The last step involves the polycondensation, where the geopolymer gel sets and forms a three-dimensional aluminosilicate network (Duxson et al., 2006; Hajimohammadi et al., 2010). Mabroum et al. summarized the general mechanism of geopolymerization schematically, as shown in Fig. 2.1 (Mabroum et al., 2020):

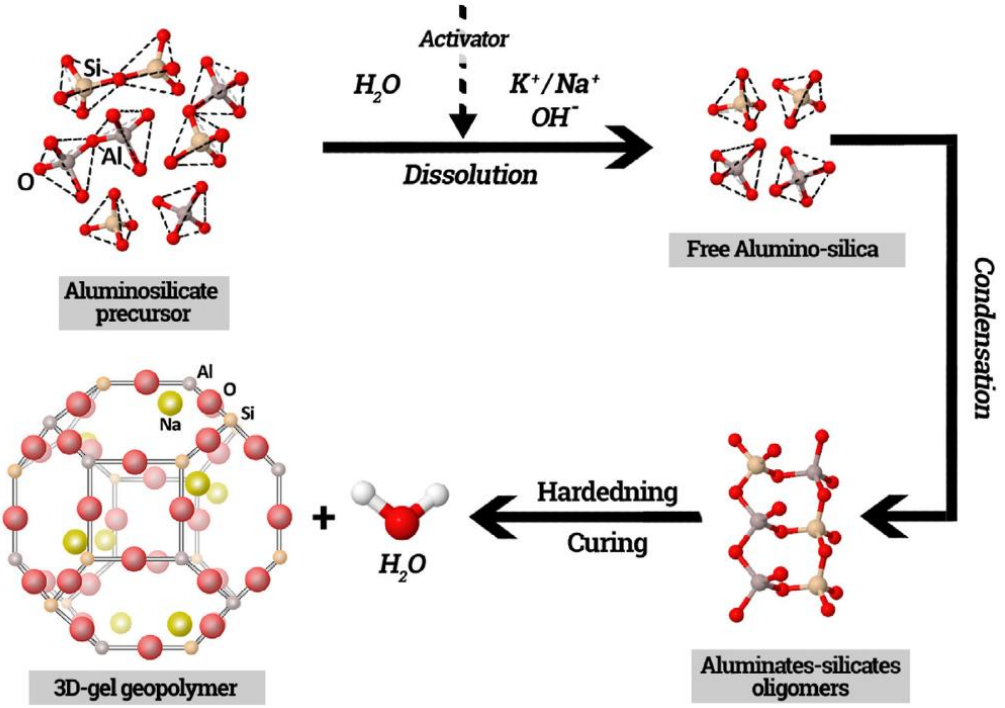

Figure 2.1 General mechanism of geopolymerization (Mabroum et al., 2020)

2.2.2 Aluminosilicate sources

AAMs and geopolymers can be produced from a wide range of aluminosilicate-rich mineral sources, such as metakaolin (Mikhailova and Rovnaník, 2016; Vlček et al., 2021; Zhang et al., 2016), industrial byproducts (Duxson et al., 2007b), and natural minerals (Nana et al., 2021). The utilization of byproducts, especially in concrete production, presents several environmental benefits such as reducing energy usage and greenhouse gas emission associated with Portland cement manufacture. Moreover, the industrial wastes may contain toxic chemicals and heavy metals; therefore, utilizing them in geopolymer can help to reduce

the environmental impact such as land pollution and groundwater contamination caused by their disposal.

a. Metakaolin

Metakaolin is produced by the calcination of kaolin at high temperatures, usually at a temperature ranging between 550 ℃ and 850 ℃ (He et al., 2016; Mo et al., 2014; Vlček et al., 2021). Kaolin composes of kaolinite, a clay mineral consisting of secondary minerals such as anatase, quartz, halloysite, and nacrite (Zain et al., 2017). Kaolin has a crystalline structure; thus it is a less reactive material. Kaolinite layers have hydrogen bonding between hydroxyl sites on the gibbsite basal plane and oxygens of the silicon tetrahedral sheet (Hu and Liu, 2003). To increase its reactivity, kaolin is calcinated to obtain amorphous metakaolin. During the calcination process at high temperature, the hydroxyl bound ions in kaolin are removed, resulting in disordered alumina and silica layers yielding highly reactive material. The main phase of metakaolin was amorphous with minor α-quartz (He et al., 2016). Metakaolin is an ideal solid for manufacturing geopolymers because it has a more consistent ratio of silicon to aluminium (Si/Al) compared to other aluminosilicate sources.

b. Fly ash

Fly ash is an industrial waste produced from the burning of coal in a boiler. Due to its pozzolanic activity, fly ash is commonly used as a partial replacement of OPC in concrete production. It is also the most common aluminosilicate source used to produce geopolymer. The reason lies in the fact that many industries and power plants use coal which generates huge amounts of ashes. The abundance of byproducts from the coal power plant is considered one of the environmental issues as it may contain toxic substances and heavy metals that can harm the ecosystem. The chemical composition and the properties of fly ash depend on the type of coal, combustion process, and efficiency of emission control devices.

The ASTM C168 has classified the fly ash type: Class C fly ash or high calcium fly ash, is produced from lignite or sub-bituminous coal, whereas class F fly ash or low-calcium fly ash is produced from anthracite or bituminous coal.

Wilczyńska-Michalik et al. study the importance of combustion technology on the composition of coal by-products including fly ash (Wilczyńska-Michalik et al., 2014). The ashes generated from two types of boilers, namely pulverized boiler (conventional) and hybrid boiler, are rich in glass and mullite but exhibit differences in their contents (silica and alumina content) and shapes. Fly ash from pulverized boilers mainly has a spherical aluminosilicate form, while fly ash from the hybrid boiler has lower aluminosilicate spheres. Different combustion process also affects the value of a loss on ignition (LOI). LOI is a measurement of unburnt carbon remaining in the ash.

The use of fly ash in concrete is beneficial in reducing the water demand and improving workability. In addition, a study by Saha (Saha, 2018) showed that the addition of class F fly ash (up to 40 wt%) as partial replacement of OPC reduced the porosity of the concrete; thus, fly ash concrete exhibited lower water sorptivity and chloride permeability. Moreover, the author found that the drying shrinkage was reduced with increasing fly ash content. Although fly ash is commonly used in geopolymer production, one factor limiting the use of fly ash geopolymer in construction is its low compressive strength. This is attributed to the low reactivity of fly ash; therefore, an initial heat curing is required to accelerate the geopolymerization process and gain higher compressive strength (Rickard et al., 2012).

c. Ground granulated blast-furnace slag (GGBS)

Blast-furnace slag is a byproduct of the iron and steel manufactory. It is removed from the top of molten iron during the extraction from the ore in a blast furnace (Yildirim and Prezzi,

2011). If the molten slag is cooled and solidified by rapid water quenching to a glassy state, no crystallization occurs, and granulated slag particles are obtained. When crushed or ground to very fine particles, ground granulated blast-furnace slag (GGBS) has cementitious properties, making it suitable as an admixture or partial substitution of Portland cement in concrete. Using GGBS in such an application reduces the energy demand that would be required for the calcination of limestone during the manufacturing process of cement. GGBS consists primarily of CaO, SiO_2, Al_2O_3, and Fe_2O_3 (Yildirim and Prezzi, 2011). The Fe_2O_3 content depends on the efficiency of the furnace. Other compounds, such as MgO may also be present as impurities.

The use of GGBS in fly ash-based geopolymer is crucial to eliminate the use of heat curing (Zannerni et al., 2020). Mixing fly ash and GGBS enables geopolymer cured at ambient temperature due to the increased amount of C-(A)-S-H (Saha and Rajasekaran, 2017). Fig. 2.2 presents the effect of GGBS addition on compressive strength in which the strength increased as the amount of GGBS increased (Saha and Rajasekaran, 2017). Similar to Portland cement paste, C-A-S-H of geopolymer significantly contributes to the formation of denser microstructure, hence high compressive strength is obtained. Moreover, in Fig. 2.2, the compressive strength is also affected by the molarity of the alkaline solution. Further explanation regarding the effect of alkaline solution on the properties of geopolymer is provided in the next section.

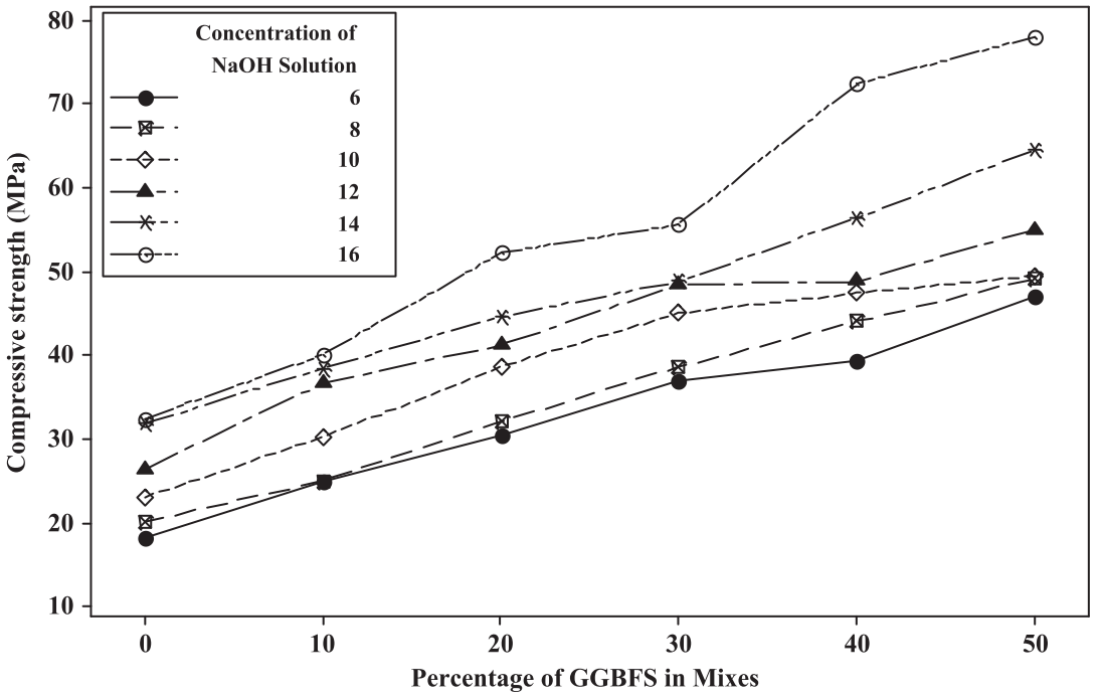

Figure 2.2 Effect of GGBS on compressive strength of geopolymer (Saha and Rajasekaran, 2017)

2.2.3 Alkaline solutions

As described in section 2.2.1, a chemical activator is required to initiate the geopolymerization reaction, mainly to dissolve the aluminosilicate precursors. The alkali hydroxides and alkali silicates commonly used as activators in geopolymer production are sodium and/or potassium. Sodium hydroxide is the most commonly used hydroxide activator because it is the cheapest and most widely available among other alkali hydroxides. Moreover, geopolymers prepared using NaOH solution present higher compressive strength compared to KOH-activated geopolymer, as shown in Fig. 2.3 (Okoye et al., 2015). However, the use of NaOH causes some problems, including the high tendency to efflorescence (formation of sodium carbonate in the surface), which is considered as a major factor limiting the extensive application of geopolymer.

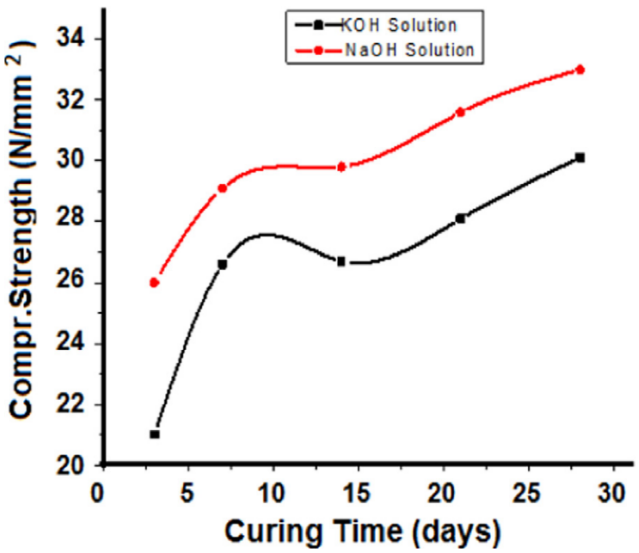

Figure 2.3 Compressive strength of geopolymer activated by KOH and NaOH (Okoye et al., 2015)

Geopolymer synthesized using potassium activator solutions has less unreacted aluminosilicate particle than sodium geopolymer, thus the efflorescence will be less in potassium-activated geopolymer. Potassium activating solutions have a higher pH than sodium solutions, thus promoting the dissolution faster, resulting in less unreacted materials (Duxson et al., 2005). However, the high cost of potassium hydroxide and potassium silicate makes the potassium activator solutions less favorable in the geopolymer for structural application.

The properties of geopolymer are also affected by the concentration of alkali solution. In a study by Saha and Rajasekaran (Saha and Rajasekaran, 2017), the compressive strength of geopolymer was found to be increased when the concentration of sodium hydroxide solution increased (see Fig. 2.2). This is attributed to the high concentration of sodium hydroxide solutions accelerating the dissolution of aluminosilicate sources and promoting the polycondensation.

2.2.4 Curing conditions

Curing condition is supposed to be another critical factor affecting the properties of reaction products of geopolymer. High-temperature curing is favorable but not necessary because elevating curing temperature will accelerate the geopolymerization reaction processes. Fly ash/slag blend geopolymer can set rapidly at ambient temperature; however, ambient-cured geopolymer suffers from severe efflorescence (more detail in the section for efflorescence). According to a study by Sajan et al. (Sajan et al., 2021), the optimum curing temperature for fly ash-based geopolymer is 60 ℃, at which the geopolymer samples exhibited the highest compressive strength of 36.21 MPa after 14 days curing as shown in Fig. 2.4.

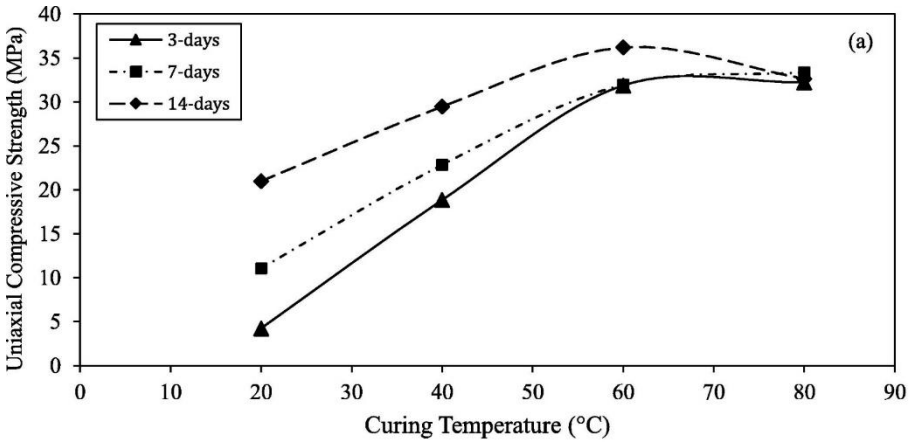

Figure 2.4 Influences of curing temperatures on the compressive strength (Sajan et al., 2021)

Lee et al. investigated the influence of sealed and unsealed curing on the compressive strength of geopolymer (Lee et al., 2016). The result shows that the compressive strength of sealed specimens is higher than that of unsealed specimens, as shown in Fig. 2.5. The lower strength of the unsealed specimen could probably be attributed to the loss of water that caused microcracking.

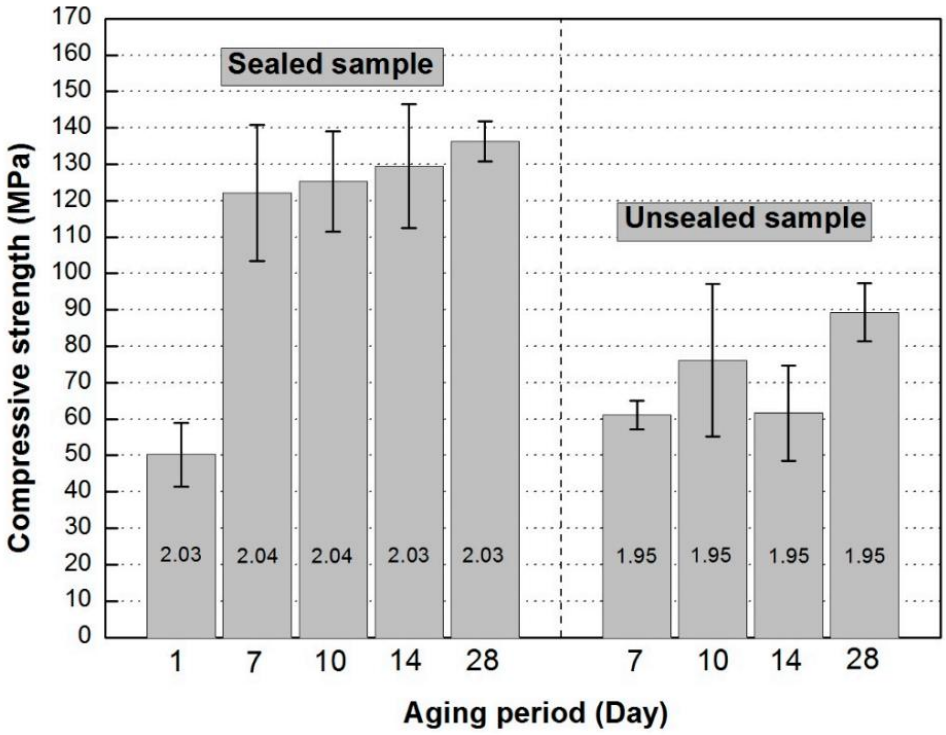

Figure 2.5 Compressive strength of sealed and unsealed geopolymer specimens (Lee et al., 2016)

2.3 Geopolymer Composites

As mentioned earlier, geopolymer presents ceramic-like properties, including brittle behavior and low flexural strength. Brittleness refers to the tendency of a material to fracture abruptly before significant plastic deformation occurs. In brittle materials, cracks propagate rapidly, resulting in low tensile strength. Flexural strength is an indirect way to measure tensile strength. High flexural strength is essential for stress-bearing restorations when high stress is applied on the materials. The high brittleness and low flexural strength of geopolymer have limited the application of this material in the construction industry.

2.3.1 Fiber-reinforced geopolymers

Similar to Portland cement concrete, the brittle behavior of geopolymer can be reduced by adding appropriate fiber reinforcement. Carbon fibers, in particular, have advantages over other types of fibers owing to their high modulus; thus, it is widely used in construction.

Therefore, incorporating carbon fiber in concrete attracts more and more attention as it can increase the flexural strength of concrete. Zhang et al. (H. Y. Zhang et al., 2014a) developed fiber-reinforced metakaolin/fly ash (MK/FA) based geopolymers for fire resistance application. The results showed that the addition of chopped carbon fibers (CF) improved the bending strength either at ambient temperature or under high temperatures but had no significant influence on compressive strength (see Fig. 2.6).

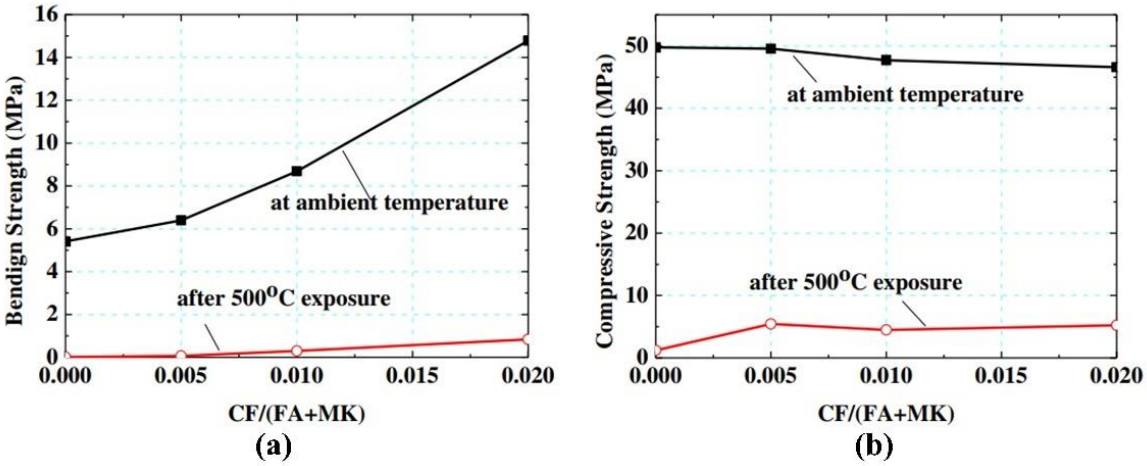

Figure 2.6 Effect of CF content on bending strength and compressive strength of geopolymers (H. Y. Zhang et al., 2014a)

Yan et al. (Yan et al., 2016) also used carbon fiber in their study and investigated its effect on the microstructure and mechanical strength of geopolymer produced from metakaolin and silica sol. The addition of carbon fiber remarkably improved the flexural strength of geopolymers. Lin et al. (Lin et al., 2008) pointed out the fiber size has a significant influence on the mechanical properties and fracture behavior of geopolymer. The lengths of the carbon fibers used in their study were 2, 7, and 12 mm. Geopolymer reinforced by carbon fibers of 7 mm in length shows a maximum flexural strength and the highest work of fracture (see Fig. 2.7), which are increased by 4.4 times and 118 times, respectively compared to the reference sample containing no fibers. This is attributed to the fiber bridging

and pulling-out. Further, they explained that longer fibers (12 mm) restrict deformation, while short fibers create friction due to the increased number of fiber ends.

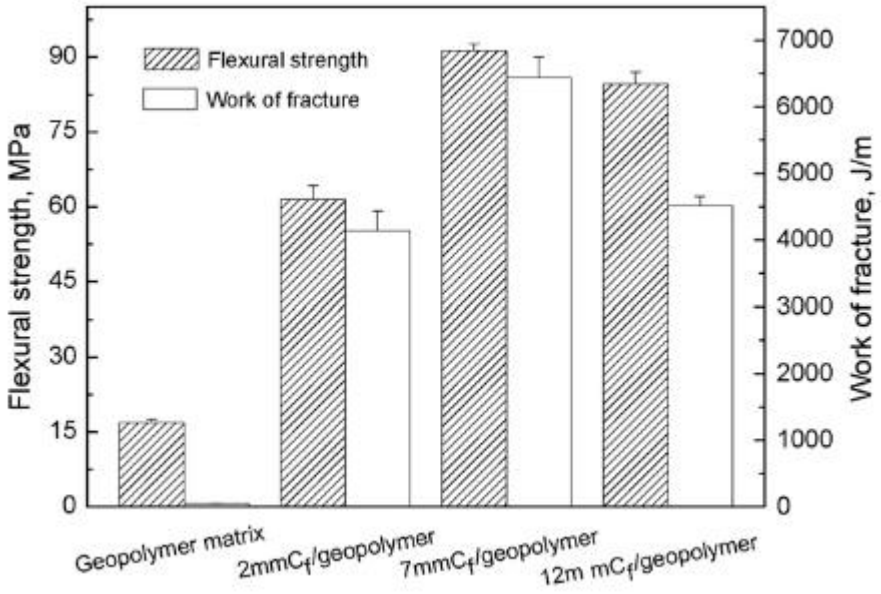

Figure 2.7 Flexural strength and work of fracture of geopolymer and geopolymer composite under various fiber length (Lin et al., 2008)

2.3.2 Epoxy resin-reinforced geopolymers

Although incorporating carbon fiber could significantly improve the flexural strength of geopolymer as shown in the previous section, it adversely affects the compressive strength (Payakaniti et al., 2018) due to the incompatibility between the fibers and geopolymer matrix. The incorporation of organic resin appears to be an effective way to improve flexural and compressive strength. The excellent compatibility between the geopolymer matrix and the resin can be achieved even without using compatibilizers (Colangelo et al., 2013; Roviello et al., 2013).

Zhang et al. (Zhang et al., 2012) developed a geopolymer composite reinforced by resin and investigated the effect of high temperature on the mechanical properties of the synthesized specimens. Incorporating a small amount of resin (1 wt%) could improve the compressive strength and flexural strength of geopolymer, as shown in Fig. 2.8. Although

epoxy resin is a flammable polymer, it did not negatively affect the resistance of geopolymer at high temperatures.

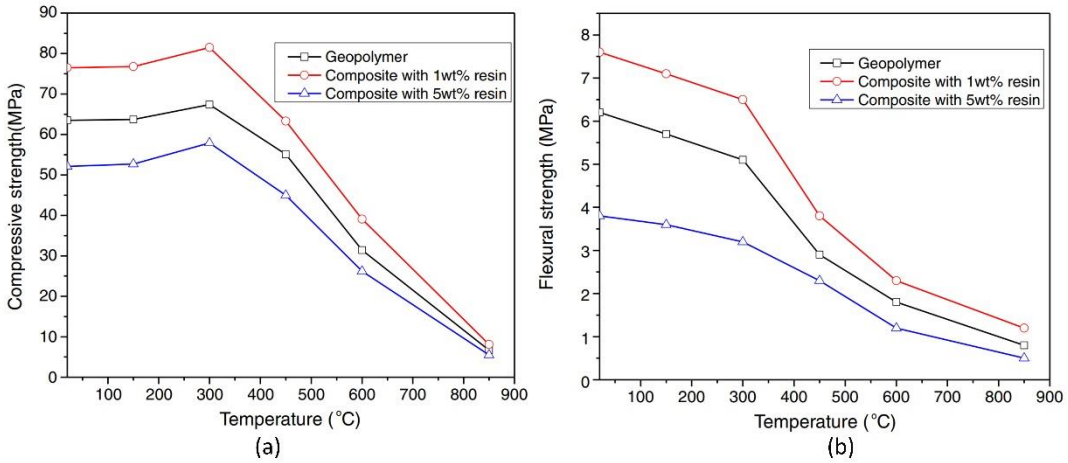

Figure 2.8 Compressive strength (a) and flexural strength (b) of geopolymer and geopolymer composite as a function of temperatures (Zhang et al., 2012)

2.4 Fire Resistance of Geopolymer

Many researchers agree that geopolymers present better resistance to fire compared to Portland cement. Although concrete is a non-combustible material, the fire behavior of concrete has attracted great attention because of the tendency to suffer thermally explosive spalling and strength loss during and after fire exposure. The effect of fire on the mechanical properties of Portland cement concrete depends on the properties of the concrete constituents, exposure temperature (Alonso and Fernandez, 2004), external loadings, and cooling rates. The major changes occur due to the decomposition of C-S-H and portlandite. During heating, the C-S-H gel loses water molecules and OH^- groups from the interlayer space. The dehydration of C-S-H occurs at a temperature ranging from 105 to 1000 ℃, while the temperature range for CH dehydration is about 400 to 550 ℃ (Khoury et al., 2002). Tantawy (Tantawy, 2017) investigated the effect of high temperatures on the microstructure of cement paste and revealed that beyond 450 ℃, the percentage of portlandite sharply diminished and

C-S-H decomposed into C_2S and C_3S, as shown in Fig. 2.9. Furthermore, the author observed the propagation of harmful cracks and increased total porosity, resulting in severe mechanical strength loss, as shown in Fig. 2.10 (Tantawy, 2017).

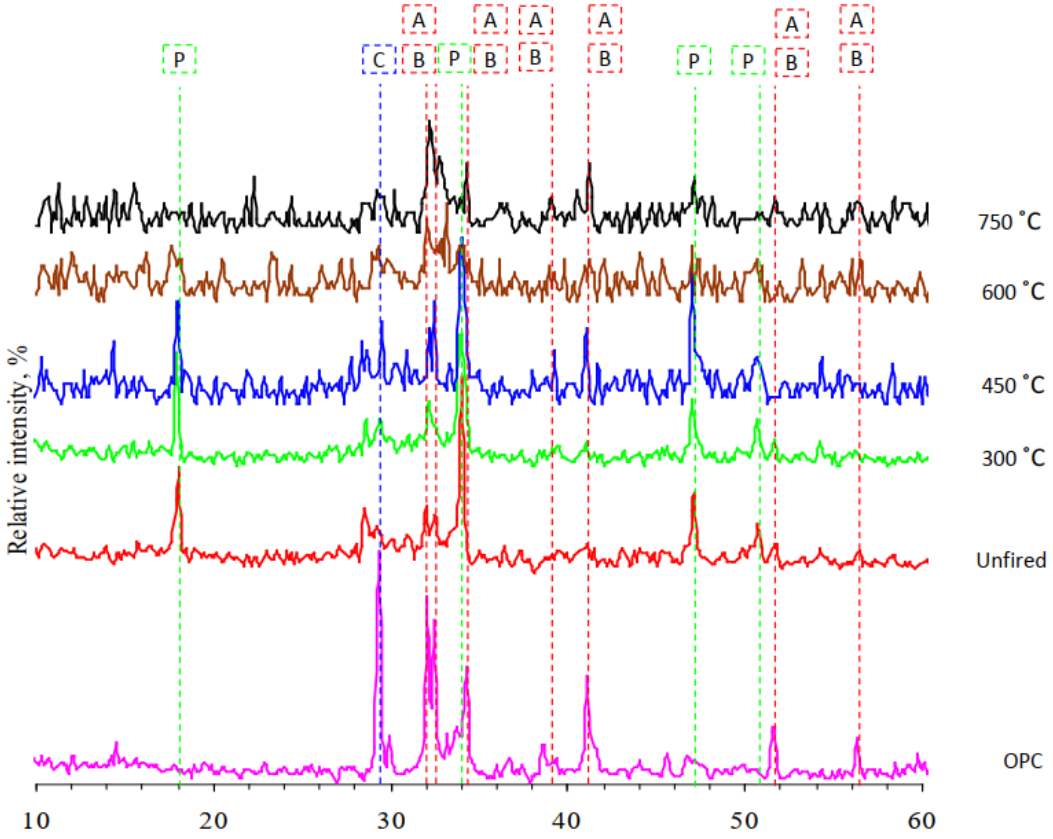

Figure 2.9 XRD patterns of cement exposed at 300 – 750 °C. (A: alite, B: belite, C: calcite, and P: portlandite) (Tantawy, 2017)

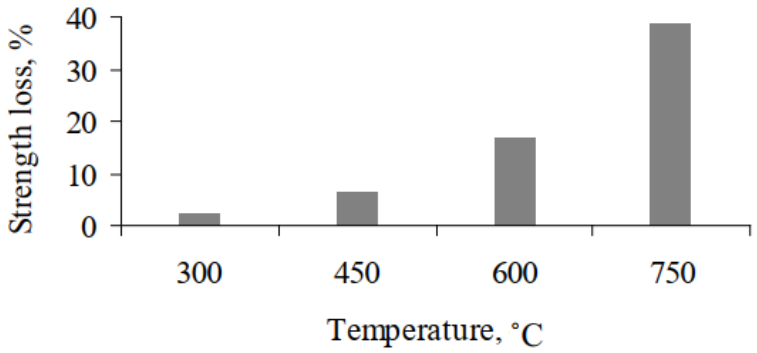

Figure 2.10 Strength loss of cement paste exposed to high temperatures (Tantawy, 2017)

Geopolymers are made of an amorphous aluminosilicate matrix; therefore the durability of geopolymer is expected to be different from that of OPC. The heat resistance of geopolymers is significantly higher than that of OPC, with very little structural damage observed up to 1000 ℃ (Davidovits, 2017; Rickard et al., 2012). When exposed to high temperatures, geopolymer undergoes thermal expansion or thermal shrinkage, causing macroscopic cracks. However, it should be noted that geopolymer materials possess better fire resistance compared to OPC due to their ceramic-like properties. At high temperatures, dehydration does not cause significant changes in the geopolymer structures, making the geopolymers exhibit high thermal stability.

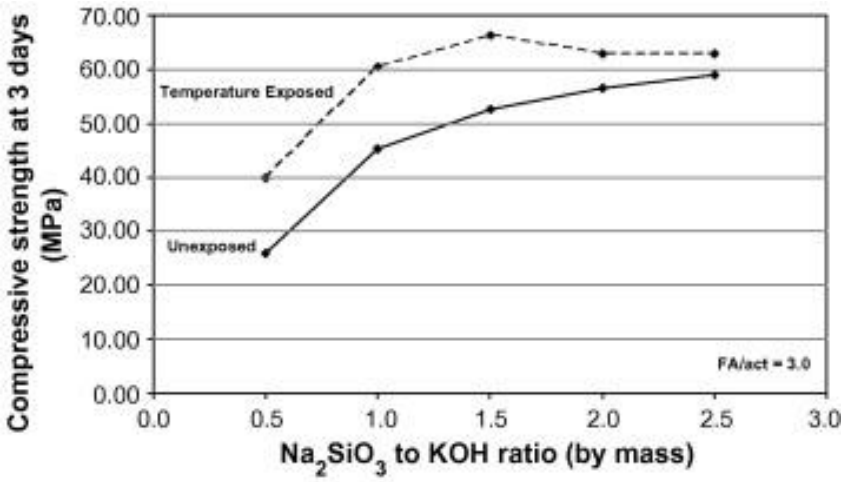

Figure 2.11 Effect of sodium silicate-to-potassium hydroxide ratio on compressive strength (Kong and Sanjayan, 2008)

Unlike Portland cement paste, some geopolymers have been observed to increase the compressive strength after elevated temperature exposure (Kong and Sanjayan, 2008; Lahoti et al., 2018). This is attributed to the alkali cations used that influence the fire resistance of geopolymer. Kong and Sanjayan (Kong and Sanjayan, 2008) produced fly ash geopolymer composites and varying sodium silicate solution to potassium hydroxide solution (Na_2SiO_3/KOH) ratio ranging from 0.5 to 2.5 and heated them to 800 ℃. The results showed that the compressive strength was significantly improved as the ratio increased (see

Fig. 2.11). Interestingly, the compressive strength of exposed specimens was higher than that of unexposed ones.

A similar result was shown by the study of Lahoti et al. (Lahoti et al., 2018), which observed the strength enhancement of K-geopolymer after exposure to high temperatures, while Na-geopolymer exhibited a reduction in strength (see Fig. 2.12). This increase was attributed to the low diffusion coefficient of K^+ at high temperatures, resulting in a higher melting temperature of geopolymer.

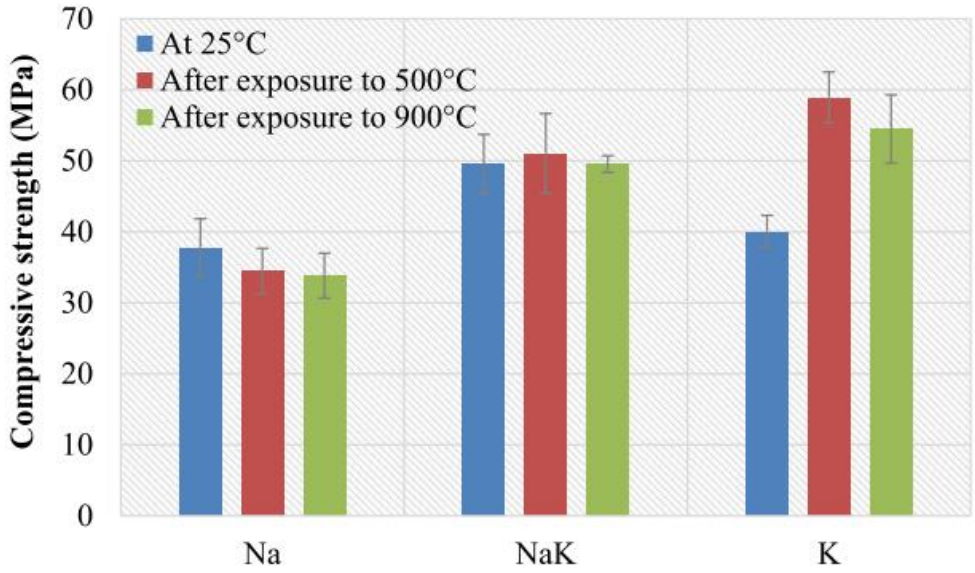

Figure 2.12 Compressive strength of geopolymer at ambient temperature and after exposure (Lahoti et al., 2018)

2.5 Efflorescence in Alkali Activated Materials

Efflorescence is a phenomenon that describes the deposits of crystalline salt on the surface of building materials such as bricks, concretes, and masonries. In normal mortars or concretes, efflorescence is not expansive and can be washed out easily, but it is aesthetically undesirable. It is caused by the migration of salt to the surface of porous materials. Efflorescence on masonries and mortars is generally formed by carbonates or sulfates. In

this case, the presence of water is essential because the water will dissolve the salts, as well as transport them to the surface.

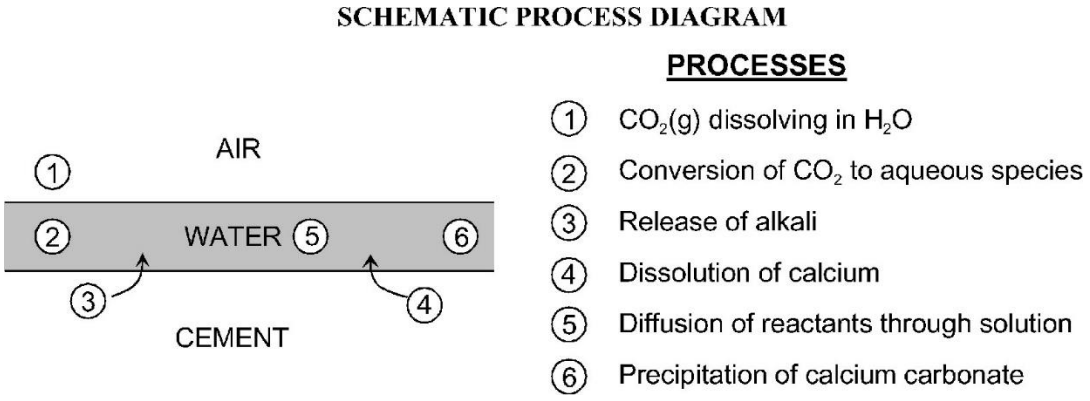

Figure 2.13 Schematic process of efflorescence in cement-based materials (Dow and Glasser, 2003)

According to the study by Dow and Glasser, efflorescence is controlled by six processes, as shown in Fig. 2.13 (Dow and Glasser, 2003). The first step of efflorescence occurs when the CO_2 from the atmosphere is dissolved in H_2O and converted to aqueous species. In the following process, the cement will release alkalis, and the constituent such as calcium hydroxide will be dissolved and react with aqueous species containing CO_2. Finally, the dissolved compound will diffuse through the thin solution layer and precipitate on the surface as calcium carbonate. The alkalis released from cement will promote the formation of efflorescence. The presence of soluble alkali increases the solubility of $Ca(OH)_2$, but the alkalis themselves are not constituents of efflorescence deposits. Therefore, cement with low-alkali is preferred to prevent severe efflorescence.

Efflorescence has been considered a major issue in the application of AAMs and geopolymers. Efflorescence reactions in AAMs and geopolymers are different from those occur in Portland cement-based materials. In AAMs, the efflorescence tends to occur due to the high concentration of alkali solutions used in the mixtures. As mentioned earlier, even

though OPC releases some alkalis, they are not the constituent of efflorescence deposit, while in geopolymers, the final product of efflorescence is mainly hydrated sodium carbonate as observed by XRD analysis (see Fig. 2.14), which is formed by the following chemical reactions (Zhang et al., 2018):

$$CO_2\,(g) + 2OH^-\,(aq) \longrightarrow CO_3^{2-}(aq) + H_2O$$

$$2\,Na^+\,(aq) + {CO_3}^{2-}\,(aq) + n\,H_2O \longrightarrow Na_2CO_3 \cdot nH_2O\,(s)$$

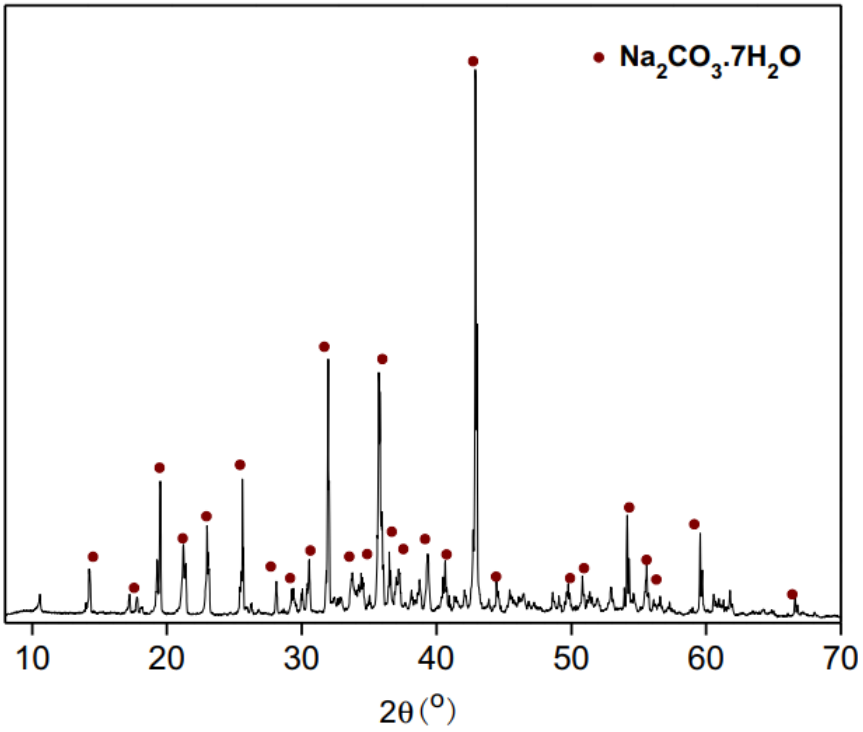

Figure 2.14 XRD pattern of efflorescence product scraped from the surface of geopolymer (Z. Zhang et al., 2014)

AAMs and geopolymers contain much higher soluble alkali concentrations than conventional cement, thus efflorescence can be more severe in these materials.

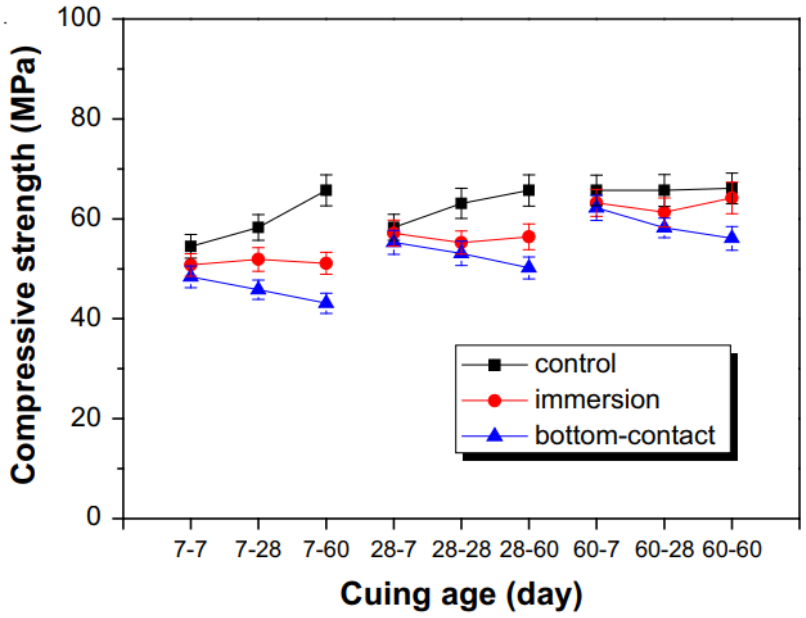

Figure 2.15 Compressive strengths of alkali-activated materials made fly ash/slag = 1 (Yao et al., 2016)

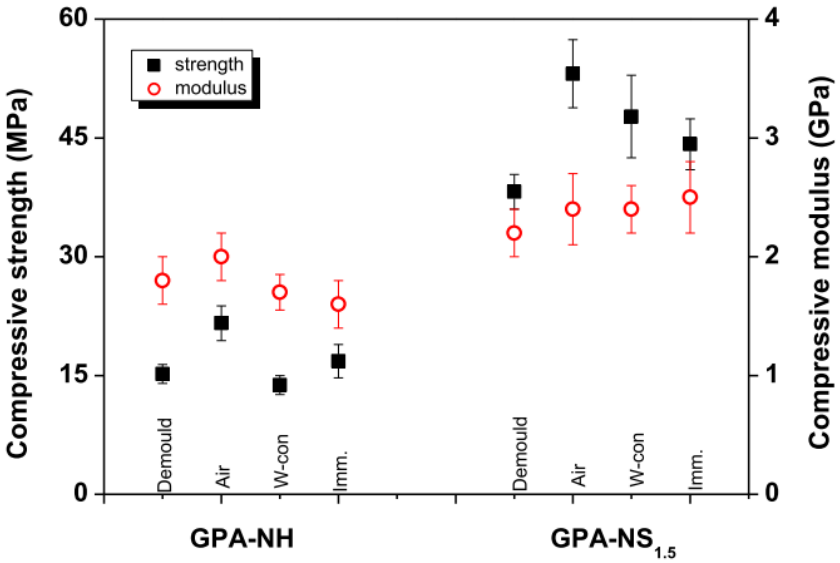

Figure 2.16 Compressive strength and modulus of geopolymer on demoulding, and after ageing under three conditions (Zhang et al., 2018).

Unlike in cement, the efflorescence in alkali-activated materials can be structurally harmful as it can cause degradation on mechanical strength (Yao et al., 2016; Zhang et al., 2018). The negative effect of efflorescence in AAMs is a combination of multiple factors,

mainly loss of alkalis and subflorescence. Yao et al. observed the gradual degradation of compressive strength of binders with bottom in contact with water, while air-cured binders continuously gain strength, as shown in Fig. 2.15 (Yao et al., 2016). Zhang et al. observed that the fully immersed samples show much less increase in compressive strength (see Fig. 2.16) due to the loss of alkalis into the water, while samples under simulated efflorescence gain strength but very limited extent (Zhang et al., 2018). This strength degradation is mainly caused by the formation of carbonate crystals within the pores or beneath the surface that damage the microstructure. In this case, the precipitation is called subflorescence. When AAM is in contact with water, subflorescence will occur when the free alkalis react with the CO_3^{2-} absorbed from the atmosphere. Subflorescence will generate a crystallization pressure; therefore, the damage of the matrix will depend on the magnitude of this pressure. Subflorescence can cause cracking and spalling if the crystallization pressure exceeds the tensile strength.

The mechanical properties of AAMs are strongly influenced by the concentration of alkali solution used in their production. Thus, the AAMs can contain 10-20 times higher alkali content than in Portland cement. However, alkali concentration becomes one of the major factors that influence the efflorescence formation in AAMs. According to Skavara et al., these alkalis are weakly bound in the structure and can readily leach into the water (Škvára et al., 2012). Therefore, the weak bond of alkalis becomes the primary cause of efflorescence formation in AAMs.

Several attempts have been made to reduce the efflorescence potential in AAMs. Najafi Kani et al. (Najafi Kani et al., 2012) reported that the use of alumina-rich cement admixtures could reduce the efflorescence in geopolymers. Zhang et al. (Z. Zhang et al., 2014) stated in their study that the efflorescence of geopolymer is strongly dependent on the type of alkali solutions, curing temperature, and the addition of slag (see Fig. 2.17). In

general, alkali silicate activator is more favorable than alkali hydroxide for achieving high compressive strength; however, in their study, ambient-cured specimens prepared using sodium silicate show more intense efflorescence deposits compared to specimens prepared using sodium hydroxide. Geopolymers cured at low temperature (23 ℃) exhibit rapid efflorescence compared to those hydrothermally cured at 80 ℃. Specimen containing 20% slag cured in both ambient and high temperature do not show any efflorescence deposit compared to those made from fly ash only.

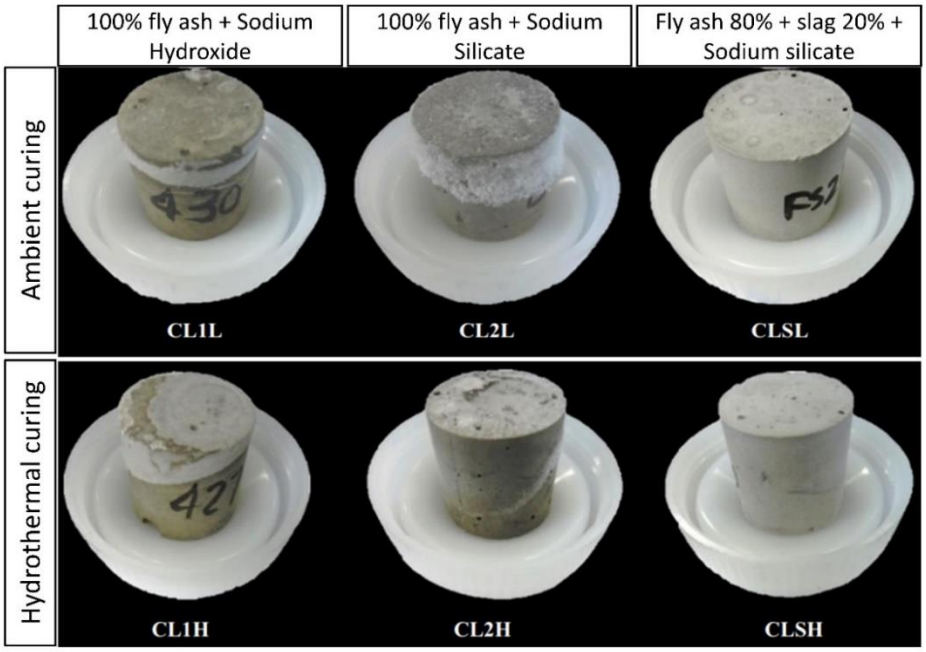

Figure 2.17 Efflorescence of ambient and hydrothermal-cured geopolymer after 24 h with the bottom in contact with water (Z. Zhang et al., 2014)

The effect of slag addition on the efflorescence of geopolymers is more related to the reduction in porosity and permeability rather than binding of alkalis. However, Yao et al. (Yao et al., 2016) found that when adding slag higher than 50%, the binders show more rapid efflorescence compared to that containing fly ash only. This finding makes the porosity a less important factor influencing the efflorescence because the higher the amount of slag, the lower the porosity is. This is probably attributed to the increasing amount of slag

increasing the formation of C-(A)-S-H gel, which has lower alkali binding property compared to N-A-S-H.

2.6 Application of AAMs and Geopolymers

The need to conserve our environment has become crucial due to the issues of climate change and global warming that have had observable effects on the environment. The largest driver of these environmental issues is the emission of gases that create a greenhouse effect such as CO_2 and methane. Due to the high CO_2 emission generated from cement industries, the primary area of application of AAMs and geopolymers is currently in the development of low-carbon construction materials as an alternative to Portland cement.

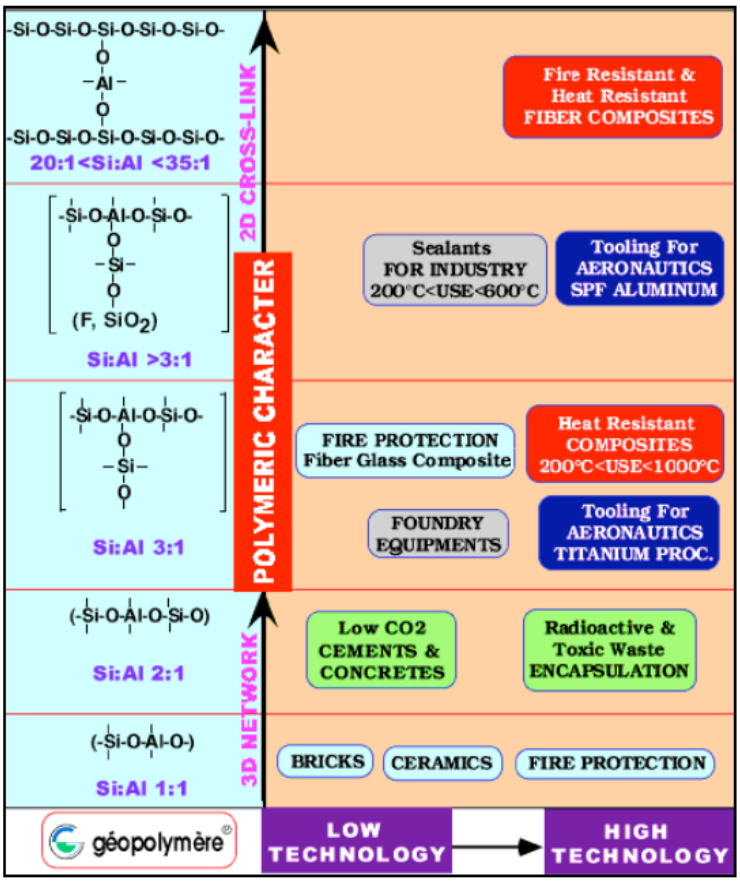

Figure 2.18 Geopolymer types involved in successful applications (Davidovits, 2002).

Davidovits summarized other successful applications of geopolymers including a low-temperature ceramic, refractory, fireproof for high-tech applications, sealants for industries, radioactive and toxic waste encapsulation, as shown in Fig. 2.18 (Davidovits, 2002).

CHAPTER 3. MATERIALS AND METHODS

3.1 Materials

3.1.1 Aluminosilicate precursors

This study utilized fly ash, ground granulated blast-furnace slag (GGBS), and silica fume (SF) to produce geopolymer and alkali-activated slag. The fly ash used is low-calcium fly ash, whereas GGBS consists of a significantly high amount of calcium. The physical and chemical properties are listed in Tables 3.1 and 3.2, respectively. The XRD patterns of each material are shown in Fig. 3.1. The XRD pattern of fly ash shows some crystalline peaks of mullite and quartz, while GGBS and silica fume show amorphous phases. The low-intensity peak of magnetite (Fe_3O_4) was observed in SF due to the iron source added during smelting in the furnace.

Table 3.1 Physical properties of raw materials

Materials	Blaine fineness (cm^2/g)	Density (g/cm^3)	Standard	Amorphous content (%)
Fly ash	3550	2.24	JIS A 6201	78.26
GGBS	4170	2.91	JIS A 6206	>90
SF	16300	2.25	JIS A 6207	>90

Table 3.2 Chemical compositions of raw materials

Component (mass%)	SiO_2	Al_2O_3	Fe_2O_3	CaO	K_2O	TiO_2	MgO	Na_2O	SO_3	P_2O_5	LOI
Fly ash	68.44	20.65	4.18	2.25	1.53	1.19	0.58	N/A	0.52	0.30	2.90
GGBS	35.45	14.06	0.27	43.78	0.23	0.56	5.84	0.24	0.62	0.01	0.05
SF	96.12	0.73	1.40	0.27	0.74	N/A	0.42	N/A	0.20	N/A	1.68

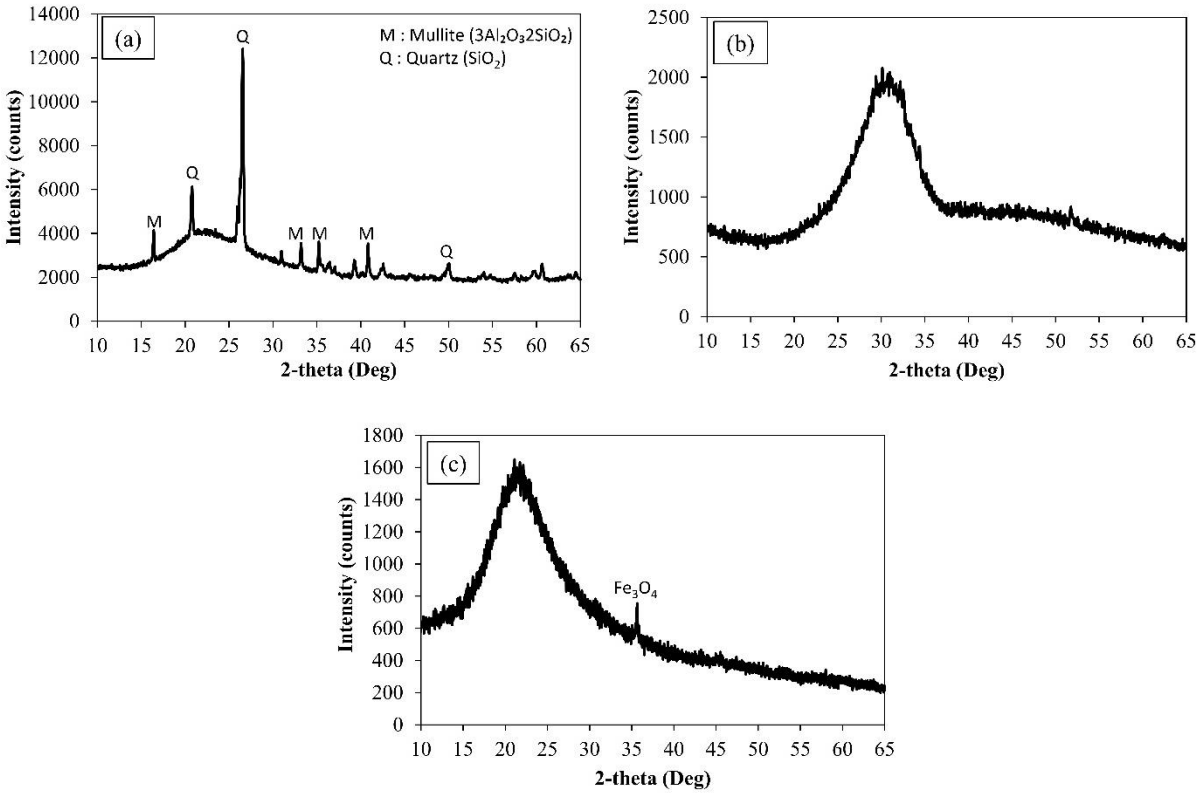

Figure 3.1 XRD patterns of raw materials: fly ash (a), GGBS (b), and silica fume (c).

3.1.2 Alkaline solutions

The alkaline solutions employed in this study were the combination of water glass (sodium silicate) and sodium hydroxide (NaOH) solution, and the combination of water glass with potassium hydroxide (KOH) solution. Sodium silicate (Na_2SiO_3) solution, KOH pellets, and NaOH pellets were purchased from Sigma Aldrich. NaOH solution was prepared in 14 M by dissolving 560 grams NaOH pellets in water to form one liter solution. Meanwhile, 14 M KOH was also prepared by dissolving 784 grams KOH pellets in water to form one liter solution.

3.1.3 Epoxy resin

Epoxy is in a family of thermosetting resin. Thermosetting refers to irreversible property. Once cured and hardened, epoxy cannot melt back because of the cross-linking. Epoxy resin

is widely used as adhesives and coatings, but recently it is also used for concrete repair. Among these thermosetting materials, bisphenol A (BPA) epoxy resin and bisphenol F (BPF) epoxy resin are commonly used in civil engineering fields.

In this study, BPF epoxy resin was used to produce geopolymer composite. BPF epoxy resin has a lower viscosity than BPA epoxy resin, making it easy to incorporate with other materials. Epoxy resin was prepared by mixing commercially available bisphenol F epoxy resin with imidazole (1-isobutyl-2-methyl imidazole) curing agent with the resin to curing agent ratio of 2.5 by mass and cured at 60 ℃ for at least 30 min or until the color switched from white to light yellow. The structural formula of bisphenol F epoxy resin and imidazole are shown in Fig. 3.2 and Fig. 3.3, respectively.

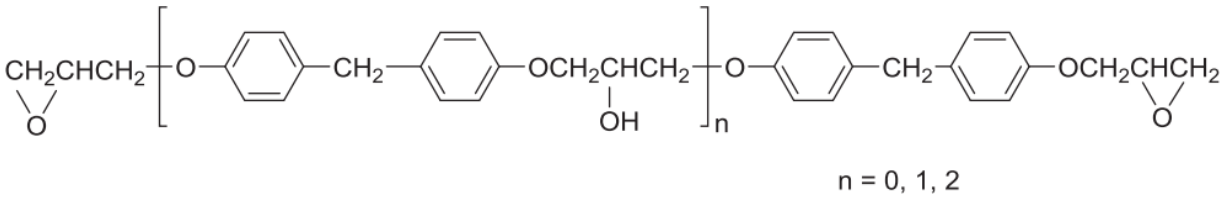

Figure 3.2 Structural formula of bisphenol F epoxy resin (Ji et al., 2017)

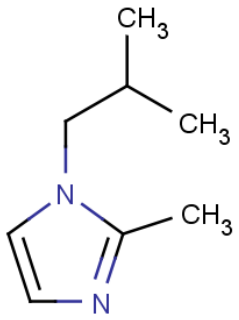

Figure 3.3 Structural formula of imidazole

3.2 Mix Design and Synthesis Procedures

3.2.1 Fly ash/GGBS-based geopolymer

Table 3.3 shows the mix proportion of fly ash/GGBS geopolymer blends. Slag was used to partially replace fly ash at percentages of 0, 15, 30, 45, and 60% because the inclusion of slag can improve the microstructure and compressive strength, as explained in the previous chapter. However, the high content of calcium makes it necessary to investigate the fire resistance of the fly ash/slag geopolymer since the inclusion of slag produces more C-(A)-S-H, which is thermally unstable.

Table 3.3 Mix proportion of fly ash/GGBS-based geopolymer

Sample ID	**Fly ash (g)**	**GGBS (g)**	**Alkali solution/ binder ratio**	**Na_2SiO_3/ NaOH**	**Na_2SiO_3 solution (g)**	**NaOH solution (g)**	**KOH solution (g)**
FAS0	700	0	0.52	1.35	210	156	0
FAS15	595	105	0.52	1.35	210	156	0
FAS30	490	210	0.52	1.35	210	156	0
FAS45	385	315	0.52	1.35	210	156	0
FAS45 (K-Geo)	385	315	0.52	0	210	0	156
FAS60	280	420	0.52	1.35	210	156	0

The geopolymer paste specimens were synthesized as follows: fly ash and GGBS were first dry-mixed together in a pan mixer. The sodium silicate and sodium hydroxide solutions were added and mixed with the solid materials rapidly to form the fresh geopolymer paste. The paste mixture was cast into cylindrical plastic molds (ϕ50 mm × 100 mm), hand-compacting, and sealed with thin plastic layers to minimize the water evaporation. After casting, the specimens were initially heated in a chamber at 70 ℃ for 24 hours and were left at room temperature (approx. 20 ℃). The specimens were demolded at the age of 3 days and stored at room temperature until the age of 28 days.

3.2.2 Epoxy resin-reinforced geopolymer composite

Table 3.4 shows the mix proportion of geopolymer composite. Geopolymer (55% fly ash and 45% GGBS) containing no epoxy resin was used as a reference. The alkaline liquid to binder (l/b) ratio and the sodium silicate to sodium hydroxide (SS/SH) ratio were maintained at constant values of 0.52 and 1.35 by mass, respectively. Geopolymer composites were prepared by adding the resin into the freshly-prepared geopolymer slurry and quickly incorporated by mechanical mixing (see Fig. 3.4 for synthesis pathways). After rapidly mixing, a part of the above mixture was poured into cylindrical plastic molds (ϕ50 x 100 mm), and the rest was cast in prismatic molds (40 × 40 × 160 mm). The top of the molds was sealed with a thin plastic layer to prevent the evaporation of water. Subsequently, some specimens were cured in an oven at 70 ℃ for 24 h to accelerate the gel formation, while others were left at ambient temperature (approx. 20 ℃). All specimens were demolded at the age of 3 days. To observe the water resistance, after demolding, some ambient-cured specimens were fully immersed in water (approx. 20 ℃) until testing days, while some were stored in a plastic bag to prevent carbonation and alkalinity loss prior to the measurements (see Fig. 3.5 for curing diagram).

Table 3.4 Mix proportion of geopolymer composite

Sample ID	Fly ash (g)	GGBS (g)	BPF Epoxy resin (g)	l/b	SS/SH ratio	SS (g)	SH (g)
FAS45 (Ref.)	385	315	0	0.52	1.35	210	156
BPF1	385	315	7 (1 mass%)	0.52	1.35	210	156
BPF2.5	385	315	17.5 (2.5 mass%)	0.52	1.35	210	156

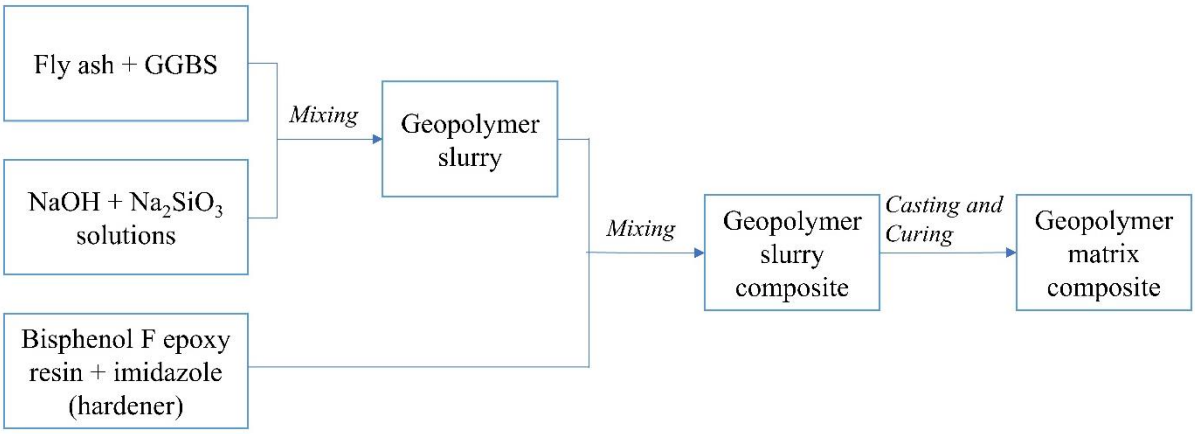

Figure 3.4 Synthesis pathways of geopolymer and geopolymer composite

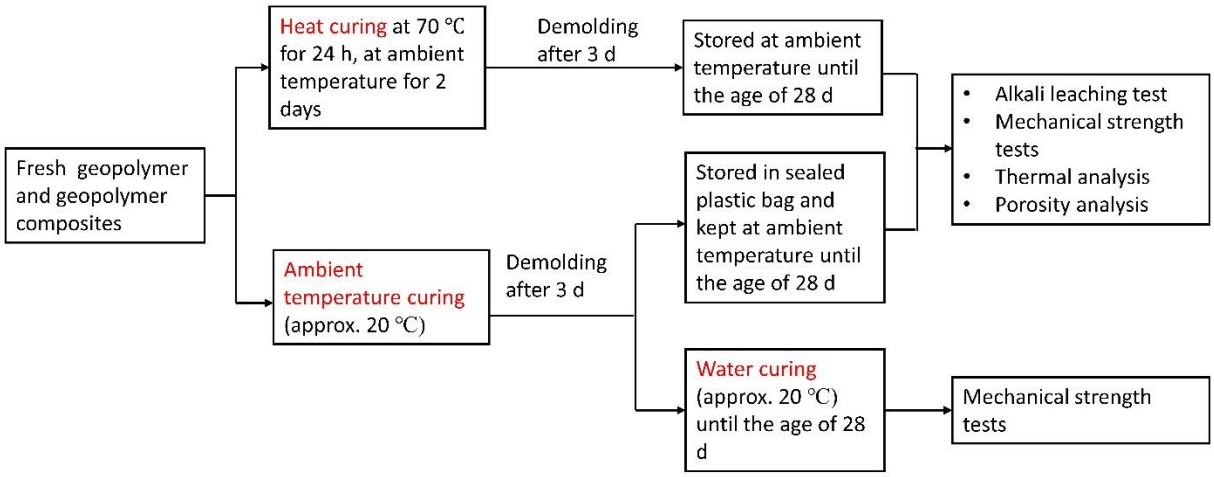

Figure 3.5 Curing diagram for geopolymer composites

3.2.3 Alkali-activated slag incorporating silica fume

Alkali-activated slag (AAS) specimens were prepared with a mix proportion listed in Table 3.5. The amount of silica fume varies as 0, 5, 10, and 15% of the total binder by mass. The alkali solutions and synthesis procedures were similar to those of geopolymer described in section 3.2.1. The fresh paste was cast into plastic bottles with a dimension of approx. 23 mm in diameter and 20 mm in height. After casting, all specimens were cured at 20 °C and demolded after 3 days. After demolding, all specimens were sealed in a plastic bag to prevent carbonation and alkalinity loss before testing at the age of 28 days.

Table 3.5 Mix proportion of alkali-activated slag incorporating silica fume

Specimens	Variables			
	l/b ratio	SS/SH	Slag [%]	SF [%]
BFS-SF0	0.52	1.35	100	0
BFS-SF5	0.52	1.35	95	5
BFS-SF10	0.52	1.35	90	10
BFS-SF15	0.52	1.35	85	15

3.3 Durability Test

3.3.1 Fire resistance test

At the age of 28 days, the prepared geopolymer paste specimens were weighed and were subjected to temperatures of 500, 750, and 950 ℃ with a heating rate of 20 ℃/min. When the target temperature was attained, it was maintained for an additional 1 hour before the furnace was shut down to allow the specimens to cool down to room temperature (see Fig. 3.6). The cooling usually takes 5 to 10 hours, depending on the target temperature (the higher the target temperature, the longer the cooling hours). After cooling down, the exposed specimens were weighed, and the mass was compared to that before exposure.

The test method was adopted from a previous study by Abdulkareem et al., but they used much lower heating rate of 4.4 ℃/min (Abdulkareem et al., 2014). This study used a higher heating rate because in actual case of fire, the temperature of fire can reach 1000 ℃ in less than one hour.

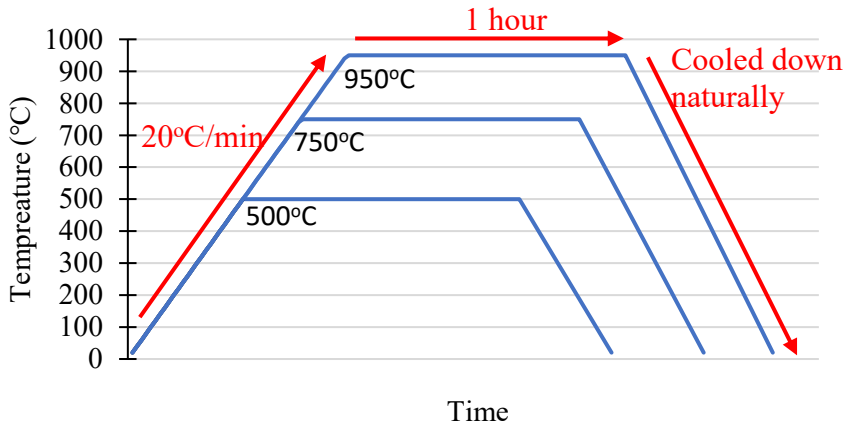

Figure 3.6 Heating regime

3.3.2 Alkali leaching test

In geopolymers and alkali-activated materials, alkali leaching has been considered one of the major issues because it is responsible for the efflorescence formation. An immersion test was performed to investigate the alkali leaching by fracturing the 28d-aged samples into the size between 2.36 and 4.75 mm and immersing them in distilled water with a solid to liquid ratio of 1:20; sealed and stored the samples at room temperature (20 ℃). The method was adopted from a study by Zhang et al. (Z. Zhang et al., 2014) with some modifications. The measurement periods were 3 h, 24 h, 3 d, 7 d, 14 d, and 28 d. The total leaching amount of sodium was calculated from the change from the initial amount of sodium in the samples measured by energy dispersive X-ray spectroscopy (EDS) to the amount of sodium in water after 28 d immersion.

3.3.3 Accelerated efflorescence test

The efflorescence formation on alkali-activated slag was investigated by partly immersing the cylindrical specimens in water individually (Z. Zhang et al., 2014), as shown in Fig. 3.7, and kept at the room temperature of 20 ℃ for 72 h. The photographs of specimens were taken at 24 h and 72 h after starting the efflorescence test.

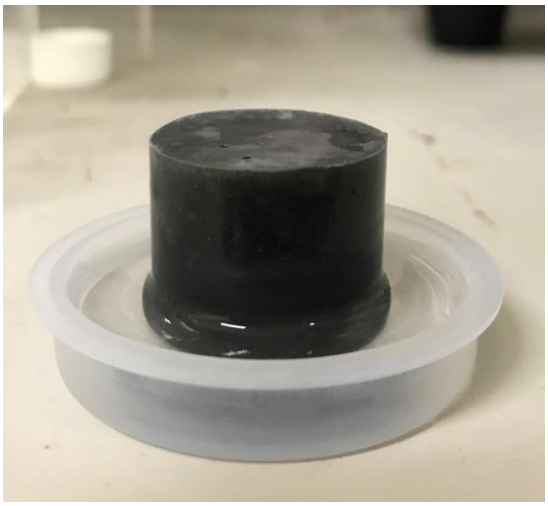

Figure 3.7 Accelerated efflorescence test on alkali-activated slag specimen

3.4 Characterizations and Measurements

3.4.1 Thermal analysis by TG-DTA

Thermogravimetric and differential thermal analysis (TG-DTA) is a useful technique to determine the thermal stability and compositions of materials. TG measures the changes in the mass of material as a function of temperature. It is most useful for dehydration, decomposition, desorption, and oxidation process. Dehydration and decomposition reactions will occur at various temperatures depending on the composition of the material.

DTA can be used to identify the chemical composition of a substance by observing the thermal behavior of a sample during heating. The term differential is used because the change in the sample is compared with standard reference material. The combination of TG and DTA yields a more straightforward interpretation than interpretation with either technique alone.

In this study, TG-DTA was performed on the powder samples. It was used to measure the mass change of sample as a function of temperature (TG), and to identify the events (exothermic or endothermic) that cause such changes. The measurement was carried out

using Simultaneous DTA-TG apparatus DTG-60H and DTG-60 with a heating rate of 20 ℃/min in air from room temperature to 1000 ℃.

3.4.2 Phase composition analysis by XRD

X-ray diffraction (XRD) is a non-destructive technique used to determine the nature of materials (crystalline or amorphous). It is also widely used for the phase identification of cement and its reaction products. Since the diffraction pattern of every material differs from each other, the materials and compounds are identified by using a database of diffraction patterns. Peak represents a lattice plane that can be characterized by the Miller index. In order for an X-ray to diffract, the sample must be crystalline, and interplanar spacing must be close to the radiation wavelength. The diffraction peak can be obtained if it follows Bragg's law. This law describes the relationship between the wavelength of incident X-ray, angle of incidence, and spacing between the crystal lattice planes of atoms expressed as:

$$n\lambda = 2dsin\theta$$

The diffraction pattern plots intensity against the angle of detector, 2-theta (2θ).

Although AAMs and geopolymers are amorphous, XRD is often used to identify newly formed phases. In this study, XRD was performed on powder samples with a Bruker AXS D2 Phaser X-ray diffractometer in 2-theta range of 10-65° using a Cu Kα X-ray source with a scanning speed and step size of 3.7 deg/min and 0.02°, respectively. The applied voltage and current were 30 kV and 10 mA, respectively.

3.4.3 Microstructural and elemental analysis by SEM-EDS

Scanning electron microscopy (SEM) is a useful method for evaluating the surface topography of various materials with high-resolution imaging. The advantages of using SEM over optical microscopy include the higher magnification and the possibility of getting more information such as the chemical composition and crystal structure of materials. SEM

produces images by scanning the surface with a focused beam of electrons. A beam of the electron is produced at the top of the microscope by an electron gun. The interaction of the electron beam with the specimen produces secondary and backscattered electrons. The primary electron beam also produces X-rays, which are used to identify elements with the technique called energy dispersive X-ray spectroscopy (EDS).

For non-conductive materials, samples are typically coated with a thin layer of conductive materials before the measurement to enable high-quality imaging. Gold is often used because of its high conductivity, hence high electron output for secondary electrons. However, for high resolution, platinum is preferred.

In this study, SEM was performed using JEOL JSM-6010PLUS, in which EDS was used for elemental analysis. It was carried out at 15 kV of accelerated voltage. All samples were coated with platinum (Pt).

3.4.4 Flame Atomic Absorption Spectroscopy

Atomic absorption spectroscopy is one of the most widely used techniques to measure the concentrations of elements in solutions. Its measurement principle is based on the Beer-Lambert law. Beer-Lambert law predicts a linear relationship between absorbance and concentration (Swinehart, 1962). In order to have atomic absorption, the ground-state atoms of the element should be produced. The free atoms are produced in an atomizer, and the process is called atomization. This is a crucial step because it determines the sensitivity of the reading. Atomic absorption equipment is equipped with an atomizer; the most common is flames and furnaces. The concentration of the sample is measured by comparing its absorbance to a linear calibration curve.

In this study, flame atomic absorption spectroscopy (FAAS) was employed to measure the concentration of Na+ leached into deionized water. It was conducted using

FAAS Shimadzu AA-6800. The analyte (sample being analyzed) was mixed with a particular concentration of HNO_3. It is useful for keeping the elements in the solution until they reach the flame of FAAS.

3.4.5 Mechanical strength

a. Compressive strength test

The test was performed to measure the maximum amount of compressive load the specimen can withstand before fracturing. Compressive strength test was conducted on cylindrical specimens, using a universal testing machine with a compression capacity of 250 kN and a displacement-controlled loading rate of 0.2 mm/min. The test was performed for three specimens, and an average was taken.

b. Flexural strength test

Flexural strength is defined as the maximum stress at which a material exhibits deformation due to a flexural load (Saikia and De Brito, 2012). Flexural strength is important in designing structural elements like beams, pavements, and slabs, as they are often subjected to flexing or bending. In this study, the flexural strength of prismatic specimens (160 × 40 × 40 mm) was measured using a three-point-bending test in accordance with JIS R 5201 (physical testing methods for cement). The test was repeated for three specimens, and an average was taken.

3.4.6 Mercury Intrusion Porosimetry (MIP)

MIP is an analytical technique used to characterize the porosity of materials, including the total pore volume, pore size distribution, bulk, and apparent density, which involves the intrusion of mercury into the material as a function of pressure. Since mercury does not wet the solid simultaneously, it must be forced using pressure into the pores. The relationship

between pressure (P) and capillary diameter (d) is described by Washburn as (Gardner, 1921):

$$P = \frac{-4\gamma \cos\theta}{d}$$

where θ is the contact angle and γ is the surface tension of mercury. The Washburn equation is based on the model of a cylinder. Therefore, the equation connects the pressure at which the cylindrical pores are intruded by mercury with their diameter. However, very few materials actually fulfill the requirement of this model (cylinder with the same diameter in both of its openings). Pore shapes in cement pastes are not cylindrical, according to the study by Diamond (Diamond, 2000). Therefore, some researchers agree that the MIP result does not represent the actual pore size. However, this technique provides a useful comparative indication of the total porosity of the specimens.

In this study, an MIP test was employed using a Quantachrome Poremaster 60 with a contact angle of 140 °. The samples were prepared in particle sizes between 2.36 – 4.75 mm. These samples were stored in acetone for at least 24 h to lead to the rapid evaporation of water. Subsequently, the samples were oven-dried at a temperature of 70 ℃ for 8 h to enable the appropriate evacuation. The pore size distribution was measured in the range of 0.0045 – 200 μm.

3.4.7 Water absorption of alkali-activated slag

Water plays a crucial role in the transport processes of concrete and other materials because it acts as the medium for aggressive agents. Therefore, water absorption behavior plays an important role in the durability of concrete. Water absorption usually indicates the degree of porosity of materials expressed in percentage under specific conditions.

In order to understand the capillary porosity, a water absorption test was performed. The water absorption of cylindrical specimens was measured with the following procedures: At the age of 28 d, specimens were dried at a temperature of 80 ℃ until a stable mass (m_0) was reached. Subsequently, the specimens were immersed in water at a temperature of 20 ℃ for 48 h. After the desired immersion period, specimens were taken out from the water, and the mass was weighed (m_1) immediately. The percentage of the water absorption (W_A) was determined using the following equation:

$$W_A = \frac{m_1 - m_0}{m_0} \times 100$$

CHAPTER 4. PROPERTIES OF GEOPOLYMER AT HIGH TEMPERATURES

The effect of high temperature on a building material is a complex mechanism because it is influenced by many factors. Visual inspection can provide useful information regarding the effect of fire on concrete since most damages such as cracks are macroscopically manifested. However, the investigation on material level must be considered since the individual materials comprise and, therefore, influence the overall performance of concrete at high temperatures. The composition of geopolymer is one of the crucial factors influencing the fire resistance of this material. This chapter presents the investigation results on the fire resistance of fly ash-based geopolymer with the addition of GGBS. In addition, the behavior of geopolymer activated with the combination of potassium hydroxide and sodium silicate solution (K-Geo) at high temperature was compared with geopolymer activated with sodium hydroxide and sodium silicate solutions (Na-Geo).

Moreover, fire resistance investigation on ordinary Portland cement (OPC) paste was also provided and compared to geopolymers. The preliminary research results were published in the author's publication (Saludung et al., 2019). The parameters studied include thermal stability, compressive strength, phase stability, and microstructural changes after elevated temperature exposure.

4.1 Effect of GGBS Addition on Fire Resistance of Geopolymer

4.1.1 Thermal analysis

Figure 4.1 shows the TG-DTA curves of geopolymer without GGBS (FAS0) and with 60% GGBS (FAS60). The TG curves are used to demonstrate changes in mass with the increase of temperature. At exposure temperatures ranging from room temperature (approx. 20 °C) to 200 °C, a mass loss of 12.6% was recorded for FAS0, which was lower than that of FAS60

(15.1% mass loss). The first significant mass loss that occurs at this temperature range is associated with the evaporation of free water and some physically and chemically bound water. The mass loss rate stabilizes after 200 ℃ up to 700 ℃, corresponding to the further removal of chemically bound water and hydroxyl groups.

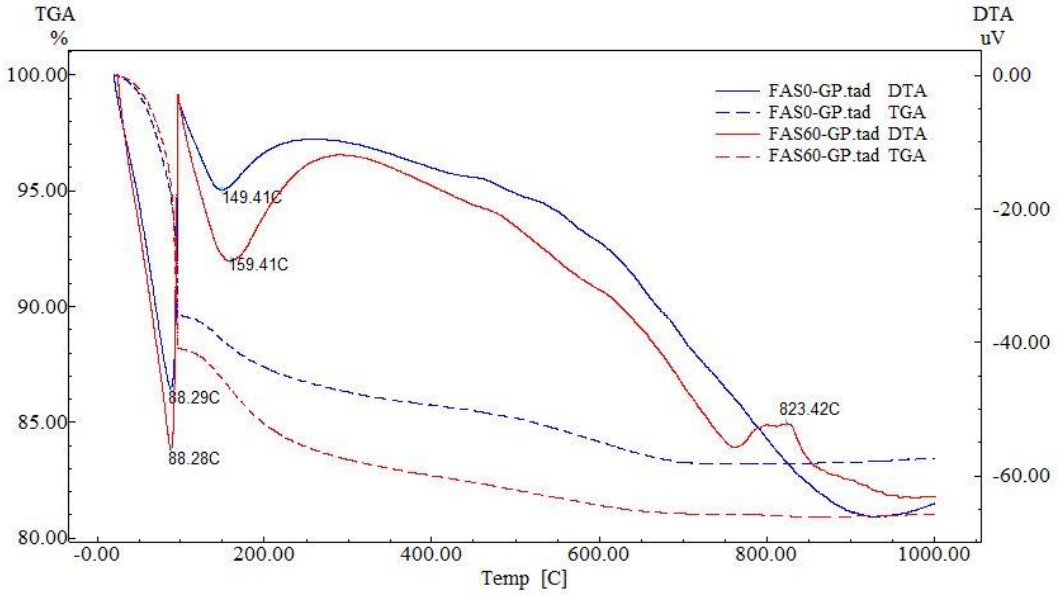

Figure 4.1 TG-DTA curves of geopolymer without GGBS and with 60% GGBS

The DTA curves show two major endothermic peaks centered at approx. 88 ℃ and 149-159 ℃ in both specimens. The first and second endothermic peaks correspond to the evaporation of free water and removal of chemically bound water molecules, respectively. Moreover, an exothermal event was observed in specimen containing 60% GGBS, indicated by a peak centered at 823 ℃. The exothermal event was probably attributed to the formation of crystalline phases (see section 4.1.3 for phase change). The detail regarding the thermal properties of all specimens is summarized in Table 4.1.

The TG-DTA curves of FAS15, FAS30, and FAS45 are provided in the appendix. All specimens, except for FAS60, present a similar residual of mass at 1000 ℃. The lowest residual of FAS60 could be due to the higher moisture present in its structure. Moreover, a

high rate of water loss in FAS60 (see mass loss before 200 ℃) compared to other mixtures could indicate its poorer heat resistance performance.

Table 4.1 Thermal properties of fly ash/slag geopolymer paste

Sample ID	Mass loss before 200 ℃ (mass%)	Mass loss ending temperature (℃)	Residual at 1000 ℃ (mass%)
FAS0	12.6	700	83.4
FAS15	11.7	710	84.1
FAS30	11.3	750	84.2
FAS45	12.6	700	83.1
FAS60	15.1	670	81.0

4.1.2 Effect of high temperature on compressive strength

The compressive strength of unexposed and exposed geopolymers under different dosages of GGBS is shown in Fig. 4.2(a). The addition of GGBS was found to improve the initial compressive strength. The improvement is due to the formation of calcium silicate hydrate gel since significant amounts of calcium were dissolved from GGBS.

Exposure to elevated temperature dramatically reduces the compressive strength of all specimens. Fig. 4.2(b) represents the percentage of retained compressive strength after elevated temperature exposure. Specimens containing slag undergo significant compressive strength loss, resulting in a low percentage of retained compressive strength compared to that made of 100% fly ash. Fly ash geopolymer has large numbers of interconnected pores, which facilitate the escape of moisture when heated, resulting in minimal damage to the matrix. Regardless of the amount of GGBS, reduction of compressive strength along with the temperature follows a similar trend. A rise in temperature could affect the pore structure by reducing the specific area of reaction products. High temperatures contribute to the

formation of large pore structures and result in the reduction of compressive strength. Although the investigation on porosity is not provided, the SEM analysis can give useful information regarding microstructural changes induced by thermal exposure in the sample (see section 4.1.4 for microstructural analysis by SEM). Moreover, since C-S-H was formed and is the main source of geopolymer strength, the heat exposure causes this phase to decompose, resulting in a significant loss of compressive strength.

Specimen containing 60% GGBS presents the highest initial compressive strength up to 92 MPa, but it could only retain 6.37% of initial strength after exposure to 950 °C. This proves that material with extremely high compressive strength does not necessarily provide good fire resistance. Moreover, surface spalling was found to occur only in this mixture. Increasing the GGBS content up to 60% can increase the formation of C-S-H gel and make the microstructure highly dense, thus having low permeability. If the material contains high moisture and the permeability of the material is low, damage may occur in the form of surface spalling.

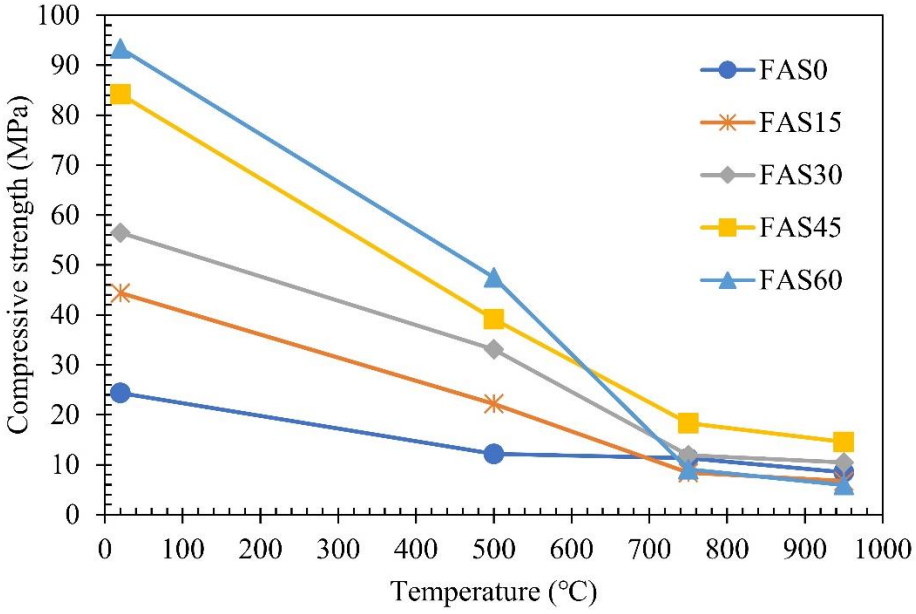

(a)

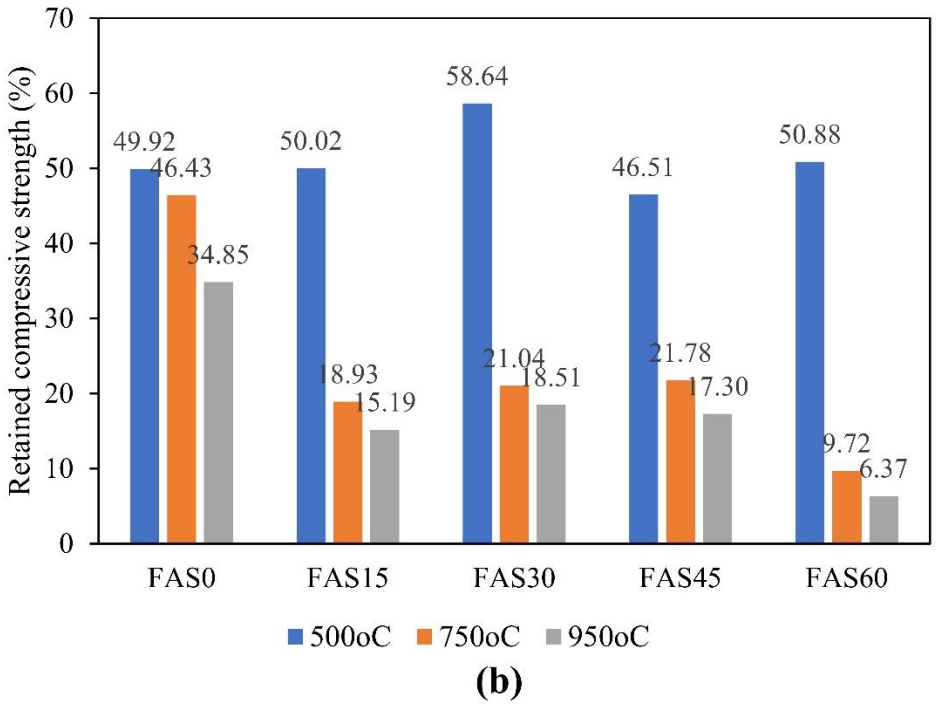

Figure 4.2 Compressive strength of unexposed and exposed geopolymer (a) and retained compressive strength after heat exposure (b).

4.1.3 Phase change after exposure

Figure 4.3 presents the XRD patterns of unexposed and exposed specimens. The unexposed geopolymers contain predominantly amorphous phases, indicated by a broad hump at approximately 15 – 35° 2-theta with some low intensity peaks of mullite and quartz phases which originated from raw fly ash.

A rise in temperature affects the phase transformation of geopolymer. When specimens were heated at 750 ℃, the XRD pattern showed some new crystalline phases. FAS0 and FAS15 still maintain their amorphous structures even after exposure to 950 ℃, but at the same time, the formation of crystalline phases was observed. The decomposition of reaction products of geopolymer is likely to be different from that of OPC paste. Unlike OPC, the decomposition of geopolymer paste frees Ca, Na, Si, Al, and Mg species to crystallize to the secondary mineral phases. The formation of nepheline which is estimated

to occur at a temperature between 750 – 950 ℃, dominates the geopolymer made from 100% fly ash after exposure. Cristobalite was observed after exposure to 750 and 950 ℃ as the result of crystallization modification of quartz at high temperatures (Simon and McMahon, 1953). The addition of slag leads to the formation of other crystalline phases such as wollastonite and akermanite due to the high calcium content from slag. Increasing the slag content likely promotes crystallization of geopolymer at a lower temperature. The quartz peak in FAS45 and FAS60 vanished, and the crystallization was almost completed after exposure to 750 ℃. In the case of specimens with higher fly ash content, geopolymer was heterogeneous at the molecular level due to the existence of unreacted fly ash particles. In low-calcium geopolymer, higher energy is required for the transformation from amorphous to crystalline phases. However, the starting crystallization temperature in this study was much lower than that observed by He et al., in which the geopolymer starts to crystallize at a temperature above 1000 ℃ (He et al., 2011).

The formation of wollastonite was observed in the specimens containing slag due to the decomposition of C-(A)-S-H gel. In addition, slag consists of a significant amount of magnesium which leads to the formation of akermanite at high temperatures. The re-crystallization of geopolymer, which led to the formation of the analogies to natural minerals after elevated temperature exposure, is in contrast with the phase composition of OPC. Fig. 4.4 shows the appearance of unexposed and exposed FAS45 specimens. A significant degree of macroscopic shrinkage was observed in specimens after exposure to 500 ℃. According to Duxson et al., at a temperature between 250-600 ℃, the dihydroxylation process takes place and induces shrinkage of geopolymer (Duxson et al., 2007a). A slight change in the XRD peak at this temperature implies a slight change in the framework. The formation of crystalline phases is estimated to occur at a temperature between 500-750 ℃ and causes the specimens to expand. The expansion can cause cracks and increase the porosity; thus,

compressive strength gradually decreases, but at a slower rate than that of the specimen after exposure to 500 ℃. The crystallization of geopolymer into secondary mineral phases can either decrease the fire resistance by forming cracks or improve the fire resistance by increasing the melting temperature. It is worth noting that no sign of chipping or spalling was observed even when faster heating rate of 20 ℃ was applied. A spalling was observed in the specimen containing 60% slag due to its much denser microstructure.

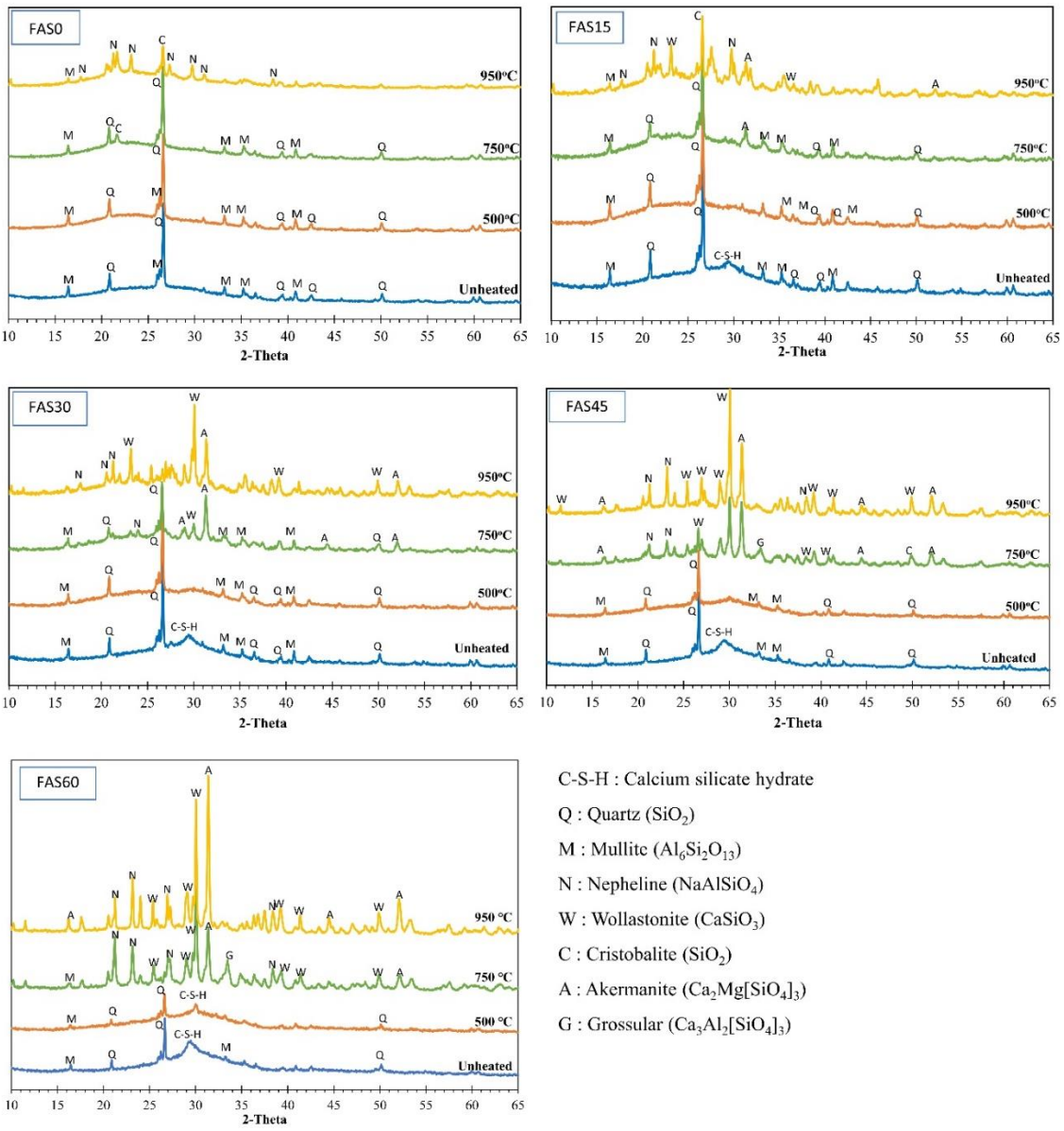

Figure 4.3 XRD patterns of unexposed and exposed geopolymer

Figure 4.4 Visual appearance of unexposed and exposed geopolymer containing 45% GGBS

4.1.4 Microstructural change

Fig. 4.5 shows the microstructure of geopolymers depicted at 500× magnification. Two mixes were selected for comparison: specimens without GGBS and with 60% GGBS. Before heating, the regular spherical grains can be observed in the binder made from 100% fly ash. It was observed that the addition of GGBS was found to produce a denser structure. According to the literature, the presence of calcium leads to the formation of C-S-H, which produces a compact microstructure (Saha and Rajasekaran, 2017; Wang and Scrivener, 1995).

SEM micrographs also represent the microstructural evolution of geopolymer pastes observed from 20 ℃ to 1000 ℃. The changes in compressive strength after elevated temperature exposure are due to the changes in the microstructure of the material. For specimen containing 60% GGBS, the higher the temperature, the coarser the microstructure becomes. This was attributed to the decomposition of C-S-H gel which creates a porous microstructure.

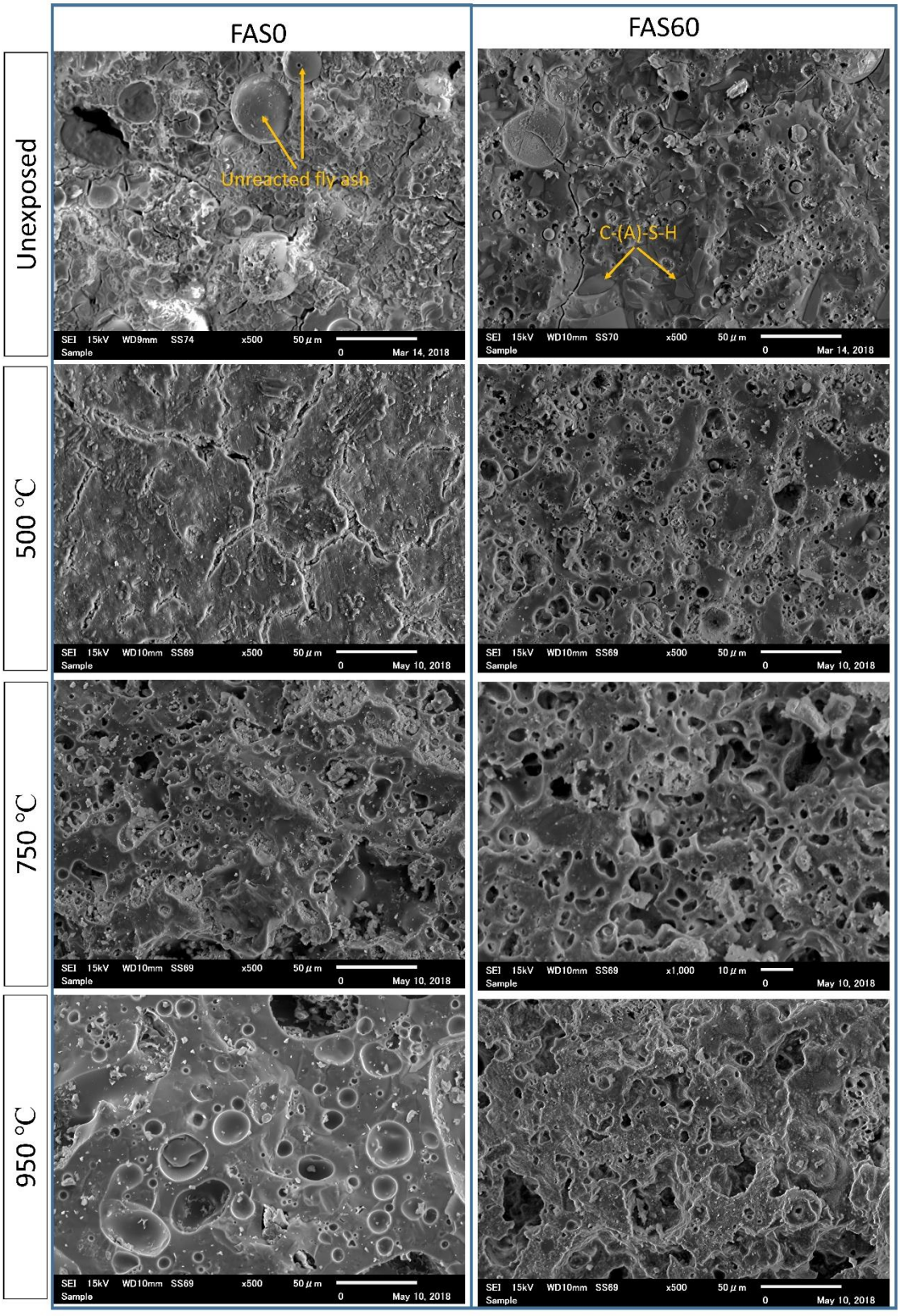

Figure 4.5 SEM micrograph of unexposed and exposed FAS0 and FAS45

Geopolymer without GGBS (FAS0) behaved differently. The cracks are visible in FAS0 after heating at 500 ℃, but no large pores were observed. At some level of heat, the gel formation of fly ash geopolymer was still progressed. However, the specimen does undergo some level of high-temperature thermal shrinkage, resulting in the formation of macrocracks, hence reducing the strength significantly. After heating at 750 ℃, the structure of FAS0 become porous, but simultaneously, sintering and densification of the matrix initiated. It is possible that the sintering can promote crack healing; therefore, the strength decreased gradually at a slow rate compared to that in specimen containing GGBS after exposure to a temperature above 500 ℃. The effect of sintering was pronounced after temperature exposure to 950 ℃. This results in a more homogenous and denser microstructure than the unexposed FAS0 specimen.

Despite a lower initial strength of fly ash geopolymer, its behavior at elevated temperatures can be more favorable. The easy densification of fly ash geopolymer is beneficial to its application as a fire-resistant material. Moreover, despite significant degradation in microstructure and strength, fly ash geopolymers doping with GGBS up to 45% provide resistance to spalling even after exposure to 950 ℃, promising their application as fire resistance building material.

4.2 Effect of Alkali Metal Type on Fire Resistance of Geopolymer

Sodium hydroxide (NaOH) solution is the most commonly used hydroxide solution in geopolymer production. However, efflorescence (formation of a white deposit on the surface) and crystallization is less rapid in geopolymer prepared using KOH. Moreover, some previous studies on fly ash geopolymers have shown that using KOH as an activator solution was beneficial to improve the fire resistance (Bakharev, 2006; Kong and Sanjayan, 2008). In this study, since the binder consists of 55% fly ash and 45% slag, the geopolymers

may perform differently from the previous studies, which used only fly ash. In addition, the behavior of OPC paste after elevated temperature exposure was also investigated and was compared to geopolymers.

4.2.1 Compressive strength

The influence of alkali metal type on the compressive strengths of unexposed and exposed fly ash/slag geopolymer specimens is presented in Fig. 4.6. Na-geopolymer presents higher initial compressive strength than K-geopolymer at the same concentration and curing condition. According to a study by Xu and van Deventer, the dissolution rate of minerals in NaOH solution is higher than in KOH solution (Duxson et al., 2005; Xu and Deventer, 2000). Thus, the geopolymer produced from NaOH could form the gel products more rapidly, resulting in higher compressive strength than that produced from KOH. In addition, it can be seen that the compressive strength of geopolymers is higher than that of OPC paste.

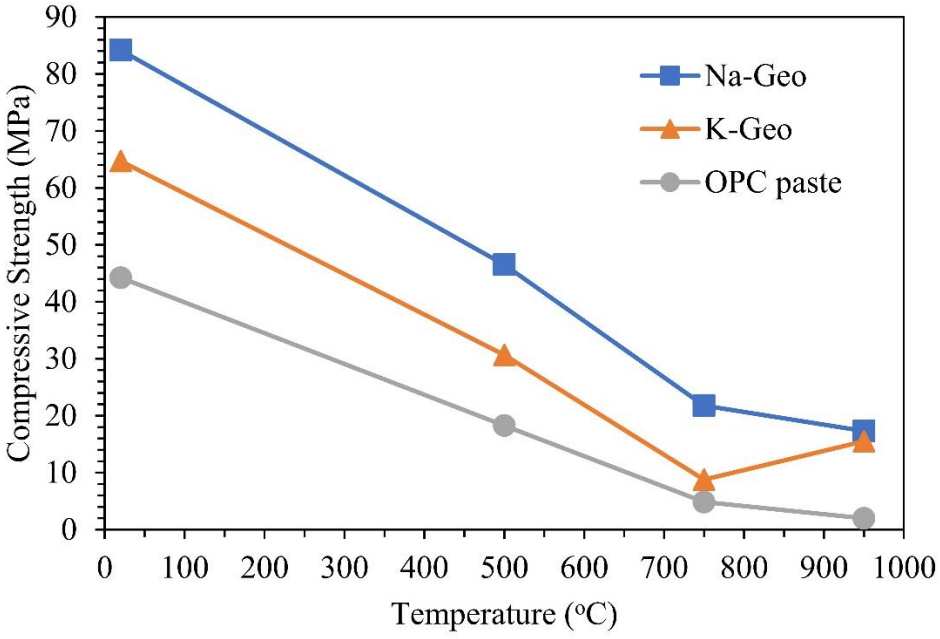

(a)

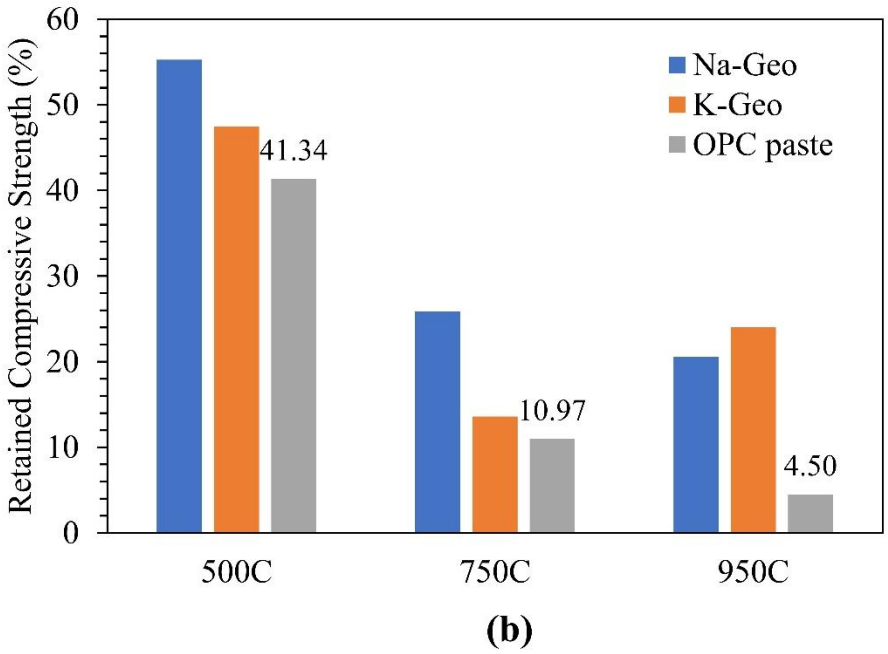

Figure 4.6 Compressive strength (a) and the percentage of retained compressive strength of Na-geopolymer, K-geopolymer, and OPC paste heat exposure.

After exposure to high temperatures, both geopolymer and OPC pastes show significant degradation in compressive strength. Loss of strength after elevated temperature exposure was possibly connected to the deterioration of aluminosilicate gel and C-(A)-S-H (for specimen containing slag), which created a porous structure. It can be seen that the compressive strength of Na-Geo and OPC paste gradually decreased after exposure to temperature up to 950 ℃. OPC paste almost totally lost its compressive strength at 950 ℃, while Na-Geo could maintain about 24% of its initial strength. The behavior of K-Geo, when exposed to high temperature, was different from that of Na-Geo. K-Geo had gradually decreased its strength when exposed to up to 750 ℃, but then the compressive strength increased after exposure to 950 ℃. Kong and Sanjayan observed that fly ash geopolymer specimens prepared from a solution containing potassium exhibited higher compressive strength than unexposed specimens after exposure to 800 ℃ (Kong and Sanjayan, 2008). The increase of compressive strength is probably attributed to the low diffusion coefficient of K^+ at high temperatures which increased the melting temperature of the geopolymer.

However, in the presence of GGBS, the strength increment is not as much as the observation in the previous study. Thus, the effect of using KOH as an activator solution may be beneficial when using low-Ca precursors.

4.2.2 Phase change after exposure

Fig. 4.7 and Fig. 4.8 present the XRD patterns of Na-Geo and K-Geo, respectively, before and after exposure to elevated temperature. The unexposed Na-Geo and K-Geo show almost similar XRD patterns, but the C-S-H peak in K-Geo is sharper than that in Na-Geo. This indicates that the C-S-H formed in K-Geo could be more ordered than that in Na-Geo.

After exposure to 500 ℃, there is no crystallization occuring in both Na-Geo and K-Geo. However, the C-S-H reduces its intensity, indicating that the decomposition of this phase occurs at a temperature below 500 ℃. At 750 ℃, some new crystalline phases such as nepheline, akermanite, wollastonite, grossular, and cristobalite were formed in Na-Geo, and the specimen shows almost complete crystallization at this exposure temperature. By contrast, an amorphous hump was still observable in K-Geo after exposure to 750 ℃, even though some low intensity peaks of wollastonite and cristobalite were observed. After exposure to 950 ℃, both Na-Geo and K-Geo show a complete crystallization. At this temperature, akermanite and leucite ($KAlSi_2O_6$) were observed in K-Geo. Based on the XRD results, it is clear that the type of alkali metal in solution influences the crystallization temperature and mineral formation in geopolymer at high temperatures.

On the other hand, the XRD pattern of unexposed and exposed OPC specimens is presented in Fig. 4.9. OPC paste mainly consists of portlandite, with some low intensity peaks of C_2S (belite), C_3S (alite), ettringite, and calcite. At 500 ℃, the portlandite peak was still observable, and it started to decrease considerably at 750 ℃. At 750 ℃, the CaO peak was formed, and considerable amounts of C_2S and C_3S were observed. Calcite peak vanished

at 950 ℃, which indicates a complete decomposition of calcite at a temperature between 750 and 950 ℃.

Moreover, the peak intensities of CaO and C_3S increased considerably with the increase of exposure temperature up to 950 ℃ due to the further decomposition of portlandite, calcite, and C-S-H. This result indicates that OPC paste behaved differently from the geopolymer materials. Unlike geopolymer, OPC products are represented by the compounds not having analogies to natural minerals, thus resulting in lower heat resistance. The higher heat resistance of geopolymers is believed due to the recrystallization of the reaction products into secondary mineral phases, which increases the melting temperature of geopolymers.

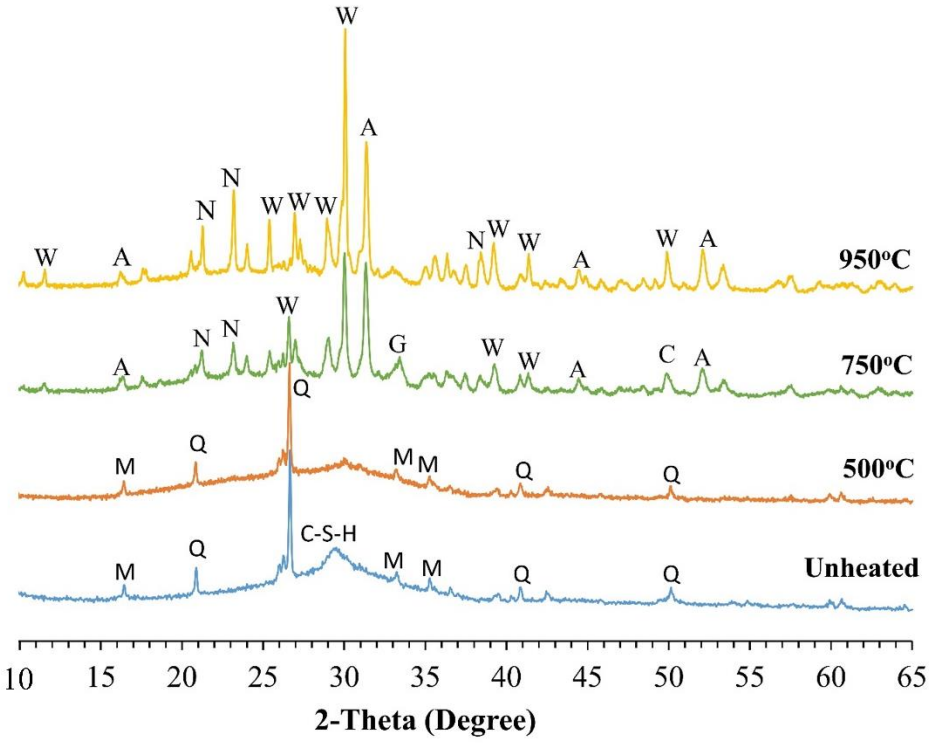

Figure 4.7 XRD pattern of unexposed and exposed Na-geopolymer (M: mullite, Q: quartz, G: grossular, C: cristobalite, W: wollastonite, A: akermanite, N: nepheline).

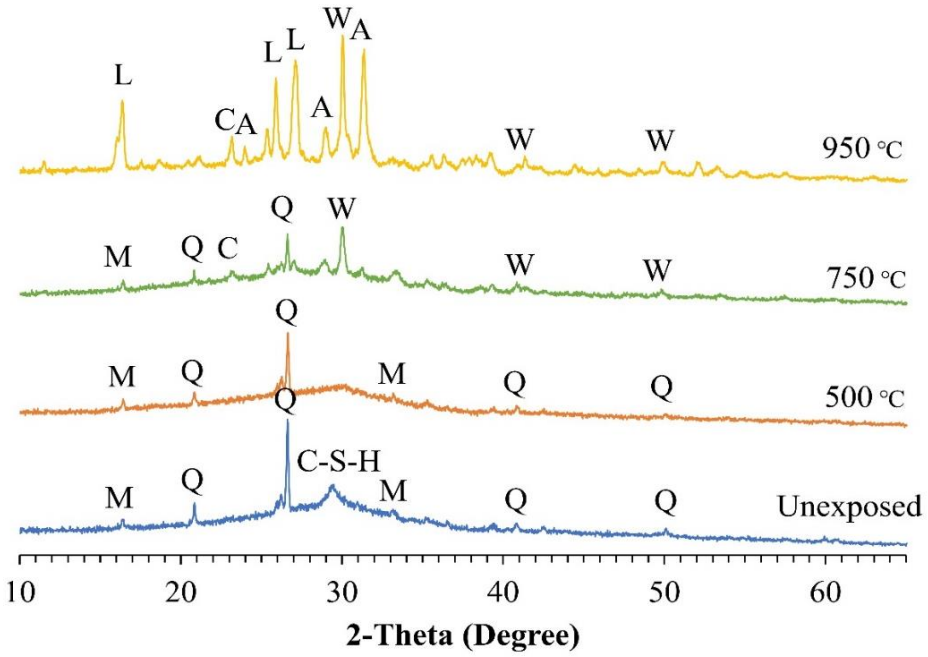

Figure 4.8 XRD pattern of unexposed and exposed K-geopolymer (M: mullite, Q: quartz, C: cristobalite, W: wollastonite, A: akermanite, L: leucite).

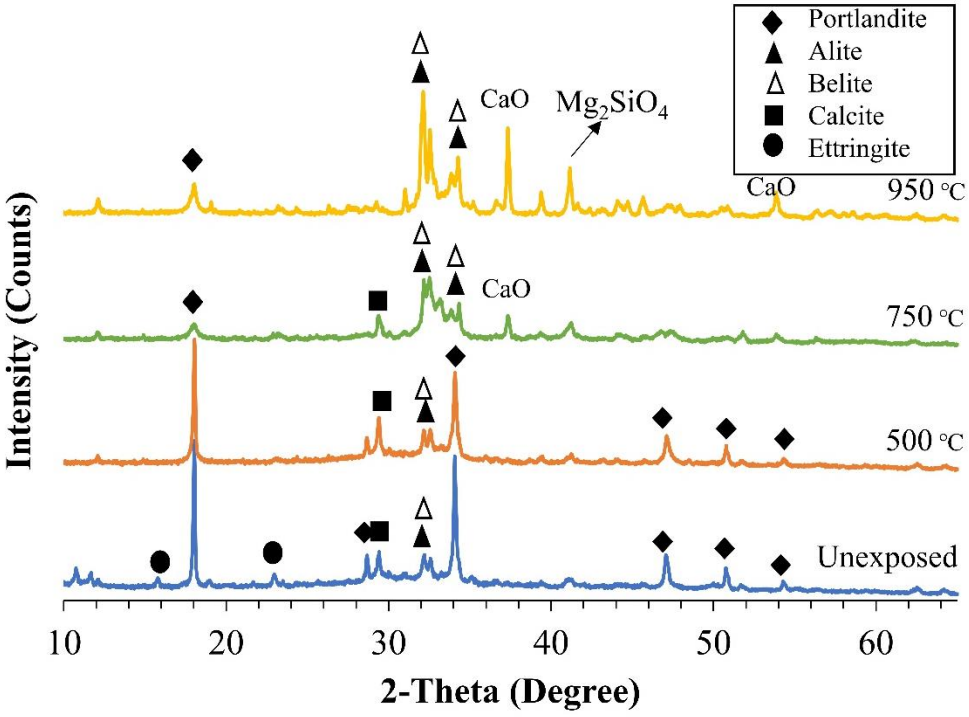

Figure 4.9 XRD pattern of unexposed and exposed OPC paste.

4.2.3 Microstructural change

Fig. 4.10 compares the microstructure of Na-Geo and K-Geo before and after elevated temperature exposure. There is no clear difference in the microstructure of unexposed Na-Geo and K-Geo observed by SEM analysis. However, SEM images confirm the pore structure coarsening of specimens when exposed to temperatures up to 750 ℃, which is responsible for the significant compressive strength loss.

At the exposure temperature of 950 ℃, it is evident that the densification of pore structure occurs in both K-Geo and Na-Geo specimens due to sintering, but the sintering is more pronounced in K-Geo. When a material is kept heating, each material composition has a temperature where it becomes soft and undergoes liquid sintering. The liquid sintering leads to the closure of accessible pores and pore channels, resulting in matrix densification. The densification of the matrix by sintering corresponds to the slight increase in compressive strength of K-Geo when exposed to 950 ℃. However, the reason why K-Geo undergoes more rapid sintering at a temperature between 750 and 950 ℃ than Na-Geo is still unclear.

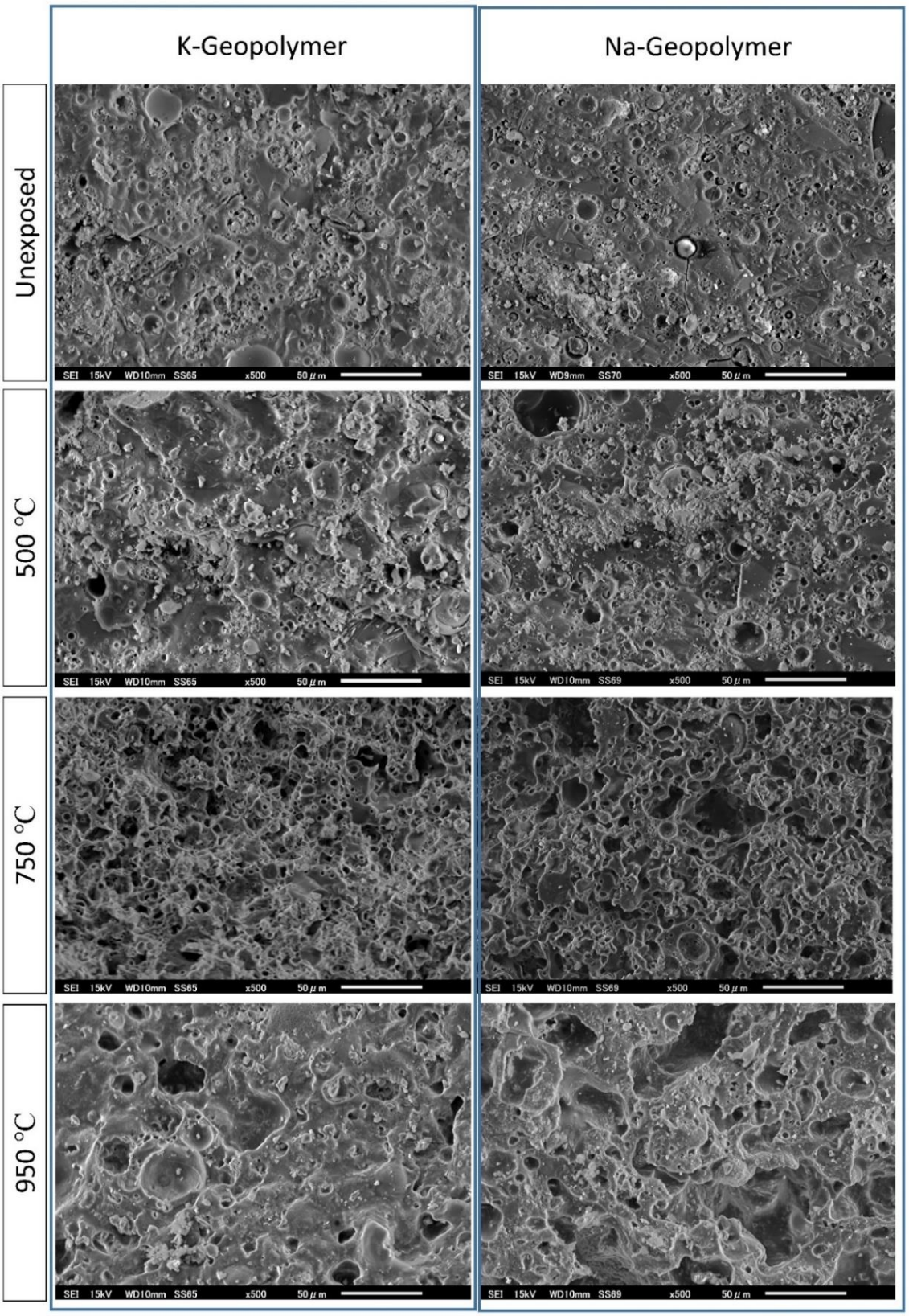

Figure 4.10 SEM micrograph of unexposed and exposed Na-geopolymer and K-geopolymer

4.3 Summary

Remaining a stable structure at high temperatures, geopolymers represent a potential alternative binder to be applied as heat-resistance materials. Based on the experimental results, geopolymer produced from fly ash exhibited a lower degradation rate after elevated temperature exposure, indicated by a lower degree of compressive strength loss and still maintaining its amorphous structure even after exposure to 950 ℃.

It is worth noting that adding Ca from GGBS could significantly increase the initial strength, but once applied for heat-resistance materials, an increased Ca content may cause serious structural damage. The role of calcium seems to be effective at a limited content. This study found that using too much GGBS to replace fly ash (more than 45% replacement ratio) may harm the structure due to a significant compressive strength loss and explosive surface spalling.

Using activator solutions from the combination of KOH solution with water glass may improve the fire resistance of geopolymer. The densification of pores in K-Geo by sintering was observed at a temperature lower than that in Na-Geo. However, despite increasing the strength after exposure to 950 ℃, K-Geo presents an almost similar compressive strength value to the Na-Geo at this exposure temperature. It is assumed that the effect of using KOH solution may be beneficial for the fire resistance of geopolymer with low GGBS content.

On the other hand, it was evident that the geopolymer materials performed high heat resistance in terms of phase stability and compressive strength loss when compared to OPC material. Unlike geopolymer which re-crystallized at high temperature, OPC paste presents an increase in the amount of belite and alite. The formation of CaO was also observed due to the thermal decomposition of calcium hydroxide and calcium silicate hydrate. This indicates the potential application of geopolymer as an alternative material to OPC.

CHAPTER 5. EFFECT OF SILICA FUME ON EFFLORESCENCE FORMATION AND ALKALI LEACHING OF ALKALI-ACTIVATED SLAG

Alkali-activated slag (AAS) appears as one of the alternative binders for concrete production. In terms of mechanical properties, AAS binders offer extremely high compressive strength compared to OPC and alkali-activated fly ash, but this is not the focus of this study. This study aims to investigate the effect of silica fume on the efflorescence formation in alkali-activated slag (AAS). The study of efflorescence is of large practical importance since this phenomenon has been considered one of the main issues limiting the application of AAMs in the civil engineering field. Unlike OPC materials in which efflorescence is considered harmless, efflorescence in AAMs can be structurally harmful. As mentioned earlier, the efflorescence is strongly affected by the alkali concentration in the solution, as a higher concentration of alkali hydroxide solution results in a higher rate of efflorescence formation. However, a high concentration of alkali solution is required to produce high-strength AAMs. The composition of raw materials is another important factor affecting efflorescence formation. In this study, various amounts of SF were used as an additional silica source in AAS production. A high concentration of sodium hydroxide (14 M) was employed in the production of AAS to obtain a clear observation result regarding the effect of SF addition into the AAS binder. All contents in this chapter have been explained in author's publication (Saludung et al., 2021a).

5.1 Effect of SF on the Properties of Reaction Products

5.1.1 Thermal analysis of AAS products

Figure 5.1 shows the TG-DTA analysis of AAS under various dosages of SF. All specimens present a sharp decrease in mass before 200 °C due to evaporation of free water, as shown by TGA curves. Since the main hydration product in AAS binder is C-(A)-S-H phase

(Puertas et al., 2011; Wang and Scrivener, 1995; Ye and Radlińska, 2016), the second mass loss between 200 ℃ and 600 ℃ could be attributed to the removal of physically and chemically bound water from C-(A)-S-H. The temperature at which the C-(A)-S-H starts to decompose is estimated to be around 105 – 110 ℃, similar to that of C-S-H decomposition in Portland cement paste (Wang and Scrivener, 1995), while a complete decomposition occurs at a temperature range of 600 – 800 ℃. In this study, C-(A)-S-H was estimated to be completely decomposed at approx. 600 – 650 ℃ as above this temperature, a stable mass was observed.

The detail regarding the thermal properties of AAS is summarized in Table 5.1. The inclusion of SF seems to increase the total mass loss. BFS-SF0 presents the highest residual amount at 1000 ℃, which could be attributed to the lower amount of water molecules (physically and chemically bound in the structure) than specimens containing SF. The water loss behavior could give useful information regarding porosity. The lower water content of BFS-SF0 can indicate a low porosity. This statement is supported by the results of the water absorption test and MIP analysis provided in Section 5.6.

Mass losses from TG analysis are related to the phase changes represented by DTA. The DTA curves show two major endothermic peaks at approx. 86-90 ℃ and 165-173 ℃ in all test samples, while the exothermic peak was observed at approx. 788-795 ℃ in BFS-SF10 and BFS-SF15 only. The first and second endothermic peaks correspond to the evaporation of free water and removal of chemically bound water molecules, respectively. By comparing the peaks broadening (the second endothermic peak), it can be seen that by increasing the SF dosages, the amount of water is higher in these forms, which could be related to the higher porosity. The exothermal event was probably attributed to the formation of wollastonite ($CaSiO_3$) due to the thermal decomposition of C-S-H (Tajuelo Rodriguez et al., 2017). The formation of wollastonite occurs at a certain temperature, depending on the

amount of calcium and silicon in reaction products. The temperature required for the transformation of C-S-H to wollastonite is raised with an increasing Ca/Si ratio. Since BFS-SF0 and BFS-SF5 have higher Ca/Si ratios than BFS-SF10 and BFS-SF15 (the detailed information regarding the Ca/Si ratio is provided in section 5.4), the formation of wollastonite may occur at higher temperatures (>1000 ℃). A further study on the XRD analysis of the AAS sample exposed to elevated temperature is required to validate the formation of wollastonite.

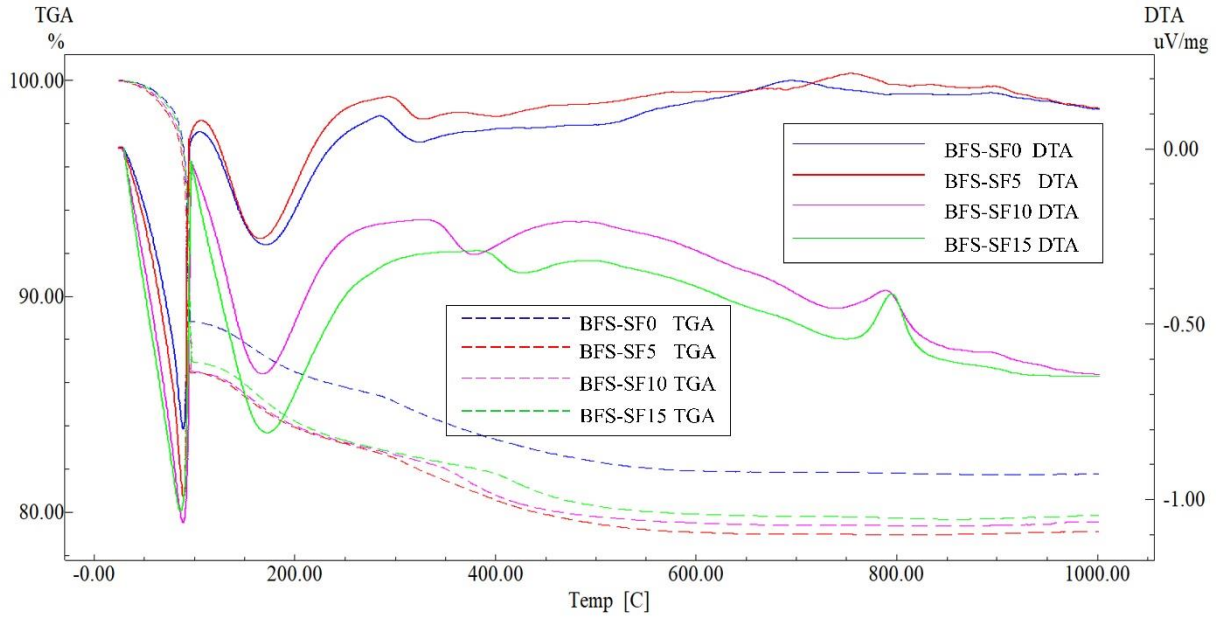

Figure 5.1 TG-DTA curves of AAS products under various dosages of silica fume

Table 5.1 thermal properties of AAS products

Samples	Temperature at 5 % mass loss (˚C)	Mass loss ending temperature (˚C)	Residual at 1000˚C (mass%)
BFS-SF0	92	600	82
BFS-SF5	91	650	79
BFS-SF10	93	650	80
BFS-SF15	92	650	80

5.1.2 Phase composition of reaction products

XRD patterns of raw GGBS and SF are presented in Fig. 5.2(a). Both raw materials show a completely amorphous structure; the reaction between these materials with alkaline solution results in amorphous AAS with a poorly crystalline C-S-H (Lee and Lee, 2015; Puertas et al., 2011), indicated by a broad diffraction peak centered at 29-30° 2-theta, as shown in Fig. 5.2(b). Aluminate-substituted calcium silicate hydrate (C-A-S-H) was formed in AAS due to the higher Al/Si ratio, but lower Ca/Si ratio compared to that of C-S-H in OPC. Puertas et al. suggest that the atomic scale structure of C-(A)-S-H in AAS might be close to tobermorite (Puertas et al., 2011).

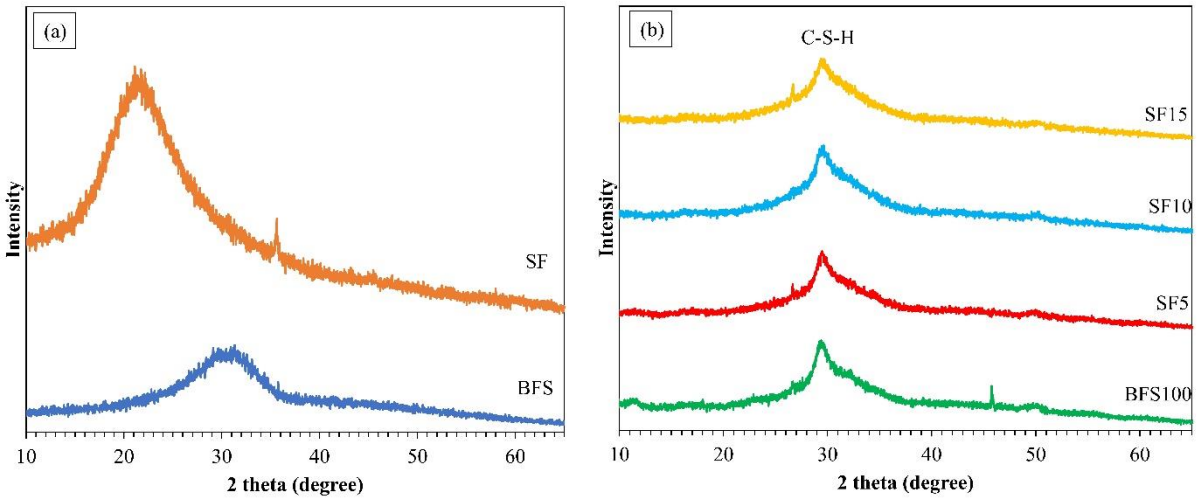

Figure 5.2 XRD patterns of raw materials (a) and AAS products with the addition of SF (b).

The addition of SF seems to promote the formation of amorphous C-(A)-S-H. The C-(A)-S-H peak in BFS-SF0 has a sharper peak than that in specimens containing SF; as the amount of SF increases, the C-(A)-S-H peak becomes wider, indicating that there is an increase in amorphicity of the gel. The result is in complete agreement with the previous study by Ye and Radlinska (Ye and Radlińska, 2016), which reported that the presence of additional Si from sodium silicate solution reduces the crystallinity of C-S-H. It is suggested

that the Ca/Si ratio influences the C-S-H crystallinity in the alkali-activated binder. In this study, the presence of additional Si from SF reduces the Ca/Si ratio, indicating C-(A)-S-H formed in the specimen without the addition of SF (BFS-SF0) can be more ordered than the C-(A)-S-H formed in the specimens containing SF.

5.2 Alkali Leaching and Efflorescence Investigation

5.2.1 Alkali leaching of AAS

In general, AAMs and geopolymers contain a significantly high amount of unreacted alkali (Na and/or K) particles, mainly due to the low extent of reaction and relatively high concentration of alkali in activator solutions. The unreacted or free alkalis are mobile; when the specimen is subjected to a humid environment, the alkalis will move to the surface and react with CO_2 in the atmosphere to form white deposits called efflorescence. Since efflorescence formation is strongly related to free alkali, the alkali leaching test is considered an effective way to understand the efflorescence phenomenon in AAMs.

Figures 5.3 and 5.4 demonstrate the concentration of alkali leached in water and the total amount of alkali leaching, respectively. All mixes present a rapid alkali leaching in the early immersion period (at 3 and 24 hours) due to the high amount of free alkali. BFS-SF0 presents the highest leaching amount after 3 h and 24 h immersion and almost vanished after 28 d. This proves that the BFS-SF0 contains a much higher amount of unreacted alkali particles compared to other specimens containing SF, while the lowest alkali leaching was observed in specimen with 15% SF (BFS-SF15). This suggests that incorporating SF into the AAS binder can significantly reduce the amount of unreacted alkali particles. Since free alkalis are responsible for efflorescence formation, it is expected that the efflorescence deposits will be rapidly formed in BFS-SF0.

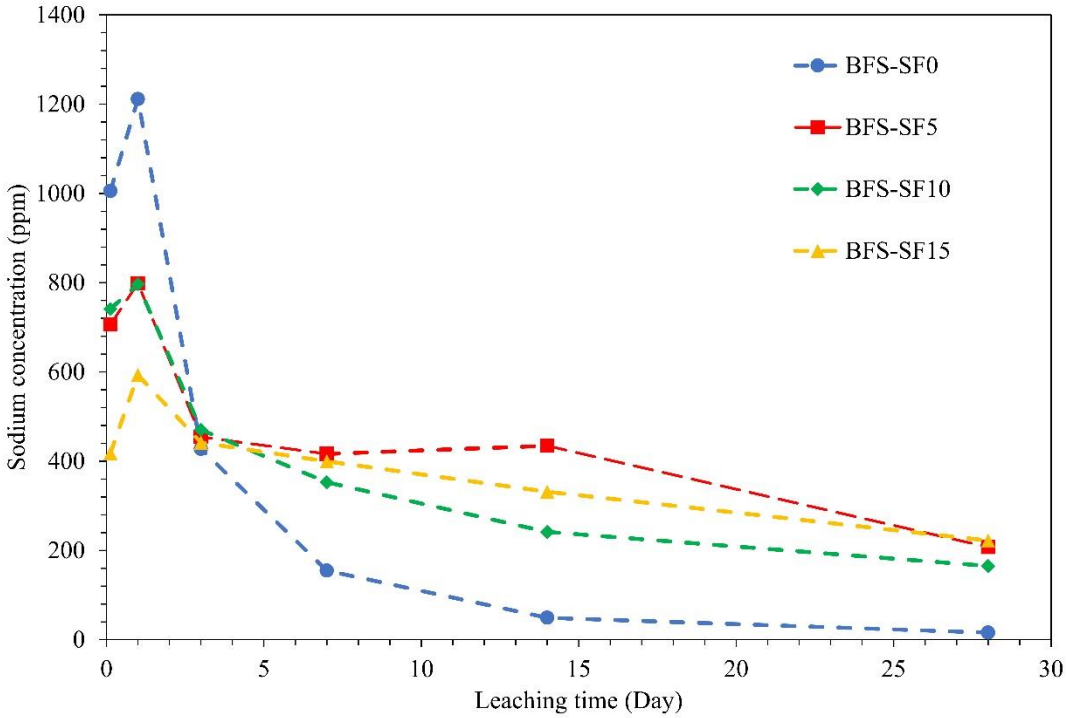

Figure 5.3 Sodium concentration in water

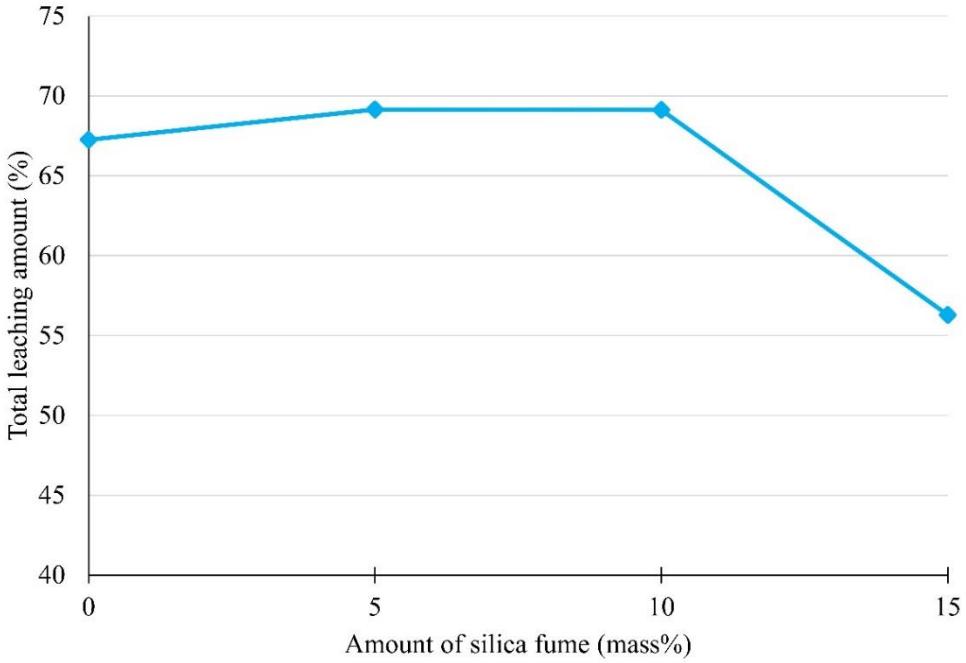

Figure 5.4 Total leaching amount of sodium after 28 days immersion in water

Although each specimen exhibits a different leaching rate, the total amount of sodium leached after 28 d was almost equal in specimens containing 0%, 5%, and 10% of SF (see Fig. 5.4). Specimen containing 15% SF exhibits the lowest total alkali leaching amount, indicating that BFS-SF15 has better alkali binding property. The total leaching amount of sodium after 28 d involved not only the unreacted sodium but also the reacted particle since sodium is only bound weakly in gel structure; hence it can be readily leached into the water. This result is in agreement with the study by Škvára et al. which observed that almost all alkalis from the alkali-activated fly ash and metakaolin are leachable into the water, indicating the weak bond of alkali (Škvára et al., 2012).

5.2.2 Efflorescence observation

Figure 5.5 demonstrates efflorescence formation on the specimens observed after putting them in contact with water for 24 h and 72 h. It can be observed that efflorescence formation on partly immersed specimens decreases with the inclusion of SF. This result, in turn, indicates that the incorporation of additional silicate from SF is helpful in reducing the efflorescence formation. Although BFS-SF5 did not show any visible efflorescence deposits, some cracks could be observed on its surface, and the specimen contracts. It could be attributed to the crystal formation inside the pore or beneath the surface (subflorescence). As the crystal grows, the crystallization pressure is generated; when this pressure exceeds the tensile strength, it can cause damage by forming cracks (Scherer, 2004). In general, a crystal formation causes the material to expand; however, due to the slow kinetics of water penetration, the crystallization pressure can be overcome by the capillary pressure, which makes the sample shrink (Scherer, 2004).

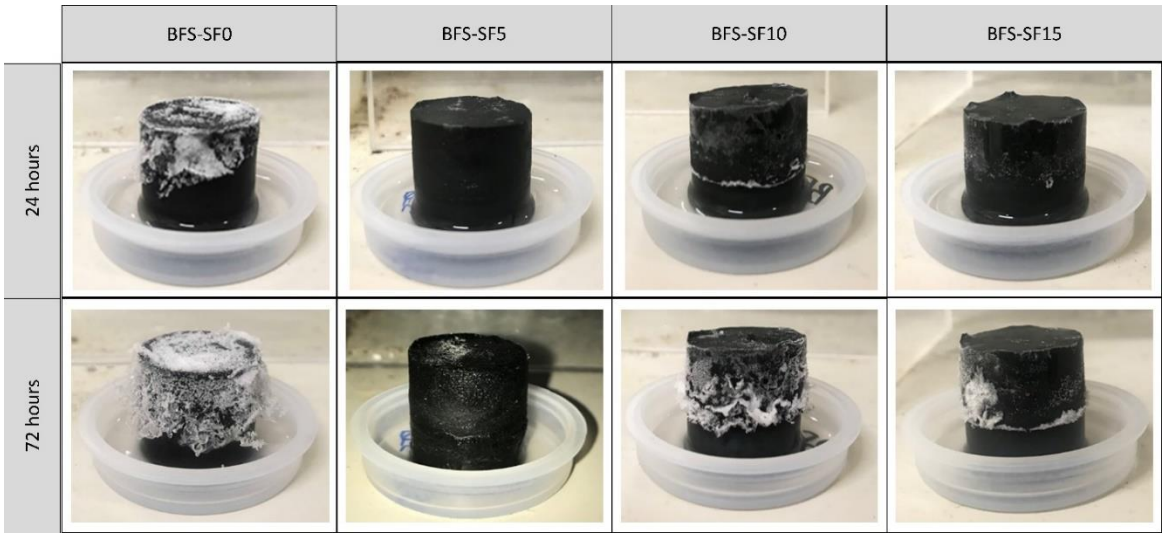

Figure 5.5 Efflorescence on 28d-aged AAS specimens after being in contact with water

In conjunction with alkali leaching, BFS-SF0 showed the fastest efflorescence as it presents the highest alkali leaching at the immersion period of 24 h. This is attributed to the high amount of unreacted sodium in BFS-SF0, proving that the efflorescence is strongly related to the free alkali. Specimens containing SF have lower efflorescence formation potential as the amount of leached sodium was lower than that in BFS-SF0 after immersion for 24 h. However, there is a peculiarity that the total amount of leached sodium was almost equal in some specimens after 28 d of immersion. The inclusion of 15% SF shows a significant reduction in the total leaching amount of sodium, resulting in little efflorescence formation.

It was clearly observed that the efflorescence was excessively formed during contact with water from 0 to 72 h. After 72 h, all water was absorbed by the specimens. If more water was added to extend the efflorescence period, no significant change was observed. Moreover, the alkali leaching occurs at a slow rate after 72 h (except for BFS-SF0). This could indicate that the free alkalis may be completely leached in an immersion period

between 24-72 h. After 72 h in contact with water, it was suggested that some reacted sodium particles started to leach from the specimens.

5.2.3 Efflorescence product

Fig. 5.6 presents the XRD pattern of efflorescence product scraped from the surface of BFS-SF0 as it exhibited excessive formation of a white deposit. It demonstrates that the efflorescence product is mainly a sodium carbonate hydrate. Unlike the efflorescence in OPC, although the precursor contains a high amount of calcium, the formation of calcium carbonate hydrate was insignificant, which suggests that Ca^{2+} is strongly bound in gel structures.

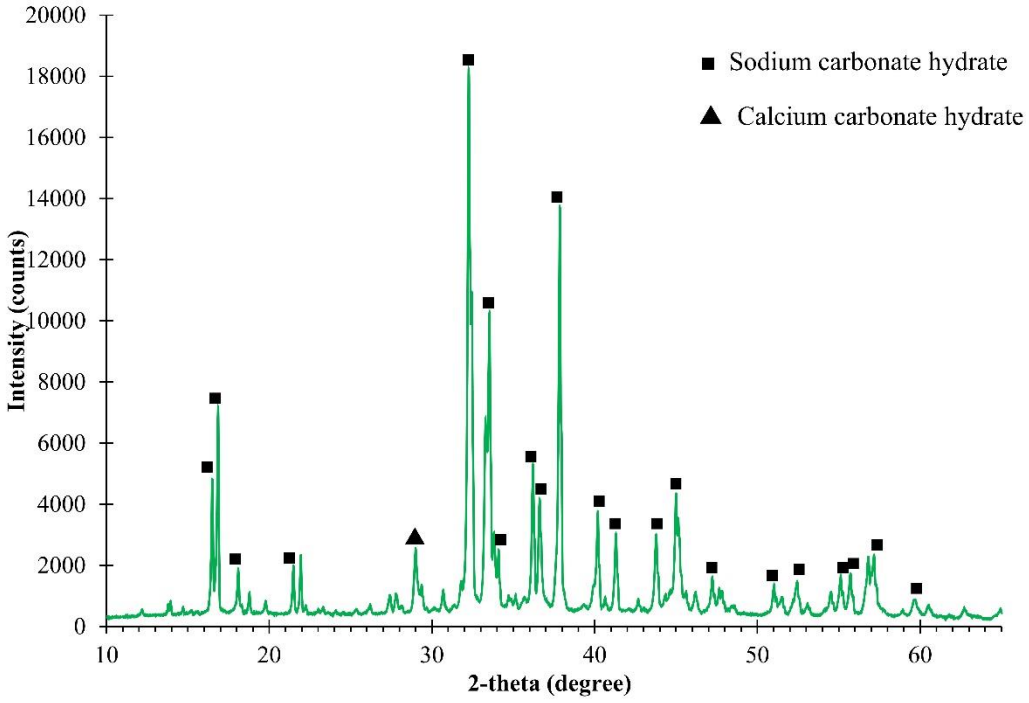

Figure 5.6 XRD pattern of efflorescence deposit

The elemental analysis of efflorescence deposit is listed in Table 5.2. The efflorescence deposit mainly consists of C, Na, and O with very small quantities of Ca and Si, which confirms the presence of sodium carbonate. A similar result was obtained by the

study conducted by Zhang et al., which observed the presence of sodium carbonate hydrate in efflorescence deposit of fly ash geopolymer (Z. Zhang et al., 2014).

Table 5.2 Elemental analysis of efflorescence deposit

Elements	C	Na	Si	Ca	S	O
Compositions (mass%)	13.88	33.96	0.20	0.82	0.29	50.86

5.3 Elemental Analysis

Table 5.3 provides the elemental analysis of unexposed ambient-cured specimens (dry), specimens after the efflorescence test (eff), and specimens after the immersion test (imm). Alkali activated slag products contain mainly Si, Al, Na, Mg, O, C, and Ca with some impurities of S and Ti. Fig. 5.7 demonstrates the atomic ratios of the reaction products of AAS under different dosages of SF and different curing conditions. The Ca/Si atomic ratios of unexposed specimens decrease as the amount of SF increases. After efflorescence and immersion tests, the Ca/Si ratio did not change significantly.

Table 5.3 Elemental analysis of unexposed specimens (dry), specimens after efflorescence test (eff), and specimens after immersion test (imm).

Elements	BFS-SF0 (mass%)			BFS-SF5 (mass%)			BFS-SF10 (mass%)			BFS-SF15 (mass%)		
	Dry	Eff.	Imm.	Dry	Eff.	Imm.	Dry	Eff.	Imm.	Dry	Eff.	Imm.
C	6.67	5.75	10.56	7.53	6.23	13.82	6.79	7.19	12.42	8.05	10.41	16.20
Si	11.50	11.94	10.97	12.43	12.50	13.49	14.69	13.95	13.94	15.62	14.13	14.00
Al	6.27	6.88	6.47	5.65	5.91	5.67	5.61	5.84	7.73	5.14	4.86	6.68
Na	8.52	5.49	N/A	8.73	7.92	0.53	8.01	7.85	0.71	8.55	8.22	1.26
Mg	3.83	4.65	7.94	3.81	4.10	5.29	3.91	3.95	10.42	3.48	3.43	6.37
O	46.61	46.00	47.77	45.29	46.21	43.88	43.44	44.39	41.91	44.02	44.62	43.47
Ca	16.27	18.32	15.97	15.84	16.27	17.16	16.78	16.04	12.00	14.18	13.49	11.59
S	1.02	0.73	N/A	0.70	0.71	N/A	0.63	0.66	N/A	0.80	0.64	N/A
Ti	N/A	0.23	0.34	N/A	N/A	N/A	N/A	N/A	0.62	N/A	N/A	0.34

Figure. 5.7(b) presents the Na/Si atomic ratios of specimens before and after the efflorescence and immersion tests. There is no significant change in the Na/Si ratio in specimens containing SF after the efflorescence test, which can indicate a lower amount of unreacted sodium. Mixture BFS-SF0 presents a significant reduction in Na/Si ratio, which is attributed to the higher amounts of unreacted sodium that migrate to the surface and precipitate. After the immersion test, Na/Si in all samples decreased considerably due to leaching. The EDS result also proves full leaching of sodium in BFS-SF0, which also indicates a weak bound of alkali in AAS system. Davidovits explained that the presence of alkali could balance the negative charge of alumina tetrahedral in the structure (Davidovits, 2017). However, the fact that alkali can be fully leached in water raises a question about the actual role of alkali in the alkali-activated binder system, whether it is an essential element in gel structure or just a residual from the activator solutions. The addition of SF seems to be beneficial in improving the alkali binding property since a small amount of sodium was still observable after 28 d immersion.

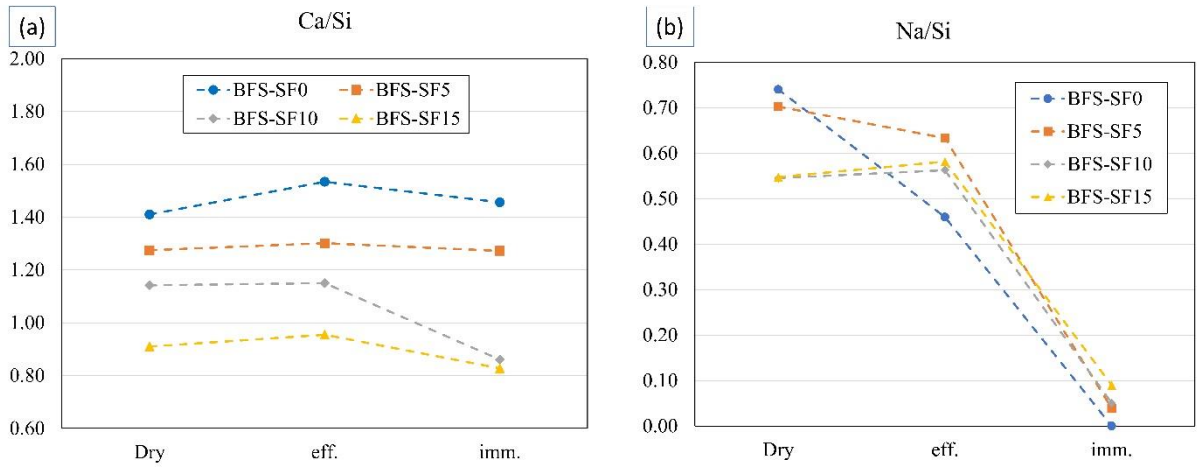

Figure 5.7 Ca/Si (a) and Na/Si (b) ratio of unexposed ambient-cured specimens (dry), specimens after efflorescence test (eff), and specimens after immersion test (imm).

In addition, the chemical composition of the AAS product may significantly affect the efflorescence and alkali leaching. It can be seen that the inclusion of 15% SF reduces the

Na/Si ratio, and consequently, the efflorescence formation and alkali leaching rate were reduced significantly.

5.4 Microstructures

Figure 5.8 shows the microstructure of BFS-SF0 and BFS-SF15 specimens before and after the immersion test. Despite rapid efflorescence formation and a higher alkali leaching rate, the ambient-cured BFS-SF0 exhibits a more compact and homogenous structure than BFS-SF15. BFS-SF15 shows a more porous microstructure because of the oxidation of free silicon from silica fume in an alkaline solution. When this process occurs, molecular hydrogen (H_2) will be released, and $Si(OH)_4$ is produced according to (Prud'homme et al., 2010) :

$$4H_2O + Si \rightarrow 2H_2\,(g) + Si(OH)_4$$

Some previous studies mentioned that the addition of SF improves the microstructure and reduces the total porosity of geopolymer and AAS concretes (Okoye et al., 2016; Rostami and Behfarnia, 2017), which are in contrast with the result of this study. This is understandable since concrete is composed of several kinds of materials with different particle sizes, and therefore, the addition of SF will fill the pores and spaces between particles. In our study, the addition of SF generates more pores, as shown by SEM images. In general, higher porosity will cause faster leaching, which leads to faster efflorescence formation, as explained by Zhang et al. (Z. Zhang et al., 2014). More detail related to porosity is explained in the section for water absorption and porosity.

Comparing the micrograph of BFS-SF0 before and after immersion (at 1000× magnification), the crack widths are smaller in samples after immersion. A similar result was obtained for BFS-SF15. The reduction in crack widths after the immersion test could be attributed to the higher moisture due to the availability of water, hence extending the period

of reaction of the materials. This results in the improvement of gel formation that finally refines the cracks.

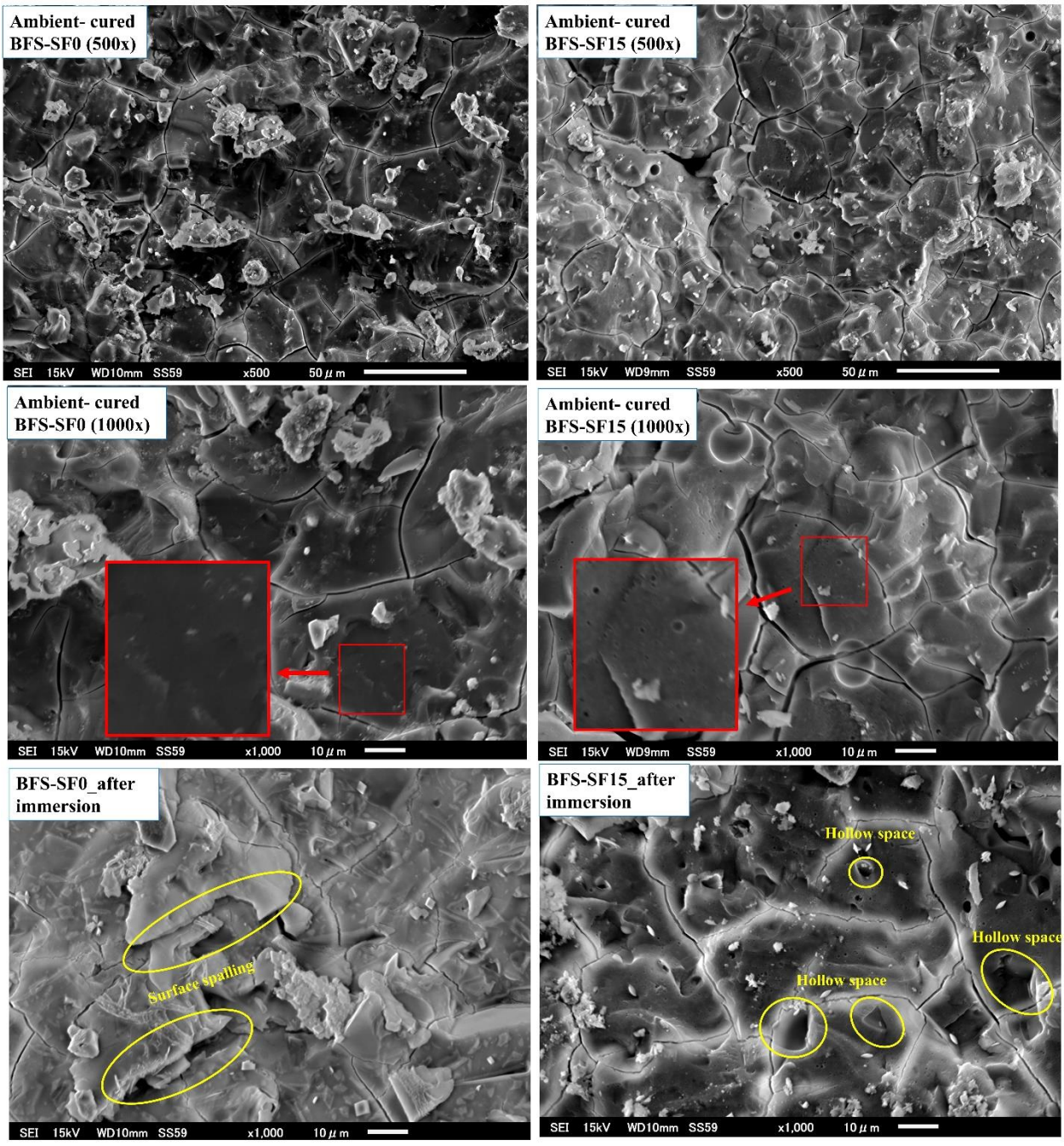

Figure 5.8 Micrograph of AAS specimens: BFS-SF0 (left) and BFS-SF15 (right) after ambient temperature curing and immersion test.

Although the crack width is reduced with high moisture contents, alkali leaching presents an adverse impact on microstructure, which is the formation of some hollow spaces

as the result of the removal of some compounds from the matrix. This phenomenon, in turn, results in coarse microstructure when compared to their corresponding samples cured at ambient temperature. In this case, the sodium-based compound is the most prone compound to be washed away since the EDS results proved that Na/Si ratio is reduced significantly after immersion. In addition, in the BFS-SF0 sample, damage on the surface (surface spalling) was observed. In fact, because of its very compact microstructure, further gel and crystal formation can generate pressure, resulting in surface spalling.

5.5 Porosity and Water Absorption

Figure 5.9(a) presents the effect of SF on the water absorption of AAS specimens. BFS-SF0, which showed rapid efflorescence formation and alkali leaching rate, corresponds to the lowest water absorption among the four series of specimens. The water absorption of specimens increases with an increase in SF content. However, the inclusion of 15% SF shows a slight decrease in water absorption compared to the specimen containing 10% SF.

In addition to water absorption, an MIP test was performed to evaluate the pore size distribution, and the result was presented in Fig. 5.9(b). As explained earlier in Chapter 3, the MIP result does represent the actual pore size, but it can be used as a comparative indication of the total porosity of the specimens. The total porosity of AAS under different dosages of SF presents a similar tendency to the water absorption. Mixture BFS-SF0 shows the lowest total pore volume. Increasing the SF content increases the total porosity. Unlike in mortar and concrete, the porosity of which decreased with the inclusion of SF, paste specimens present the increase in total pore volume with the increased amount of SF.

Specimens with 0%, 5%, and 10% SF present a plateau in similar pore size (approx. 100-1000 nm). Increasing the amount of SF up to 15%, the increment of pore diameter is observed in pore less than 100 nm. BFS-SF15 shows lower water absorption and total pore volume than BFS-SF10 because BFS-SF15 has a smaller pore size.

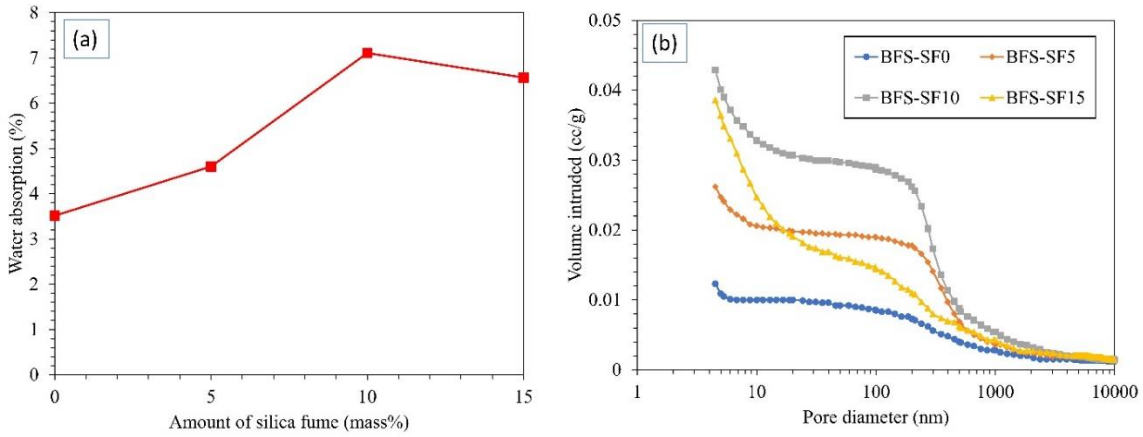

Figure 5.9 Water absorption (a) and pore size distribution (b) of AAS products under various dosage of SF

A specimen without SF shows lower water absorption and total pore volume but faster alkali leaching, and rapid efflorescence formation compared to specimens containing SF. Therefore, in this study, porosity becomes a less important factor that influences the alkali leaching and efflorescence formation.

5.6 Summary

From the above-mentioned experimental results, the following conclusion can be drawn:

a. The inclusion of SF reduces the alkali leaching rate and the efflorescence formation. This was attributed to the fact that incorporating SF into the AAS system reduces the Na/Si atomic ratio; thus less sodium particles will remain unreacted in the matrix.
b. The efflorescence deposition rate strongly depends on the free alkali content; specimens with a higher amount of unreacted sodium exhibited faster efflorescence. The inclusion of 15% SF exhibited the best performance as it presents the lowest alkali leaching rate and total alkali leaching, which results in the lowest efflorescence formation.
c. The elemental analysis by EDS proved that the alkali could be completely leached from the test sample after being immersed in water for 28 d. Samples containing SF exhibited

good alkali binding property since a small amount of sodium was observable after immersion when compared to the sample containing 0% SF.

d. After immersion, some hollow spaces were formed in the sample due to the removal of some compounds. However, immersion in water led to the crack's refinement because of the presence of moisture that extended the reaction period and gel period.

Some previous studies suggested that porosity has a strong correlation to alkali loss, but it is not the case in this study. Water absorption and porosity tests performed in this study exhibit that porosity becomes the less important factor in alkali leaching and efflorescence formation in alkali-activated slag; specimen without SF presents lower porosity and water absorption but faster alkali leaching and rapid efflorescence formation when compared to specimens containing SF which have higher porosity.

CHAPTER 6. ALKALI LEACHING AND MECHANICAL PERFORMANCE OF EPOXY RESIN-REINFORCED GEOPOLYMER COMPOSITE

This chapter provides the results of an experimental investigation on the alkali leaching and mechanical performances of fly ash/slag-based geopolymer reinforced by bisphenol F type epoxy resin. Epoxy resin is widely used as a coating material, but recently it has been applied as repair material in concrete production. Geopolymers are known to have brittle properties, thus having low flexural strength. It is expected that incorporating epoxy resin into the geopolymer system can improve the flexural strength of the geopolymer.

The dissolution behavior of OPC is determined predominantly by chemical composition and particle fineness. Meanwhile, in geopolymer, the dissolution is not only controlled by these properties, but it is also strongly controlled by the concentration of alkali hydroxide solution. The results of the previous study (Saludung et al., 2019) suggested that the role of sodium remains unclear since ambient-cured alkali-activated binder leached alkalis at a fast rate. Since the alkalis can be leached out easily in water, in this study, the effect of alkali leaching on mechanical strength was investigated by curing the fly ash/slag-based geopolymer specimens in water to leach some alkalis. Interestingly, incorporating a small amount of epoxy resin improves not only the mechanical strengths but also the alkali binding property. Part of the results and discussions of this experimental study has been published in author's research paper (Saludung et al., 2021b).

6.1 Phase Composition

Figure 6.1 represents the XRD patterns of neat geopolymer and geopolymer composite doping with 2.5% epoxy resin after curing for 28 days. It can be seen that the major components of geopolymer made from fly ash and slag are amorphous, as reflected by the broad hump from 15 to 35° 2-theta, with some crystalline phases of mullite ($Al_6Si_2O_{13}$) and

quartz (SiO_2) originated from fly ash. The replacement of fly ash by slag leads to the formation of poorly crystalline Al-substituted C-S-H gels (C-A-S-H), as indicated by the peak centered around 29° 2-theta (Saha and Rajasekaran, 2017; Z. Zhang et al., 2014).

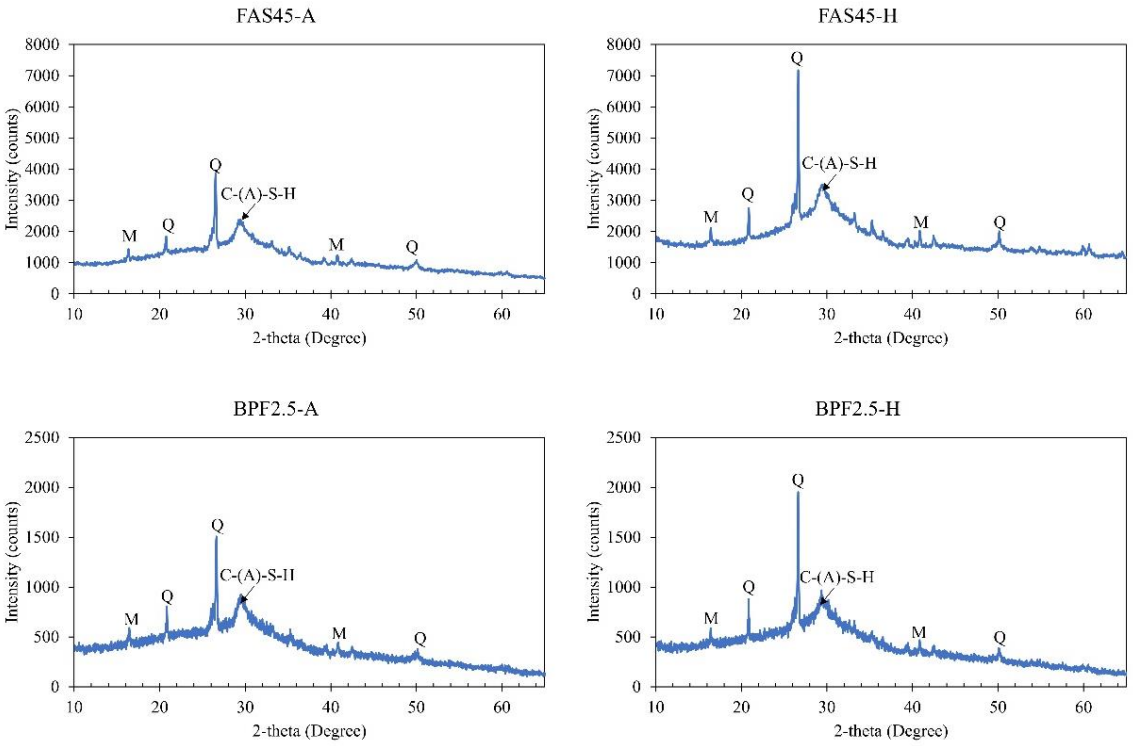

Figure 6.1 XRD pattern of neat geopolymer and geopolymer composite doping with 2.5% epoxy resin after curing for 28 days (A=ambient curing, H=Heat curing).

The neat geopolymer and geopolymer composite present similar diffraction patterns; however, the intensity of diffraction peaks in the geopolymer composite is much lower than that in neat geopolymer. For instance, the quartz peak in FAS45-H shows higher intensity than that in BPF2.5-H. Intensity is proportional to the number of scatterers per unit area of a given atomic plane. Peak intensity also reflects the absorption and the amount of phase in the mixture (Jian, 2003). Therefore, the addition of epoxy resin may affect the amount of gel phases formed in the system. Moreover, regardless of the epoxy resin doping amount, the intensity of diffraction peak in the ambient-cured specimen is lower than that in heat-cured specimens, indicating that curing temperature also influences the reaction products.

6.2 Thermal Analysis

The TG-DTA analysis was performed on the neat geopolymer and geopolymer composites after curing. The sharp decrease in mass before 200 ℃ observed in all specimens in Fig. 6.2 is attributed to the evaporation of free water that commences at the temperature ranges from room temperature to 100 ℃ and the removal of physically and chemically bound water at a temperature above 110 ℃ from geopolymer structure and C-(A)-S-H gel (Khoury et al., 2002). Further loss in mass could be attributed to the further decomposition of C-(A)-S-H. The effect of epoxy resin on the mass loss was insignificant as neat geopolymer (FAS45-A), and geopolymer composites present almost similar total mass. In geopolymer composite, the mass loss could also be attributed to the decomposition of epoxy resin. However, since only a small amount of epoxy resin was incorporated, the total mass loss does not vary significantly. The ambient-cured FAS45 (FAS45-A) shows higher total mass loss than the heat-cured FAS45 (FAS45-H), which could be attributed to the higher amount of water in the ambient-cured specimen (see Fig. 6.2(a)). The detail about thermal properties of overall samples is provided in Table 6.1. The water loss behavior can provide some useful information regarding the pore structure. Since ambient-cured FAS45 losses much water, it could contain large pores compared to the heat-cured specimen. The detail regarding porosity is provided in section 6.5.

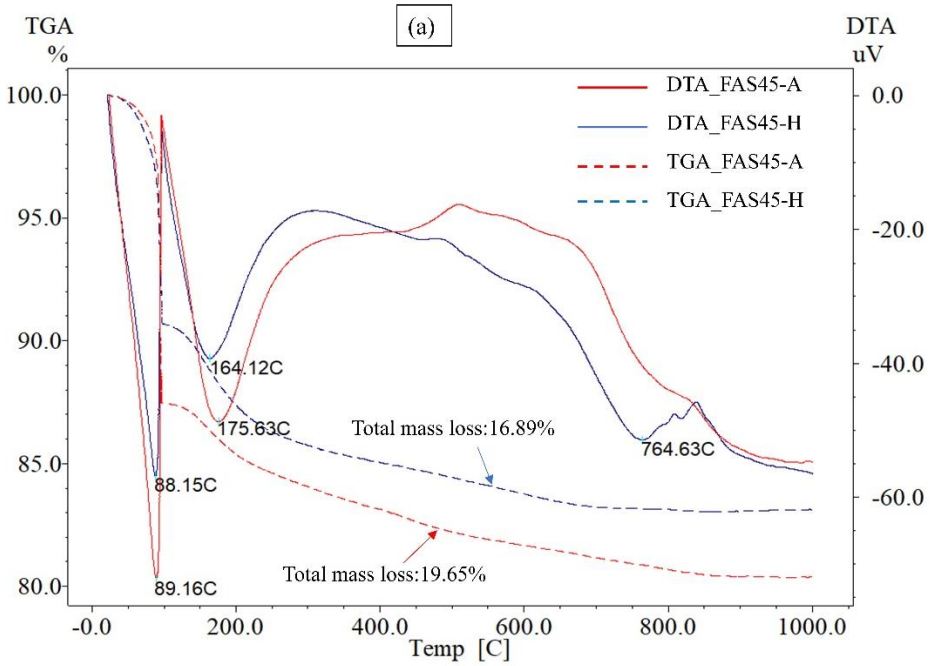
(a)
TGA
%
DTA
uV
DTA_FAS45-A
DTA_FAS45-H
TGA_FAS45-A
TGA_FAS45-H
100.0
95.0
90.0
85.0
80.0
0.0
-20.0
-40.0
-60.0
164.12C
175.63C
Total mass loss:16.89%
764.63C
88.15C
89.16C
Total mass loss:19.65%
-0.0
200.0
400.0
600.0
800.0
1000.0
Temp [C]

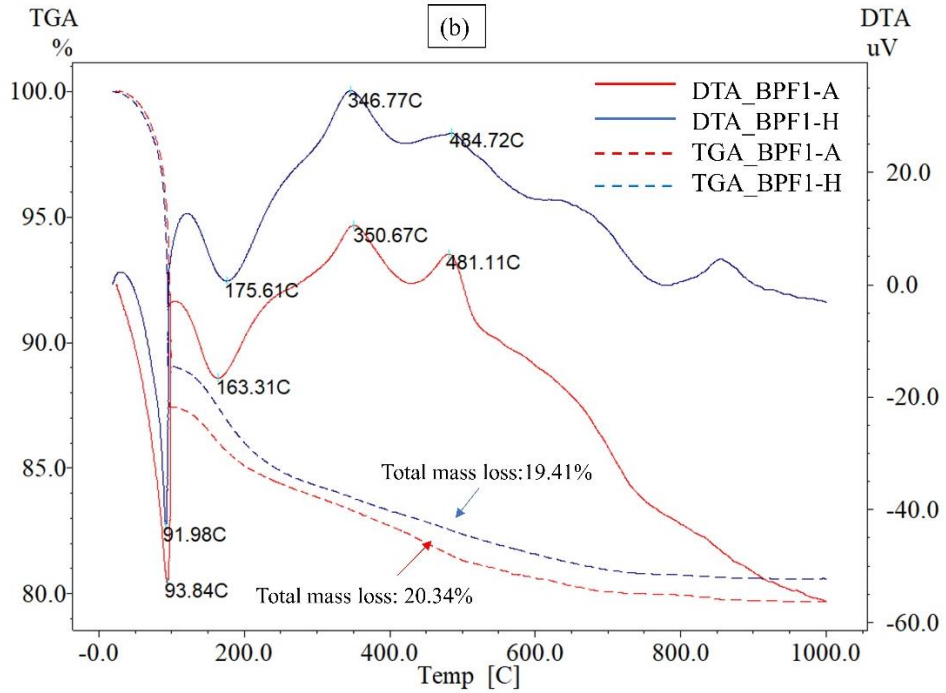
(b)
TGA
%
DTA
uV
DTA_BPF1-A
DTA_BPF1-H
TGA_BPF1-A
TGA_BPF1-H
100.0
95.0
90.0
85.0
80.0
20.0
0.0
-20.0
-40.0
-60.0
346.77C
484.72C
350.67C
481.11C
175.61C
163.31C
Total mass loss:19.41%
91.98C
93.84C
Total mass loss: 20.34%
-0.0
200.0
400.0
600.0
800.0
1000.0
Temp [C]

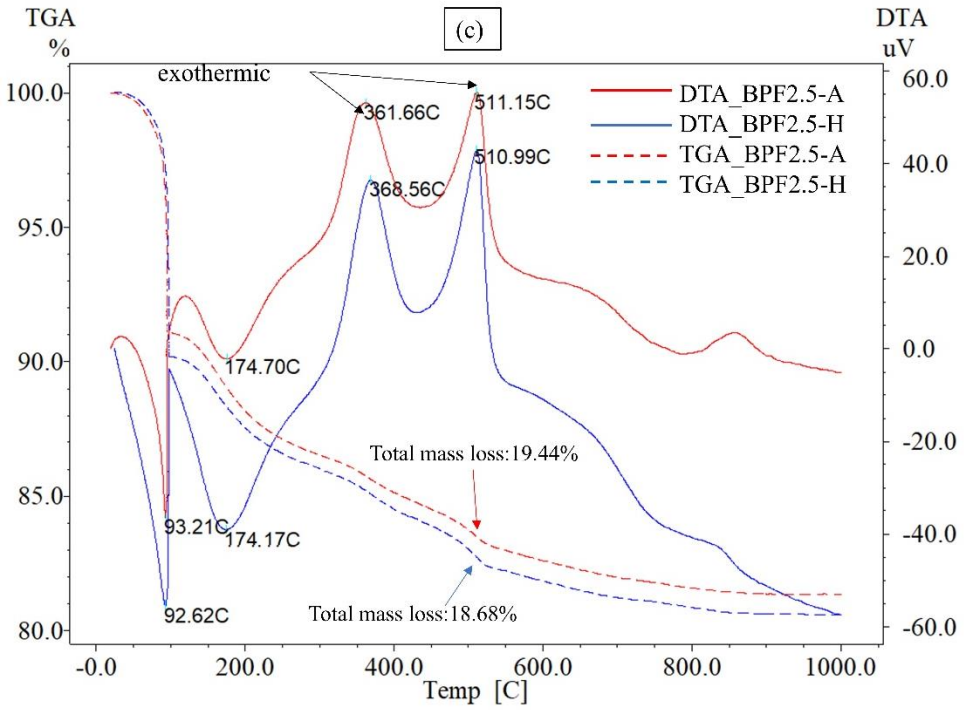

Figure 6.2 TG-DTA curves of FAS45 (a), BPH1 (b), and BPF2.5 (c). (A= Ambient curing, H= Heat curing).

Table 6.1 Thermal properties of geopolymer composites cured at ambient condition (A) and initially high temperature (H).

Sample ID	**Temperature at 5% mass loss (ºC)**	**Mass loss ending temperature (ºC)**	**Residual at 1000 ºC (mass%)**
FAS45-A	94	840	80.35
FAS45-H	93	710	83.11
BPF1-A	94	850	79.66
BPF1-H	93.5	850	80.59
BPF2.5-A	96	830	80.56
BPF2.5-H	94.5	860	81.32

Mass losses from TG analysis are related to the phase changes represented by DTA curves. The DTA analysis shows two major endothermic peaks in all samples, which correspond to the free water evaporation (first endothermic peak) and the removal of

physically and chemically bound water (second endothermic peak). The decomposition of epoxy resin is an exothermic event because it releases energy in the form of heat (Salasinska et al., 2019). Therefore, Figs. 6.2(b and c) show that the DTA curve of specimens containing epoxy resin also presents two major exothermic peaks observed at around 346-368 ℃ and 481-511℃.

6.3 Alkali Leaching

As mentioned earlier in the previous chapter, the alkali is weakly bound in the gel structure and can leach out easily in water. The leaching of alkali can be minimized by applying heat curing; however, this limits the application of geopolymer to precast concrete only.

Figures 6.3 (a) and (b) present the alkali leaching rate and total leaching amount of alkali, respectively. For ambient-cured specimens, the inclusion of epoxy resin significantly reduces the alkali leaching rate at the early immersion period and the total alkali leaching after 28 d immersion. This could be attributed to the chemical interaction between resin and alkali solution. Al-Borno et al. reported that the carboxyl group results from the hydrolysis of the ester linkages could react with NaOH (Al-Borno et al., 2015). Therefore, it is suggested that the additional chemical reaction between the epoxy resin and NaOH consumes more sodium, resulting in the decrease of the amount of unreacted sodium particles; however, this reaction can possibly hinder the polycondensation reaction.

The reduction in the amount of unreacted sodium can reduce the efflorescence potential, hence promising the extensive application of ambient-cured geopolymer. Although heat-cured specimens show significantly lower alkali leaching than ambient-cured specimens, the effect of epoxy resin on the alkali leaching rate and total alkali leaching in heat-cured specimens was insignificant. This indicates that the effect of high temperature curing seems to be more predominant than the effect of epoxy resin in reducing the unreacted sodium particles.

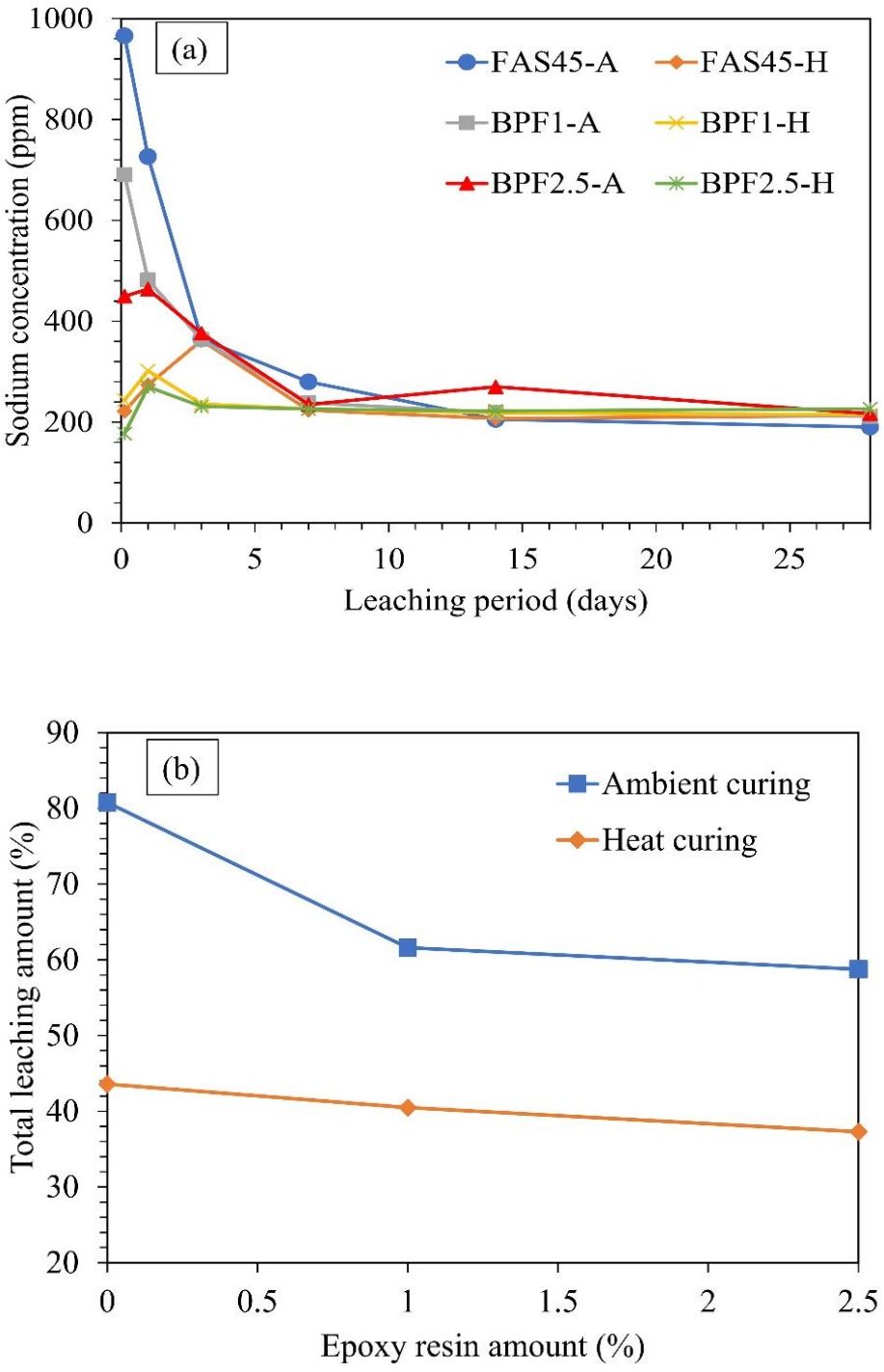

Figure 6.3 Sodium concentration in water (a), and total leaching amount of sodium after 28 days immersion (b). (A= Ambient curing, H= Heat curing).

6.4 Mechanical Strength at Various Curing Conditions

The compressive and flexural strengths of geopolymer and geopolymer composites cured at ambient temperature, high temperature (70 °C), and in water at 20 °C were measured and

discussed. Water curing was applied to observe the effect of alkali leaching on the mechanical strengths of specimens since the specimens could leach significant amount of alkali when immersed in water.

6.4.1 Compressive strength

The influence of BPF epoxy resin on compressive strength is shown in Fig. 6.4. Incorporating epoxy resin into the geopolymer matrix was observed to have slight enhancement on the 28d-aged compressive strength when cured initially at 70 ℃. For specimens cured at ambient temperature, the inclusion of 1% epoxy resin (BPF1-A) exhibits maximum compressive strength at the age of 28 d, while the inclusion of 2.5% epoxy resin resulted in the same compressive strength value as a reference.

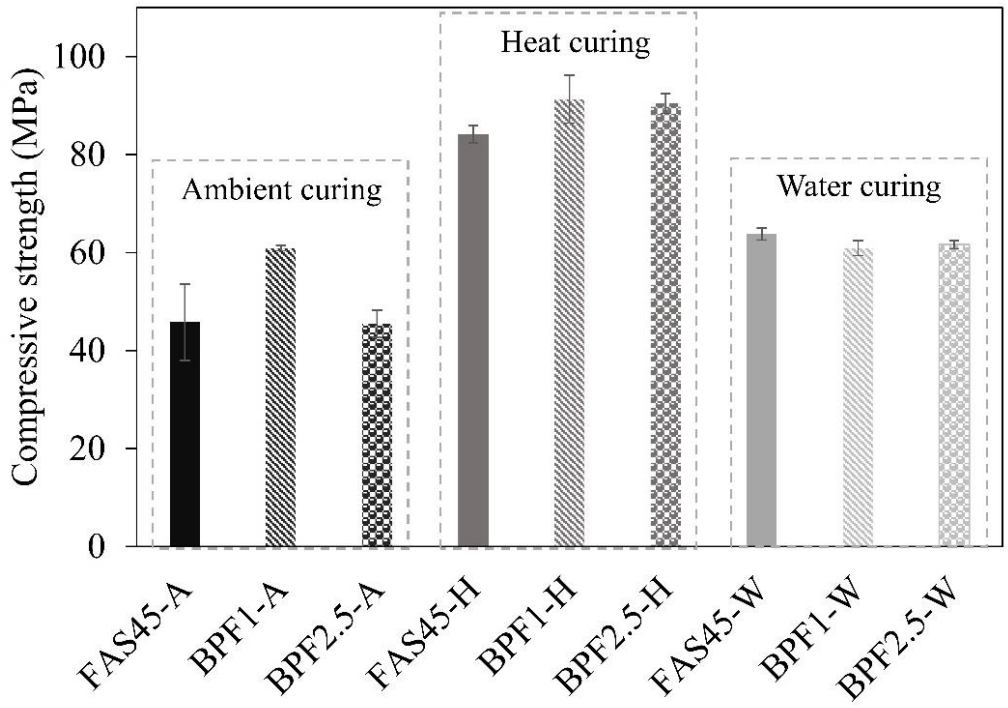

Figure 6.4 Compressive strength of neat geopolymer (FAS45) and geopolymer composites (BPF1 and BPF2.5) at different curing conditions.

The improvement of compressive strength by 1% epoxy resin could be due to the filling effect. Although the addition of epoxy resin up to 2.5% can significantly reduce the amount of unreacted sodium, the compressive strength was adversely affected. This could be due to the higher dosage of epoxy resin reduces the homogeneity of the matrix, resulting in a coarser microstructure.

The influence of epoxy resin on the compressive strength of the specimens cured in water was insignificant since all mixtures show almost similar compressive strength values. However, it is noteworthy that the compressive strength of water-cured specimens was high compared to their corresponding samples cured at ambient temperature (except for BPF1-A and BPF-W which show almost similar compressive strength values). As mentioned earlier, immersion in water causes significant alkali leaching; however, the compressive strength value indicates that the alkali leaching did not negatively influence the compressive strength.

6.4.2 Flexural strength

The flexural strength of all mixtures at 28 days is shown in Fig. 6.5. Geopolymer containing 1% epoxy resin displayed the highest flexural strength at all curing conditions. The reason could be that epoxy resin could absorb part of the load by plastic deformation. For higher resin content (2.5%), the flexural strength tends to decrease up to a value equal or higher than the flexural strength of the neat geopolymer. The reason for the decrease of flexural strength at this epoxy resin dosage remains unclear, but it could be partly due to the crack formation caused by inhomogeneous microstructure.

In addition, flexural strength is also affected by curing conditions. Regardless of the epoxy resin amount, ambient-cured specimens show the highest flexural strength, followed by the heat-cured and water-cured specimens. Heat curing showed a beneficial effect on compressive strength but an unbeneficial impact on flexural strength. Despite accelerating

the gel formation increasing the compressive strength, the heat curing process caused some level of material drying and cracking. As a result, heat-cured specimens became brittle and had low flexural strength. Meanwhile, the lowest flexural strength of water-cured specimens could be attributed to the water absorption.

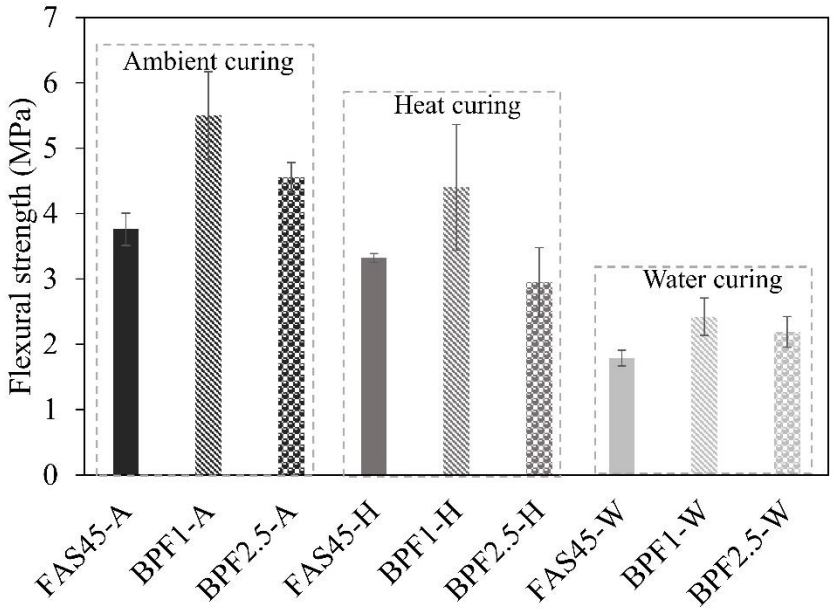

Figure 6.5 Flexural strength of neat geopolymer (FAS45) and geopolymer composites (BPF1 and BPF2.5) at different curing conditions.

6.4.3 Flexural/compressive strength ratio

Figure 6.6 presents the flexural and compressive strength (F/C) ratio. Some previous studies used the value of F/C ratio to evaluate the effect of using reinforcements in improving the strengths of geopolymer and OPC concretes (Ruan et al., 2018; Yu et al., 2012). The value of the F/C strength ratio can also reflect to the brittleness of a material, the lower the ratio, the more brittle the material (Chen et al., 2018a; Tian et al., 2020; Wang et al., 2019). For ambient curing, the increase in epoxy resin content leads to the increase of the F/C strength ratio, thus suggesting the positive role of epoxy resin in reducing the brittleness of geopolymer. However, the F/C strength ratio shows the maximum value for heat and water-cured specimens when 1% epoxy resin was added. In addition to the effect of curing

conditions, specimens cured in ambient condition show the highest F/C value, thus suggesting that ambient-cured geopolymer is less brittle than heat-cured and water-cured geopolymer.

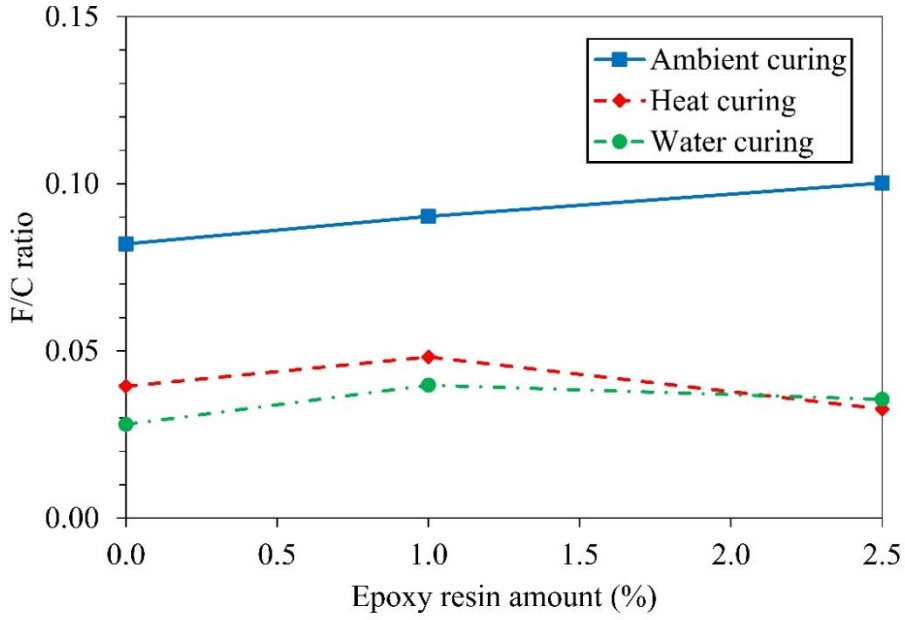

Figure 6.6 Flexural and compressive strengths (F/C) ratios

6.5 Porosity

Figures 6.7 present the pore size distribution of neat geopolymer and geopolymer composite. It can be seen that the distribution of pore sizes of the specimens varies significantly depending on the amount of epoxy resin and curing conditions. Fig. 6.7(a) shows that all ambient-cured specimens present a plateau in a similar pore size where the largest pore volume is associated with pores between 0.1 and 1 μm. However, in the case of ambient-cured BPF2.5, bigger pores are predominant, even though its compressive strength shows similar value to the reference. When increasing the curing temperature, the increment of the pore volume is observed in pores less than 0.02 μm. High-temperature curing promotes gel formation, resulting in a more compact microstructure compared to those cured at ambient temperature. It can be seen that the total pore volume of the heat-cured specimens decreased

with the increased amount of epoxy resin. As a result, a slight enhancement in compressive strength was observed in heat-cured specimens.

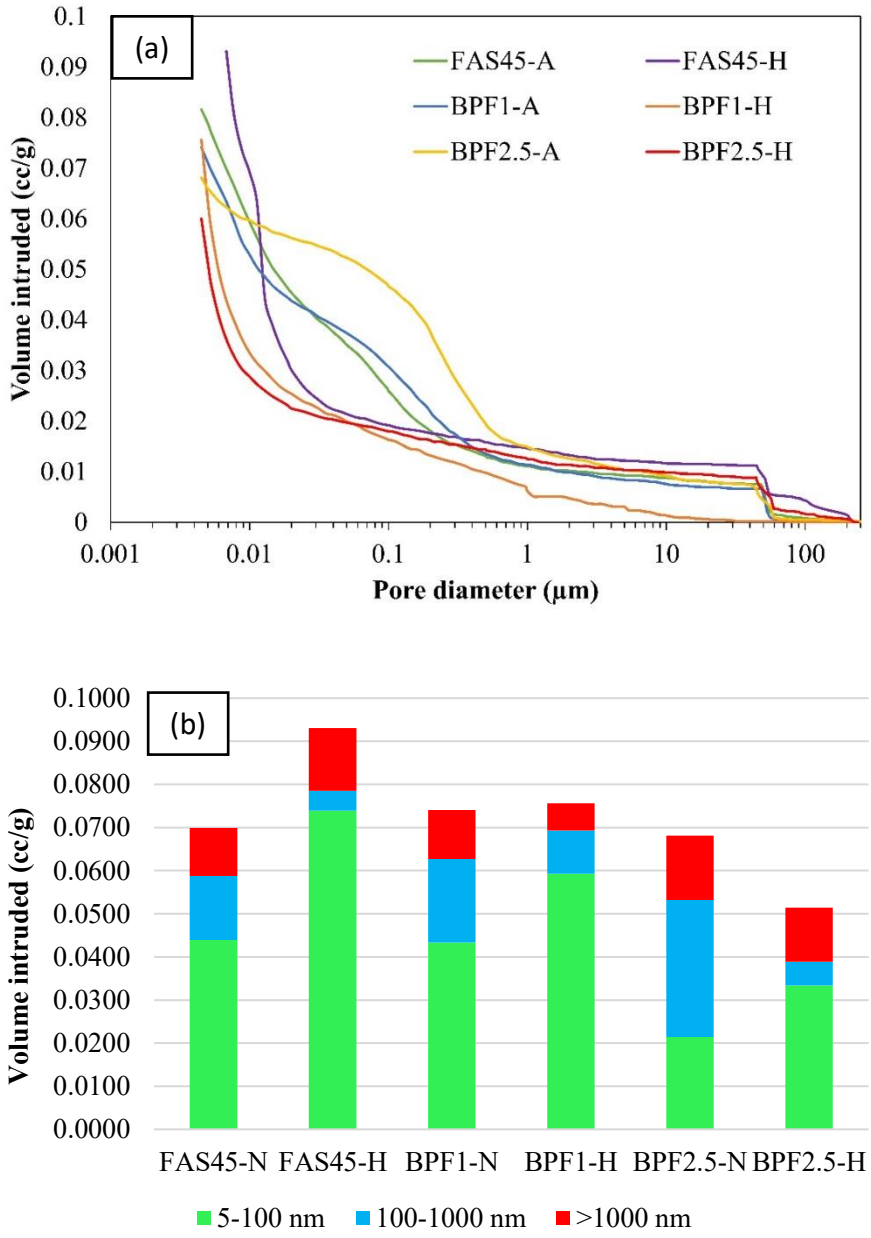

Figure 6.7 Pore size distribution (a) and pore size classification (b) of neat geopolymer and geopolymer composites cured at ambient (A) and initially high temperatures (H).

Fig. 6.7(b) shows that the heat-cured specimens contain higher proportion of small capillary pores (pores with diameter ranges from 5–100 nm) and a less proportion of large capillary pores (pores with diameter ranges from 100-1000 nm) compared to ambient-cured

specimens. The addition of epoxy resin likely reduces the total porosity of geopolymer cured at high temperature. However, for those cured at ambient temperature, the addition of 2.5 % epoxy resin increased the proportion of bigger pores. This could be the reason why the compressive strength of ambient-cured specimen decreased at this epoxy resin dosage.

6.6 Microstructure by SEM

Figure 6.8 presents the SEM micrographs of specimens. Some cracks are observable in all specimens cured at both ambient and high temperatures. However, it is worth noting that the ambient-cured specimens (left figures) present larger cracks width compared to heat-cured specimens. This could be attributed to the low reactivity of fly ash at ambient temperature, resulting in slow gel formation. In comparison to ambient-cured specimens, a denser microstructure was observed in specimens cured initially at 70 °C, which is attributed to the formation of C-(A)-S-H gel. Moreover, higher curing temperature will result in a higher rate of geopolymerization, which accelerates the formation of a three-dimensional geopolymer network, resulting in a more homogenous and denser microstructure.

It is likely that the inclusion of epoxy resin reduces the homogeneity of the microstructure. This is probably because the addition of epoxy resin hindered the polycondensation reaction of the geopolymer system. However, the compressive strength and flexural strength are not negatively affected. It is also worth pointing out that, if we compare the neat geopolymer with the geopolymer composite cured initially at 70 °C, the number and the extension of the microcracks is reduced by the addition of 1% epoxy resin.

Although the MIP analysis shows that ambient-cured BPF2.5 predominantly consists of bigger pores compared to FAS45 (Ref.) and BPF1, no agglomeration of epoxy resin was observed, indicating that the epoxy resin is well dispersed in the geopolymer system.

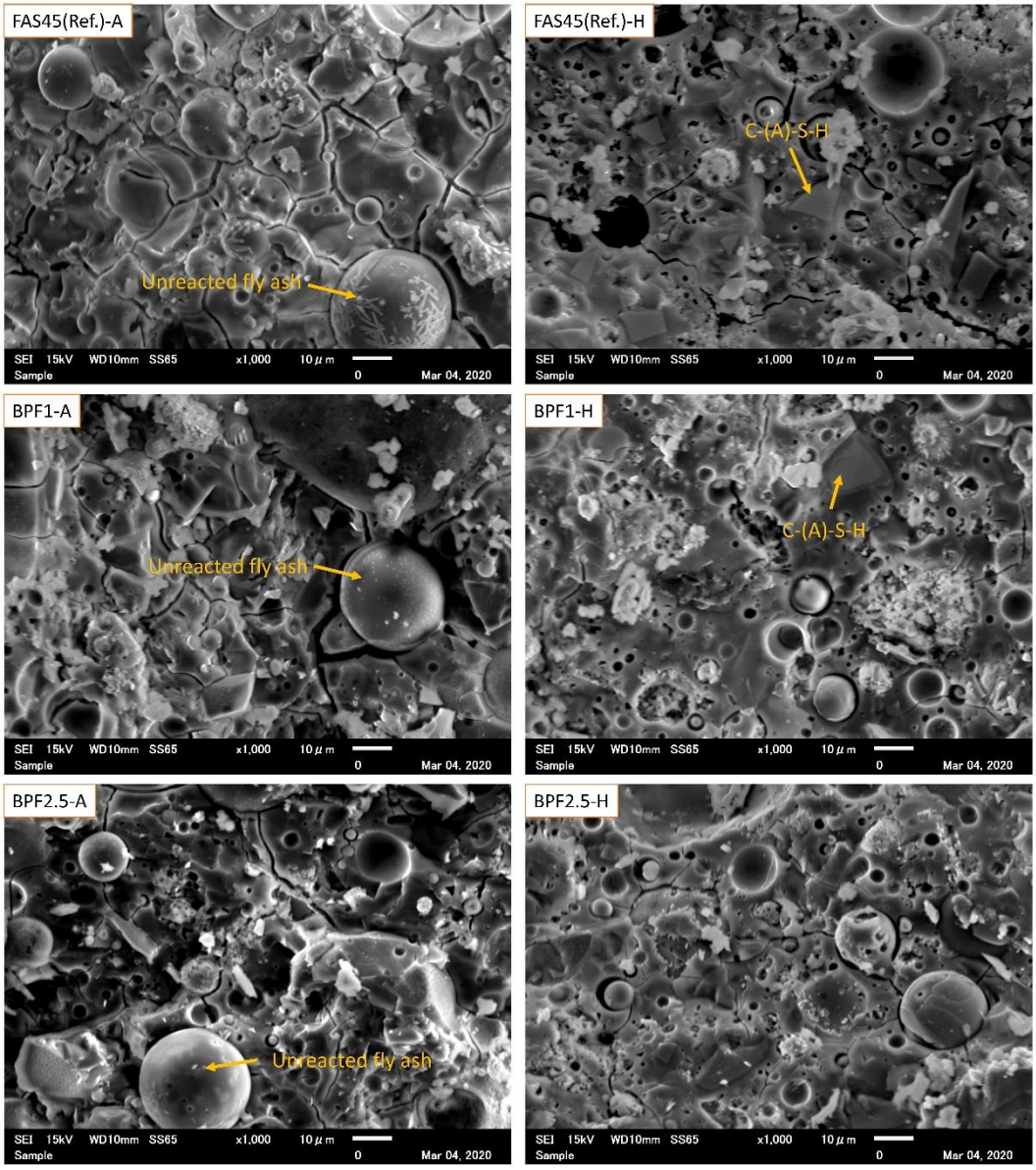

Figure 6.8 SEM micrographs of neat geopolymer and geopolymer composites cured at ambient (A) and initially high temperatures (H).

6.7 Summary

From the experimental results, the following conclusion can be drawn.

a. The addition of epoxy resin reduces the alkali leaching rate and total alkali leaching of ambient-cured geopolymer after immersion test for 28 d, while no significant influence of epoxy resin on alkali leaching was observed on heat-cured specimens.

b. The compressive strength of the ambient-cured specimen was up to maximum value while doping 1% epoxy resin.
c. Geopolymer composite doping with 1% epoxy resin displays the highest flexural strength at all curing conditions. Water curing causes significant loss of alkalis; however, a slightly higher compressive strength of water-cured specimens compared to ambient-cured specimens proved that alkali leaching did not negatively influence the compressive strength.

The improvement of mechanical strengths and alkali binding property of ambient-cured geopolymer by adding epoxy resin can lead to the extensive application of geopolymer binder in the construction industry.

CHAPTER 7. GENERAL CONCLUSIONS AND RECOMMENDATIONS

7.1 General Conclusions

Based on the results of experimental work reported in this study, the following conclusion can be drawn:

1. The addition of GGBS significantly increased the compressive strength, reaching a value of 94 MPa at 28 days when 60% GGBS was incorporated and cured initially at high temperature. However, the addition of GGBS reduced high temperature resistance of fly ash geopolymer due to the decomposition of the reaction products at high temperature. Despite a lower initial strength (24 MPa) at 28 days, geopolymer produced from full fly ash exhibited a lower degradation rate than the FA/GGBS geopolymer blends.
2. Geopolymers undergo phase transformation from amorphous to crystalline phases having an analogue to natural minerals. The crystallization of fly ash geopolymer is estimated to occur a temperature between 750 – 950 ℃, while in geopolymer containing GGBS (≥ 30%), the crystallization occurs at a lower temperature (>750 ℃).
3. Despite a significant loss in compressive strength, the sintering in fly ash geopolymer specimen leads to the formation of a liquid phase, which allows the joining of particles, resulting in the densification of pores and crack healing. By contrast, the sintering effect on high-Ca geopolymer was insignificant, probably because the matrix was dominated by the C-S-H gel.
4. Potassium geopolymer presents an increase of compressive strength after exposure to 950 ℃ due to sintering that occurs at a temperature lower than that of sodium geopolymer.
5. Alkali-activated slag specimen rapidly leached alkali when fully immersed in water. Incorporating silica fume into AAS could significantly reduce the alkali leaching at early

immersion period. This is crucial since the alkali leached at very early immersion period could be responsible for the efflorescence formation.

6. Accelerated efflorescence test shows that AAS specimens without silica fume exhibited more rapid efflorescence formation than specimens containing silica fume when putting in contact with water for 24 hours. This indicates that efflorescence could be related to the unreacted alkali particles, which can be leached from the specimen at a very early immersion period (from 0 to 24 hours).
7. Despite rapid efflorescence formation, AAS specimen without silica fume presents a highly dense structure with almost no pores observed by SEM. Incorporating a small amount of silica fume leads to a formation of some micropores due to the oxidation of free silicon in alkali environment.
8. Water absorption and porosity tests showed that the total porosity increased by the addition of silica fume. Despite a more compact microstructure, specimen without silica fume performed faster alkali leaching than specimens containing silica fume, indicating that porosity becomes a less important factor in the efflorescence formation of AAS, which is in contrast with the previous studies.
9. Reducing the Na/Si ratio by adding silica fume was found to be an effective way to control the efflorescence formation in AAS.
10. In fly ash/GGBS geopolymer composite, the alkali leaching of ambient-cured specimens was reduced by the addition of epoxy resin, while no significant influence of epoxy resin on the alkali leaching of heat-cured specimens.
11. The addition of epoxy resin significantly influences the compressive strength of ambient-cured geopolymers but shows an insignificant effect on the compressive strength of the heat and water-cured geopolymers. The compressive strength of the ambient-cured specimens was up to the maximum value when doping with 1% epoxy resin.

12. The addition of epoxy resin also remarkably influences the flexural strength of geopolymers. Geopolymers doping with 1% epoxy resin exhibited the maximum flexural strength at all curing conditions. Regardless of the epoxy resin dosages, ambient-cured geopolymers present the highest flexural strength, followed by heat-cured and water-cured specimens.
13. The porosity of geopolymer varies depending on the amounts of epoxy resin and curing conditions. Bigger pores are predominant in ambient-cured geopolymers doping with 2.5% epoxy resin, which could be the reason why the compressive strength of ambient-cured specimens decreased at this epoxy resin dosage. The curing temperature remarkably influences the porosity; the ambient-cured specimens are associated with pores between 0.1 and 1 μm, while in the heat-cured specimens, the increment of the pore volume is observed in pore less than 0.02 μm.
14. Specimens cured in water leached significant amounts of sodium, but they exhibited comparable, even higher compressive strength than those cured at ambient temperature. This result indicates that the alkali leaching did not affect the compressive strength adversely. The lower flexural strength of ambient-cured specimens compared to specimens cured at ambient and high temperature could be due to the water absorption.

7.2 Recommendations for Future Works

Based on the experiences gained from this study, the drawbacks of this study should be developed according to the following recommendations and considerations.

1. Although the compressive strength loss and phase change analysis performed in this study could be an indicator of how the materials resist high temperature, other parameters such as porosity measurement after exposure to high temperature is crucial to grasp the change in the pore structure of materials as the impact of temperature. Other analysis

tools such as Fourier transform infrared (FTIR) and magic angle spinning nuclear magnetic resonance (MAS NMR) spectroscopy are also useful to identify the structural change. The FTIR peak shifting has been appeared to be a sensitive tool for detecting the structural changes of materials, while MAS NMR is a useful technique to directly identify the coordination status between silica and alumina units.

2. Since the exposure temperature in this study were 500, 750, and 950 ℃, the exact temperature of phase transformation could not be confirmed. Therefore, for the future work, it is suggested to investigate the geopolymer properties at every 100 ℃ temperature increment to know when exactly the crystallization on geopolymer starts. It was assumed that the crystallization starts at a temperature above 500 ℃ for the high-Ca geopolymer, and above 750 ℃ for low-Ca geopolymer.
3. A higher temperature exposure (>1000 ℃) should be considered to observe the structural change of geopolymer because in some cases, the temperature of fire occurs in a building can exceed 1200 ℃, depending on what causes the fire.
4. Although XRD analysis on AAS shows a peak broadening as the impact of adding silica fume, other characterization tool such as FTIR is crucial to support the present XRD results.
5. The DTA peak shows an exothermic event which can indicate the phase transformation of C-S-H to wollastonite at high temperature. Further study on structural change of AAS after high temperature is required to confirm the formation of wollastonite. Wollastonite is used primarily in ceramics, therefore, understanding the formation of this phase in AAS can be beneficial for the synthesis of low-temperature ceramic through an alkali activation method.
6. The compressive strength should be measured to grasp the effect of silica fume on the mechanical properties of AAS.

7. Due to a significant alkali leaching, the heat resistance of geopolymer specimen cured in water needs to be investigated since the alkali plays a crucial role in the phase transformation of geopolymer at high temperatures. The transformation of amorphous geopolymer into alkali feldspar at high temperature is believed as one of the main reasons why geopolymer materials possess better heat resistance than Portland cement material.
8. The investigation on the effect of epoxy resin on the heat resistance of geopolymer is required because the epoxy resin will smoke and release toxic fumes when overheated. However, if combined with the flame retardant material such as geopolymer, it may provide sufficient fire retardant effect. Therefore, investigating the behavior of epoxy resin-reinforced geopolymer at elevated temperature is crucial to expand the application of this type of composite material.

References

Abdulkareem, O.A., Mustafa Al Bakri, A.M., Kamarudin, H., Khairul Nizar, I., Saif, A.A., 2014. Effects of elevated temperatures on the thermal behavior and mechanical performance of fly ash geopolymer paste, mortar and lightweight concrete. Constr. Build. Mater. 50, 377–387. https://doi.org/10.1016/j.conbuildmat.2013.09.047

Al-Borno, A., Chen, X., Kewaldas Dhoke, S., 2015. Effect of High Temperature Sodium Hydroxide Immersion on Fusion Bond Epoxy Coating. Int. J. Corros. 2015. https://doi.org/10.1155/2015/903478

Alehyen, S., Zerzouri, M., El Alouani, M., El Achouri, M., Taibi, M., 2017. Porosity and fire resistance of fly ash based geopolymer. J. Mater. Environ. Sci. 8, 3676–3689.

Alomayri, T., Low, I.M., 2013. Synthesis and characterization of mechanical properties in cotton fiber-reinforced geopolymer composites. J. Asian Ceram. Soc. 1, 30–34. https://doi.org/10.1016/j.jascer.2013.01.002

Alomayri, T., Shaikh, F.U.A., Low, I.M., 2013. Characterisation of cotton fibre-reinforced geopolymer composites. Compos. Part B Eng. 50, 1–6. https://doi.org/10.1016/j.compositesb.2013.01.013

Alonso, C., Fernandez, L., 2004. Dehydration and rehydration processes of cement paste exposed to high temperature environments. J. Mater. Sci. 39, 3015–3024. https://doi.org/10.1023/B:JMSC.0000025827.65956.18

Andrew, R.M., 2019. Global CO2 emissions from cement production, 1928-2018. Earth Syst. Sci. Data 11, 1675–1710. https://doi.org/10.5194/essd-11-1675-2019

Bakharev, T., 2006. Thermal behaviour of geopolymers prepared using class F fly ash and elevated temperature curing. Cem. Concr. Res. 36, 1134–1147. https://doi.org/10.1016/j.cemconres.2006.03.022

Bernal, S., De Gutierrez, R., Delvasto, S., Rodriguez, E., 2010. Performance of an alkali-activated slag concrete reinforced with steel fibers. Constr. Build. Mater. 24, 208–214. https://doi.org/10.1016/j.conbuildmat.2007.10.027

Bhardwaj, B., Kumar, P., 2019. Comparative study of geopolymer and alkali activated slag concrete comprising waste foundry sand. Constr. Build. Mater. 209, 555–565.

https://doi.org/10.1016/j.conbuildmat.2019.03.107

Carabba, L., Santandrea, M., Carloni, C., Manzi, S., Bignozzi, M.C., 2017. Steel fiber reinforced geopolymer matrix (S-FRGM) composites applied to reinforced concrete structures for strengthening applications: A preliminary study. Compos. Part B Eng. 128, 83–90. https://doi.org/10.1016/j.compositesb.2017.07.007

Carreño-Gallardo, C., Tejeda-Ochoa, A., Perez-Ordonez, O.I., Ledezma-Sillas, J.E., Lardizabal-Gutierrez, D., Prieto-Gomez, C., Valenzuela-Grado, J.A., Robles Hernandez, F.C., Herrera-Ramirez, J.M., 2018. In the CO2 emission remediation by means of alternative geopolymers as substitutes for cements. J. Environ. Chem. Eng. 6, 4878–4884. https://doi.org/10.1016/j.jece.2018.07.033

Chen, X., Zhu, G., Zhou, M., Wang, J., Chen, Q., 2018a. Effect of Organic Polymers on the Properties of Slag-based Geopolymers. Constr. Build. Mater. 167, 216–224. https://doi.org/10.1016/j.conbuildmat.2018.02.031

Chen, X., Zhu, G.R., Wang, J., Chen, Q., 2018b. Effect of polyacrylic resin on mechanical properties of granulated blast furnace slag based geopolymer. J. Non. Cryst. Solids 481, 4–9. https://doi.org/10.1016/j.jnoncrysol.2017.07.003

Colangelo, F., Roviello, G., Ricciotti, L., Ferone, C., Cioffi, R., 2013. Preparation and characterization of new geopolymer-epoxy resin hybrid mortars. Materials (Basel). 6, 2989–3006. https://doi.org/10.3390/ma6072989

Davidovits, J., 2017. Geopolymers: Ceramic-like inorganic polymers. J. Ceram. Sci. Technol. 8, 335–350. https://doi.org/10.4416/JCST2017-00038

Davidovits, J., 2002. 30 Years of Successes and Failures in Geopolymer Applications . Market Trends and Potential Breakthroughs . Geopolymer 2002 Conf. Oct. 28-29, 2002, Melbourne, Aust. 1–16. https://doi.org/10.1017/CBO9781107415324.004

Davidovits, J., 1991. Geopolymers. J. Therm. Anal. 37, 1633–1656. https://doi.org/10.1007/bf01912193

Diamond, S., 2000. Mercury porosimetry. An inappropriate method for the measurement of pore size distributions in cement-based materials. Cem. Concr. Res. 30, 1517–1525. https://doi.org/10.1016/S0008-8846(00)00370-7

Dow, C., Glasser, F.P., 2003. Calcium carbonate efflorescence on Portland cement and

building materials. Cem. Concr. Res. 33, 147–154. https://doi.org/10.1016/S0008-8846(02)00937-7

Duxson, P., Lukey, Æ.G.C., Deventer, J.S.J. Van, 2007a. Physical evolution of Na-geopolymer derived from metakaolin up to 1000 ° C 3044–3054. https://doi.org/10.1007/s10853-006-0535-4

Duxson, P., Lukey, G.C., Separovic, F., Van Deventer, J.S.J., 2005. Effect of alkali cations on aluminum incorporation in geopolymeric gels. Ind. Eng. Chem. Res. 44, 832–839. https://doi.org/10.1021/ie0494216

Duxson, P., Lukey, G.C., Van Deventer, J.S.J., 2006. Evolution of gel structure during thermal processing of Na-geopolymer gels. Langmuir 22, 8750–8757. https://doi.org/10.1021/la0604026

Duxson, P., Provis, J.L., Lukey, G.C., van Deventer, J.S.J., 2007b. The role of inorganic polymer technology in the development of "green concrete." Cem. Concr. Res. 37, 1590–1597. https://doi.org/10.1016/j.cemconres.2007.08.018

Ebrahimi, A., Saffari, M., Milani, D., Montoya, A., Valix, M., Abbas, A., 2017. Sustainable transformation of fly ash industrial waste into a construction cement blend via CO2 carbonation. J. Clean. Prod. 156, 660–669. https://doi.org/10.1016/j.jclepro.2017.04.037

Ferone, C., Roviello, G., Colangelo, F., Cioffi, R., Tarallo, O., 2013. Novel hybrid organic-geopolymer materials. Appl. Clay Sci. 73, 42–50. https://doi.org/10.1016/j.clay.2012.11.001

Fry, M., 2013. Cement, carbon dioxide, and the "necessity" narrative: A case study of Mexico. Geoforum 49, 127–138. https://doi.org/10.1016/j.geoforum.2013.06.003

Gagg, C.R., 2014. Cement and concrete as an engineering material: An historic appraisal and case study analysis. Eng. Fail. Anal. 40, 114–140. https://doi.org/10.1016/j.engfailanal.2014.02.004

Gardner, W., 1921. Note on the dynamics of capillary flow. Phys. Rev. 18, 206–209. https://doi.org/10.1103/PhysRev.18.206

Hajimohammadi, A., Provis, J.L., Van Deventer, J.S.J., 2010. Effect of alumina release rate on the mechanism of geopolymer gel formation. Chem. Mater. 22, 5199–5208.

https://doi.org/10.1021/cm101151n

He, P., Jia, D., Wang, M., Zhou, Y., 2011. Thermal evolution and crystallization kinetics of potassium-based geopolymer. Ceram. Int. 37, 59–63. https://doi.org/10.1016/j.ceramint.2010.08.008

He, P., Wang, M., Fu, S., Jia, D., Yan, S., Yuan, J., Xu, J., Wang, P., Zhou, Y., 2016. Effects of Si/Al ratio on the structure and properties of metakaolin based geopolymer. Ceram. Int. 42, 14416–14422. https://doi.org/10.1016/j.ceramint.2016.06.033

Hower, J.C., 2012. Petrographic examination of coal-combustion fly ash. Int. J. Coal Geol. 92, 90–97. https://doi.org/10.1016/j.coal.2011.12.012

Hu, Y., Liu, X., 2003. Chemical composition and surface property of kaolins. Miner. Eng. 16, 1279–1284. https://doi.org/10.1016/j.mineng.2003.07.006

Ji, N., Yeon, J., Seung, I., Yeon, K., 2017. Effects of curing temperature and hardener type on the mechanical properties of bisphenol F-type epoxy resin concrete. Constr. Build. Mater. 156, 933–943. https://doi.org/10.1016/j.conbuildmat.2017.09.053

Jian, Z., 2003. The Physical Meanings of 5 Basic Parameters for an X-Ray Diffraction Peak and Their Application * 22.

Ju, Y., Lee, C.H., 2017. Evaluation of the energy efficiency of the shell coal gasification process by coal type. Energy Convers. Manag. 143, 123–136. https://doi.org/10.1016/j.enconman.2017.03.082

Khan, M.Z.N., Hao, Y., Hao, H., Shaikh, F.U.A., 2018. Mechanical properties of ambient cured high strength hybrid steel and synthetic fibers reinforced geopolymer composites. Cem. Concr. Compos. 85, 133–152. https://doi.org/10.1016/j.cemconcomp.2017.10.011

Khoury, G.A., Majorana, C.E., Pesavento, F., Schrefler, B.A., 2002. Modelling of heated concrete. Mag. Concr. Res. 54, 77–101. https://doi.org/10.1680/macr.54.2.77.40895

Kong, D.L.Y., Sanjayan, J.G., 2008. Damage behavior of geopolymer composites exposed to elevated temperatures. Cem. Concr. Compos. 30, 986–991. https://doi.org/10.1016/j.cemconcomp.2008.08.001

Kuenzel, C., Grover, L.M., Vandeperre, L., Boccaccini, A.R., Cheeseman, C.R., 2013.

Production of nepheline/quartz ceramics from geopolymer mortars. J. Eur. Ceram. Soc. 33, 251–258. https://doi.org/10.1016/j.jeurceramsoc.2012.08.022

Kurad, R., Silvestre, J.D., de Brito, J., Ahmed, H., 2017. Effect of incorporation of high volume of recycled concrete aggregates and fly ash on the strength and global warming potential of concrete. J. Clean. Prod. 166, 485–502. https://doi.org/10.1016/j.jclepro.2017.07.236

Lahoti, M., Wong, K.K., Tan, K.H., Yang, E.H., 2018. Effect of alkali cation type on strength endurance of fly ash geopolymers subject to high temperature exposure. Mater. Des. 154, 8–19. https://doi.org/10.1016/j.matdes.2018.05.023

Lee, N.K., Lee, H.K., 2015. Reactivity and reaction products of alkali-activated, fly ash/slag paste. Constr. Build. Mater. 81, 303–312. https://doi.org/10.1016/j.conbuildmat.2015.02.022

Lee, S., van Riessen, A., Chon, C.M., 2016. Benefits of sealed-curing on compressive strength of fly ash-based geopolymers. Materials (Basel). 9. https://doi.org/10.3390/MA9070598

Li, G., Zhao, X., 2003. Properties of concrete incorporating fly ash and ground granulated blast-furnace slag. Cem. Concr. Compos. 25, 293–299. https://doi.org/10.1016/S0958-9465(02)00058-6

Liang, G., Zhu, H., Li, H., Liu, T., Guo, H., 2021. Comparative study on the effects of rice husk ash and silica fume on the freezing resistance of metakaolin-based geopolymer. Constr. Build. Mater. 293, 123486. https://doi.org/10.1016/j.conbuildmat.2021.123486

Lin, T., Jia, D., He, P., Wang, M., Liang, D., 2008. Effects of fiber length on mechanical properties and fracture behavior of short carbon fiber reinforced geopolymer matrix composites. Mater. Sci. Eng. A 497, 181–185. https://doi.org/10.1016/j.msea.2008.06.040

Mabroum, S., Moukannaa, S., El Machi, A., Taha, Y., Benzaazoua, M., Hakkou, R., 2020. Mine wastes based geopolymers: A critical review. Clean. Eng. Technol. 1, 100014. https://doi.org/10.1016/j.clet.2020.100014

Manz, O.E., 1999. Coal fly ash: A retrospective and future look. Fuel 78, 133–136.

https://doi.org/10.1016/S0016-2361(98)00148-3

Mikhailova, O., Rovnaník, P., 2016. Study of Metakaolin-Based Geopolymer with Addition of Polymer Admixtures. Int. J. Chem. Mol. Nucl. Mater. Metall. Eng. 10, 1423–1427.

Mo, B.H., Zhu, H., Cui, X.M., He, Y., Gong, S.Y., 2014. Effect of curing temperature on geopolymerization of metakaolin-based geopolymers. Appl. Clay Sci. 99, 144–148. https://doi.org/10.1016/j.clay.2014.06.024

Mohseni, E., Kazemi, M.J., Koushkbaghi, M., Zehtab, B., Behforouz, B., 2019. Evaluation of mechanical and durability properties of fiber-reinforced lightweight geopolymer composites based on rice husk ash and nano-alumina. Constr. Build. Mater. 209, 532–540. https://doi.org/10.1016/j.conbuildmat.2019.03.067

Najafi Kani, E., Allahverdi, A., Provis, J.L., 2012. Efflorescence control in geopolymer binders based on natural pozzolan. Cem. Concr. Compos. 34, 25–33. https://doi.org/10.1016/j.cemconcomp.2011.07.007

Najimi, M., Sobhani, J., Pourkhorshidi, A.R., 2011. Durability of copper slag contained concrete exposed to sulfate attack. Constr. Build. Mater. 25, 1895–1905. https://doi.org/10.1016/j.conbuildmat.2010.11.067

Nana, A., Epey, N., Rodrique, K.C., Deutou, J.G.N., Djobo, J.N.Y., Tomé, S., Alomayri, T.S., Ngouné, J., Kamseu, E., Leonelli, C., 2021. Mechanical strength and microstructure of metakaolin/volcanic ash-based geopolymer composites reinforced with reactive silica from rice husk ash (RHA). Materialia 16, 101083. https://doi.org/10.1016/j.mtla.2021.101083

Okoye, F.N., Durgaprasad, J., Singh, N.B., 2016. Effect of silica fume on the mechanical properties of fly ash based-geopolymer concrete. Ceram. Int. 42, 3000–3006. https://doi.org/10.1016/j.ceramint.2015.10.084

Okoye, F.N., Durgaprasad, J., Singh, N.B., 2015. Fly ash/Kaolin based geopolymer green concretes and their mechanical properties. Data Br. 5, 739–744. https://doi.org/10.1016/j.dib.2015.10.029

Özbay, E., Erdemir, M., Durmuş, H.I., 2016. Utilization and efficiency of ground granulated blast furnace slag on concrete properties - A review. Constr. Build. Mater.

105, 423–434. https://doi.org/10.1016/j.conbuildmat.2015.12.153

Payakaniti, P., Pinitsoonthorn, S., Thongbai, P., 2018. ScienceDirect Effects of carbon fiber on mechanical and electrical properties of fly ash geopolymer composite. Mater. Today Proc. 5, 14017–14025. https://doi.org/10.1016/j.matpr.2018.02.054

Poon, C.S., Lam, L., Wong, Y.L., 2000. Study on high strength concrete prepared with large volumes of low calcium fly ash. Cem. Concr. Res. 30, 447–455. https://doi.org/10.1016/S0008-8846(99)00271-9

Prud'homme, E., Michaud, P., Joussein, E., Peyratout, C., Smith, A., Arrii-Clacens, S., Clacens, J.M., Rossignol, S., 2010. Silica fume as porogent agent in geo-materials at low temperature. J. Eur. Ceram. Soc. 30, 1641–1648. https://doi.org/10.1016/j.jeurceramsoc.2010.01.014

Puertas, F., Palacios, M., Manzano, H., Dolado, J.S., Rico, A., Rodríguez, J., 2011. A model for the C-A-S-H gel formed in alkali-activated slag cements. J. Eur. Ceram. Soc. 31, 2043–2056. https://doi.org/10.1016/j.jeurceramsoc.2011.04.036

Rafieizonooz, M., Mirza, J., Salim, M.R., Hussin, M.W., Khankhaje, E., 2016. Investigation of coal bottom ash and fly ash in concrete as replacement for sand and cement. Constr. Build. Mater. 116, 15–24. https://doi.org/10.1016/j.conbuildmat.2016.04.080

Rickard, W.D.A., Temuujin, J., Van Riessen, A., 2012. Thermal analysis of geopolymer pastes synthesised from five fly ashes of variable composition. J. Non. Cryst. Solids 358, 1830–1839. https://doi.org/10.1016/j.jnoncrysol.2012.05.032

Rostami, M., Behfarnia, K., 2017. The effect of silica fume on durability of alkali activated slag concrete. Constr. Build. Mater. 134, 262–268. https://doi.org/10.1016/j.conbuildmat.2016.12.072

Roviello, G., Ricciotti, L., Ferone, C., Colangelo, F., Cioffi, R., Tarallo, O., 2013. Synthesis and characterization of novel epoxy geopolymer hybrid composites. Materials (Basel). 6, 3943–3962. https://doi.org/10.3390/ma6093943

Roviello, G., Ricciotti, L., Ferone, C., Colangelo, F., Tarallo, O., 2015. Fire resistant melamine based organic-geopolymer hybrid composites. Cem. Concr. Compos. 59, 89–99. https://doi.org/10.1016/j.cemconcomp.2015.03.007

Ruan, Y., Han, B., Yu, X., Zhang, W., Wang, D., 2018. Carbon nanotubes reinforced reactive powder concrete. Compos. Part A 112, 371–382. https://doi.org/10.1016/j.compositesa.2018.06.025

Saha, A.K., 2018. Effect of class F fly ash on the durability properties of concrete. Sustain. Environ. Res. 28, 25–31. https://doi.org/10.1016/j.serj.2017.09.001

Saha, S., Rajasekaran, C., 2017. Enhancement of the properties of fly ash based geopolymer paste by incorporating ground granulated blast furnace slag. Constr. Build. Mater. 146, 615–620. https://doi.org/10.1016/j.conbuildmat.2017.04.139

Saikia, N., De Brito, J., 2012. Use of plastic waste as aggregate in cement mortar and concrete preparation: A review. Constr. Build. Mater. 34, 385–401. https://doi.org/10.1016/j.conbuildmat.2012.02.066

Sajan, P., Jiang, T., Lau, C., Tan, G., Ng, K., 2021. Combined effect of curing temperature , curing period and alkaline concentration on the mechanical properties of fl y ash-based geopolymer. Clean. Mater. 1, 100002. https://doi.org/10.1016/j.clema.2021.100002

Salasinska, K., Barczewski, M., Borucka, M., Górny, R.L., Kozikowski, P., Celiński, M., Gajek, A., 2019. Thermal stability, fire and smoke behaviour of epoxy composites modified with plant waste fillers. Polymers (Basel). 11. https://doi.org/10.3390/polym11081234

Saludung, A., Azeyanagi, T., Ogawa, Y., Kawai, K., 2021a. Effect of silica fume on efflorescence formation and alkali leaching of alkali-activated slag. J. Clean. Prod. 315, 128210. https://doi.org/10.1016/j.jclepro.2021.128210

Saludung, A., Azeyanagi, T., Ogawa, Y., Kawai, K., 2021b. Alkali Leaching and Mechanical Performance of Epoxy Resin-Reinforced Geopolymer Composite. Mater. Lett. 304, 130663. https://doi.org/10.1016/j.matlet.2021.130663

Saludung, A., Ogawa, Y., Kawai, K., 2019. Effect of GGBS addition on Properties of Fly Ash-based Geopolymer at High Temperatures. Proc. Japan Concr. Inst. 41, 1991–1996.

Scherer, G.W., 2004. Stress from crystallization of salt. Cem. Concr. Res. 34, 1613–1624. https://doi.org/10.1016/j.cemconres.2003.12.034

Simon, I., McMahon, H.O., 1953. Study of the Structure of Quartz , Cristobalite , and Vitreous Silica by Reflection in Infrared. J. Chem. Phys. 23, 23–30.

Singh, M., Siddique, R., 2014. Strength properties and micro-structural properties of concrete containing coal bottom ash as partial replacement of fine aggregate. Constr. Build. Mater. 50, 246–256. https://doi.org/10.1016/j.conbuildmat.2013.09.026

Škvára, F., Kopecký, L., Myšková, L., Šmilauer, V.Í.T., Alberovská, L., Vinšová, L., 2009. Aluminosilicate polymers - Influence of elevated temperatures, efflorescence. Ceram. - Silikaty 53, 276–282.

Škvára, F., Šmilauer, V., Hlaváček, P., Kopecký, L., Cílová, Z., 2012. A weak alkali bond in (N, K)-A-S-H gels: Evidence from leaching and modeling. Ceram. - Silikaty 56, 374–382.

Swinehart, D.F., 1962. The Beer-Lambert law. J. Chem. Educ. 39, 333–335. https://doi.org/10.1021/ed039p333

Tajuelo Rodriguez, E., Garbev, K., Merz, D., Black, L., Richardson, I.G., 2017. Thermal stability of C-S-H phases and applicability of Richardson and Groves' and Richardson C-(A)-S-H(I) models to synthetic C-S-H. Cem. Concr. Res. 93, 45–56. https://doi.org/10.1016/j.cemconres.2016.12.005

Tantawy, M.A., 2017. Effect of High Temperatures on the Microstructure of Cement Paste. J. Mater. Sci. Chem. Eng. 05, 33–48. https://doi.org/10.4236/msce.2017.511004

Thomas, R.J., Peethamparan, S., 2015. Alkali-activated concrete: Engineering properties and stress-strain behavior. Constr. Build. Mater. 93, 49–56. https://doi.org/10.1016/j.conbuildmat.2015.04.039

Tian, Y., Yan, X., Lu, D., Wang, Z., Zhang, J., Xu, O., Li, W., 2020. Characteristics of the Cement Asphalt Emulsion Mixture With Early-Age Strength and Flowability 7, 1–8. https://doi.org/10.3389/fmats.2020.00122

Tiwari, M., Sahu, S.K., Bhangare, R.C., Ajmal, P.Y., Pandit, G.G., 2014. Elemental characterization of coal, fly ash, and bottom ash using an energy dispersive X-ray fluorescence technique. Appl. Radiat. Isot. 90, 53–57. https://doi.org/10.1016/j.apradiso.2014.03.002

Ul Haq, E., Kunjalukkal Padmanabhan, S., Licciulli, A., 2014. Synthesis and

characteristics of fly ash and bottom ash based geopolymers-A comparative study. Ceram. Int. 40, 2965–2971. https://doi.org/10.1016/j.ceramint.2013.10.012

Vlček, J., Topinková, M., Klárová, M., Maierová, P., Ovčačíková, H., Matějka, V., Martaus, A., Blahůšková, V., 2021. Alkali-activated metakaolin and fly ash as unfired ceramic bonding systems. Minerals 11, 1–16. https://doi.org/10.3390/min11020197

Wang, S.D., Scrivener, K.L., 1995. Hydration products of alkali activated slag cement. Cem. Concr. Res. 25, 561–571. https://doi.org/10.1016/0008-8846(95)00045-E

Wang, T., Song, H., Yue, Z., Hu, T., Sun, T., 2019. Cold Regions Science and Technology Freeze – thaw durability of cement-stabilized macadam subgrade and its compaction quality index. Cold Reg. Sci. Technol. 160, 13–20. https://doi.org/10.1016/j.coldregions.2019.01.005

Wilczyńska-Michalik, W., Moryl, R., Sobczyk, J., Michalik, M., 2014. Composition of coal combustion by-products: The importance of combustion technology. Fuel Process. Technol. 124, 35–43. https://doi.org/10.1016/j.fuproc.2014.02.016

Worrell, E., Price, L., Martin, N., Hendriks, C., Meida, L.O., 2001. Missions from ∗ the. Carbon N. Y. 26, 303–329.

Xu, H., Deventer, J.S.J. Van, 2000. The geopolymerisation of alumino-silicate minerals.

Yan, S., He, P., Jia, D., Yang, Z., Duan, X., Wang, S., Zhou, Y., 2016. Effect of fiber content on the microstructure and mechanical properties of carbon fiber felt reinforced geopolymer composites. Ceram. Int. 42, 7837–7843. https://doi.org/10.1016/j.ceramint.2016.01.197

Yao, X., Yang, T., Zhang, Z., 2016. Compressive strength development and shrinkage of alkali-activated fly ash–slag blends associated with efflorescence. Mater. Struct. Constr. 49, 2907–2918. https://doi.org/10.1617/s11527-015-0694-3

Ye, H., Radlińska, A., 2016. Quantitative analysis of phase assemblage and chemical shrinkage of Alkali-activated slag. J. Adv. Concr. Technol. 14, 245–260. https://doi.org/10.3151/jact.14.245

Yildirim, I.Z., Prezzi, M., 2011. Chemical, mineralogical, and morphological properties of steel slag. Adv. Civ. Eng. 2011. https://doi.org/10.1155/2011/463638

Yu, C., Ke-jin, W., Di, L., 2012. Mechanical properties of pervious cement concrete 3329–3334. https://doi.org/10.1007/s11771-012-1411-9

Zain, H., Abdullah, M.M.A.B., Hussin, K., Ariffin, N., Bayuaji, R., 2017. Review on Various Types of Geopolymer Materials with the Environmental Impact Assessment. MATEC Web Conf. 97. https://doi.org/10.1051/matecconf/20179701021

Zannerni, G.M., Fattah, K.P., Al-Tamimi, A.K., 2020. Ambient-cured geopolymer concrete with single alkali activator. Sustain. Mater. Technol. 23, e00131. https://doi.org/10.1016/j.susmat.2019.e00131

Zhang, H.Y., Kodur, V., Cao, L., Qi, S.L., 2014a. Fiber reinforced geopolymers for fire resistance applications. Procedia Eng. 71, 153–158. https://doi.org/10.1016/j.proeng.2014.04.022

Zhang, H.Y., Kodur, V., Qi, S.L., Cao, L., Wu, B., 2014b. Development of metakaolin-fly ash based geopolymers for fire resistance applications. Constr. Build. Mater. 55, 38–45. https://doi.org/10.1016/j.conbuildmat.2014.01.040

Zhang, Y.J., Li, S., Wang, Y.C., Xu, D.L., 2012. Microstructural and strength evolutions of geopolymer composite reinforced by resin exposed to elevated temperature. J. Non. Cryst. Solids 358, 620–624. https://doi.org/10.1016/j.jnoncrysol.2011.11.006

Zhang, Z., Provis, J.L., Ma, X., Reid, A., Wang, H., 2018. Efflorescence and subflorescence induced microstructural and mechanical evolution in fly ash-based geopolymers. Cem. Concr. Compos. 92, 165–177. https://doi.org/10.1016/j.cemconcomp.2018.06.010

Zhang, Z., Provis, J.L., Reid, A., Wang, H., 2014. Fly ash-based geopolymers: The relationship between composition, pore structure and efflorescence. Cem. Concr. Res. 64, 30–41. https://doi.org/10.1016/j.cemconres.2014.06.004

Zhang, Z.H., Zhu, H.J., Zhou, C.H., Wang, H., 2016. Geopolymer from kaolin in China: An overview. Appl. Clay Sci. 119, 31–41. https://doi.org/10.1016/j.clay.2015.04.023

APPENDIX

TG-DTA curve of FAS15

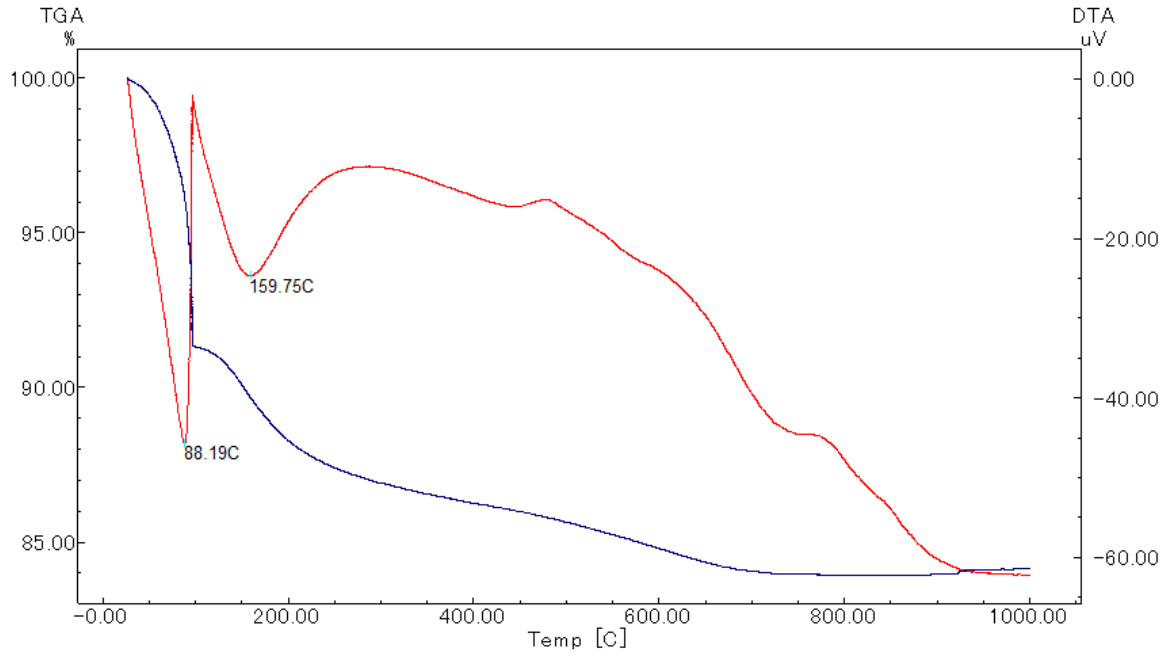

TG-DTA curve of FAS30

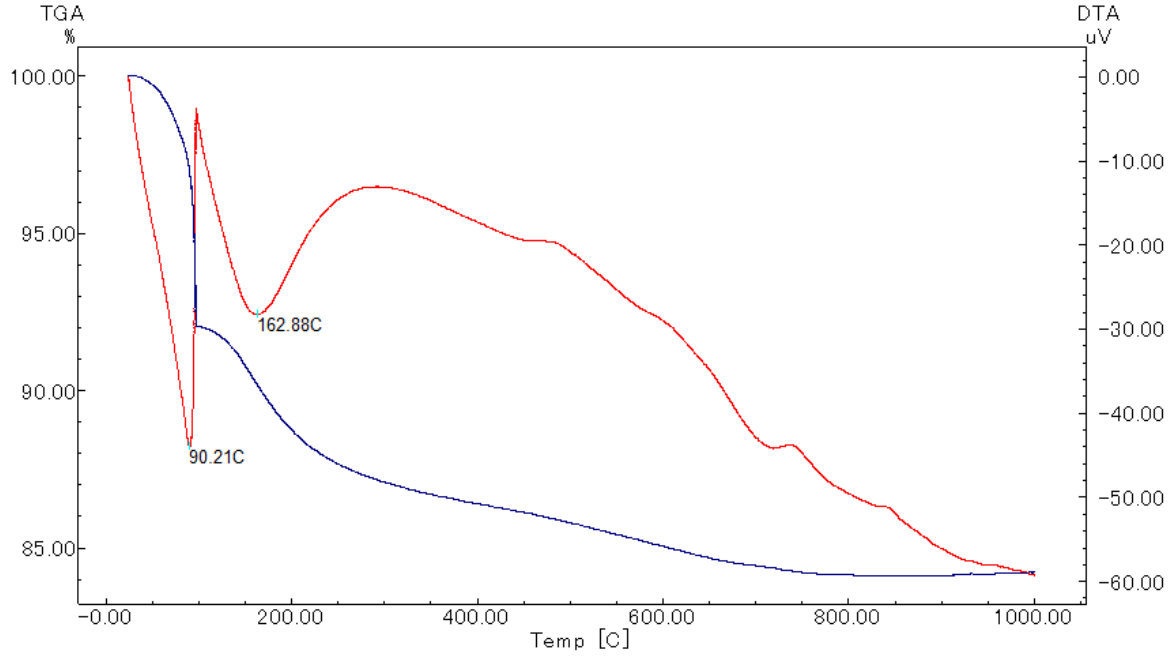

TG-DTA curve of FAS45

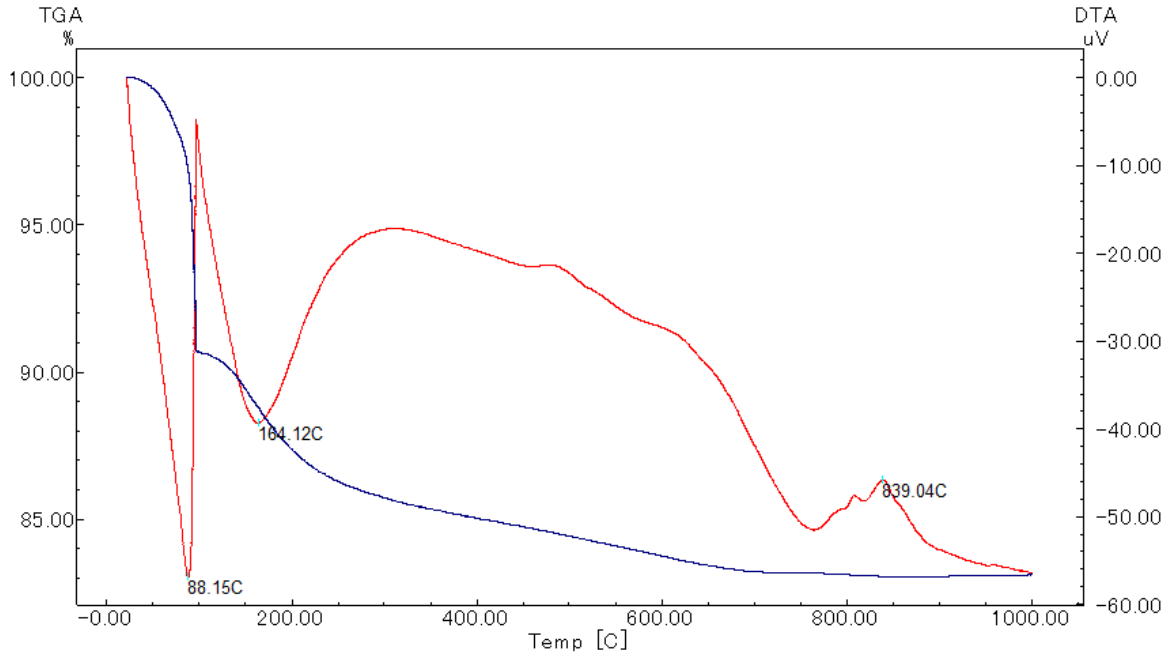

The exothermic peak observed in FAS45 could be attributed to the formation of a crystalline phase.

Microstructure analysis of FAS15, FAS30, and FAS45 at high temperature.

FAS15

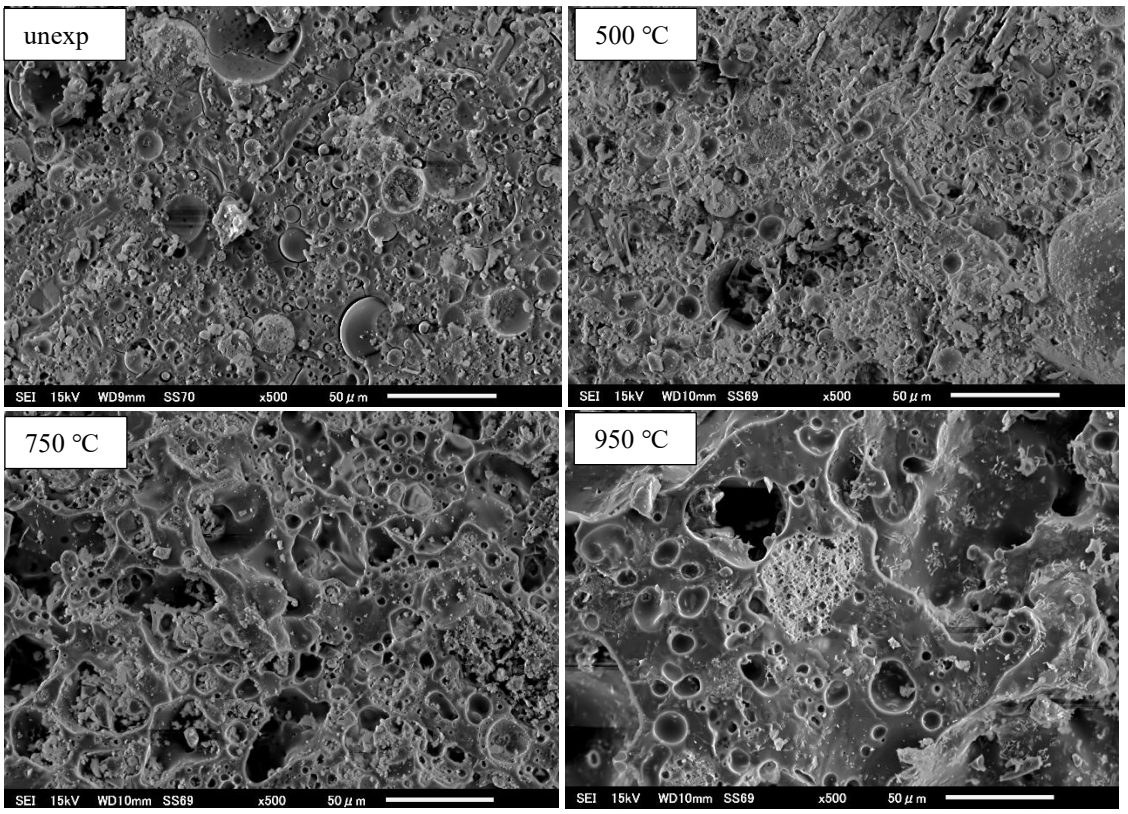

FAS30

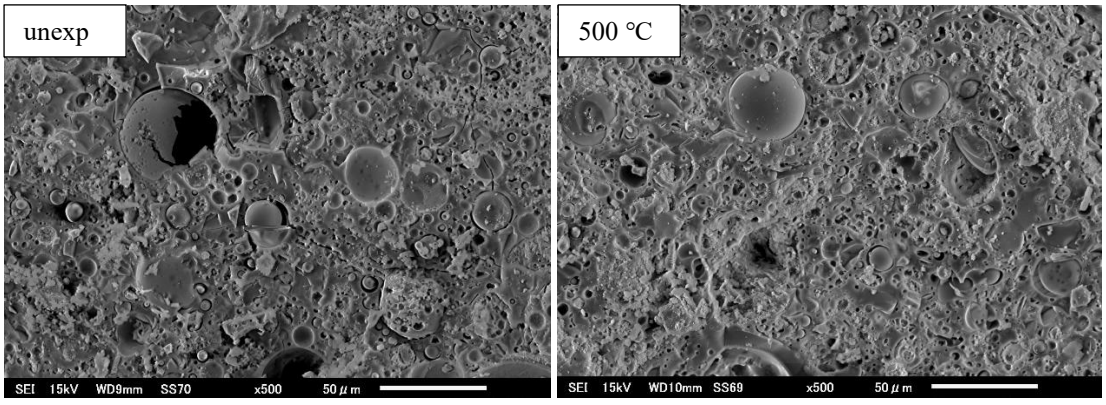

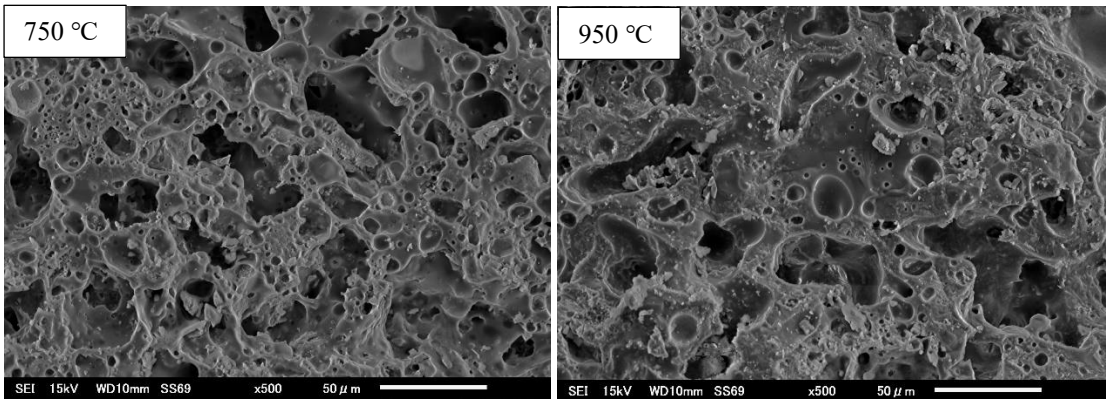
750 ℃
950 ℃
SEI 15kV WD10mm SS69 x500 50 μm
SEI 15kV WD10mm SS69 x500 50 μm

FAS45

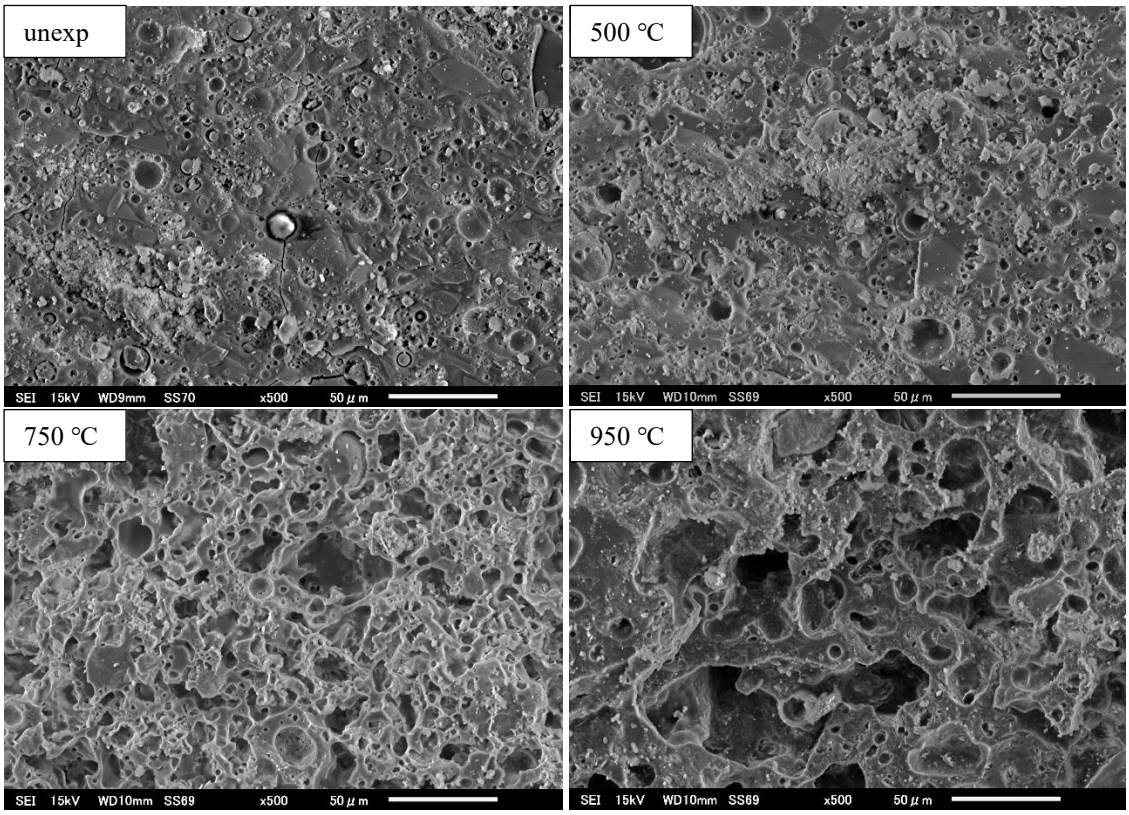
unexp
500 ℃
750 ℃
950 ℃
SEI 15kV WD9mm SS70 x500 50 μm
SEI 15kV WD10mm SS69 x500 50 μm
SEI 15kV WD10mm SS69 x500 50 μm
SEI 15kV WD10mm SS69 x500 50 μm